Insight into the Cellular and Molecular Mechanisms of Melanoma-Associated Retinopathy

Ryan Mosavi-Hecht

A DISSERTATION

Submitted to the Department of Chemical Physiology and Biochemistry
Oregon Health & Science University
School of Medicine

In Partial Fulfillment of the Requirements for the Degree of Doctor of Philosophy

November 2024

CERTIFICATE OF APPROVAL

This is to certify that the PhD dissertation of

Ryan Mosavi-Hecht

has been approved

_____

Advisor, Catherine Morgans, Ph.D.

_____

Member & Chair, Julie Saugstad, Ph.D.

_____

Member, Robert Duvoisin, Ph.D.

_____

Member, Elizabeth Berry, M.D.

_____

Member, Paul Yang, M.D, Ph.D.

_____

Outside Reader, Caroline Enns, Ph.D.

I. Table of Contents

II. Common Abbreviations

Abv	Abbreviation	Description
PNS	Paraneoplastic syndrome	A class of autoimmune disease caused by the immune response against a cancer.
MAR	Melanoma-associated retinopathy	Paraneoplastic syndrome causing visual impairment in melanoma patients.
TRPM1	Transient receptor potential melastatin 1	Cation channel expressed by ON-BCs and melanocytes. The autoantigen in MAR.
miR-211	Micro-RNA 211	Tumor suppressor microRNA encoded by intron 6 of TRPM1.
ON-BC	ON-bipolar cell	Class of retinal interneuron that responds to increments in light intensity. Post-synaptic to photoreceptors.
RBC	Rod bipolar cell	A subclass of ON-BCs that synapses with rod photoreceptors.
ONL	Outer nuclear layer	Retinal layer housing the photoreceptor nuclei.
OPL	Outer plexiform layer	First synaptic layer in the retina; the site of neurotransmission between photoreceptors, bipolar cells, and horizontal cells.
INL	Inner nuclear layer	The second cell body layer of the retina, containing bipolar cells, horizontal cells, and amacrine cells.
IPL	Inner plexiform layer	The second synaptic layer of the retina; the site of neurotransmission between bipolar cells, amacrine cells, and ganglion cells.
GCL	Ganglion cell layer	The final layer of the retinal signal pathway that houses the cell bodies of ganglion cells.
BRB	Blood-retinal barrier	A cellular barrier that restricts the passage of macromolecules from the circulation into the retina.
ERG	Electroretinogram	An exam that records the electrical activity of the retina in response to a light stimulus. Used to assess ON-BC function in MAR.
CM	Cutaneous melanoma	An aggressive form of skin cancer that arises in the pigment producing cells in the skin, melanocytes.
FcγR	Fc gamma receptor	Receptor molecules on the cell surface that bind the Fc domain on IgG antibodies.

III. Dedication

To my wife Pegga, who's determination and strength inspire me every day. Your love, support, and delectable desserts are baked into these very pages.

To my family and friends for reminding me to live and laugh.

To my high school biology teacher, Catherine Ulicny, for awakening a curiosity that would become a career.

To Oregon.

IV. Abstract

Melanoma-associated retinopathy (MAR) is a paraneoplastic syndrome that causes visual impairment in some cutaneous melanoma (CM) patients. The visual symptoms of MAR, which include poor night vision, diminished contrast sensitivity, and photopsia, are the result of an immune response against melanoma in which retinal neurons called ON-bipolar cells (ON-BCs) are caught in the crossfire. During the anti-cancer counterattack to melanoma progression, B cells produce autoantibodies against melanocyte antigens. Since ON-BCs and melanocytes both express the channel protein Transient Receptor Potential Cation Channel Subfamily M Member 1 (TRPM1), anti-TRPM1 autoantibodies generated against the tumor can cross-react with TRPM1 in ON-BCs, compromising their ability to depolarize during the light response, which results in the visual symptoms of MAR. Many aspects of MAR pathology remain obscure, such as the trigger for TRPM1 autoantibody production and the process by which they reach their target in the retina. This dissertation showcases three independent studies that address these unknown aspects of MAR in the form of a case study, a methods report, and a research article. The MAR case report in Chapter 2 analyzes disease progression, highlights an instance of successful treatment, and postulates avenues by which TRPM1 autoantibodies could cross the blood-retinal barrier to reach the retina. To investigate how autoantibodies breach ON-BCs to reach a known intracellular epitope on TRPM1, Chapter 3 describes a novel method for observing and investigating antibody internalization in retinal neurons. Finally, the implementation of this method in Chapter 4 resolves aspects of the antibody uptake mechanism employed by ON-BCs. Collectively, this work contributes substantially to our understanding of MAR pathology and provides a platform for the continued examination of neuronal antibody uptake mechanisms. These clinical findings may shape future MAR diagnosis and treatment, and the mechanism discoveries may guide strategies for therapeutic intervention or disease prevention.

Chapter 1

Introduction

❖ 1.1: Paraneoplastic Autoimmunity ❖

Paraneoplastic syndromes (PNSs) are a rare and curious class of autoimmune disorders that arise when the immune system's attack on cancerous cells invertedly damages healthy, non-cancerous tissues in the body. Unlike conventional autoimmune disease, these syndromes develop only at the emergence of a neoplasm, although in many cases symptoms present before detection of the underlying malignancy[1–3]. Despite this distinction, paraneoplastic autoimmunity can very nearly mirror the symptoms of non-paraneoplastic diseases, complicating diagnosis[4]. For example, paraneoplastic pemphigus and classical autoimmune pemphigus vulgaris both present with severe oral blistering, yet the two B-cell mediated antibody responses that drive this phenotype are distinct[4]. In instances where a tumor has not yet been discovered, paraneoplastic symptoms, especially neurological ones, can give the impression of an entirely different disease. The short-term memory loss, confusion, and psychological dysfunction that accompany paraneoplastic limbic encephalitis, for example, may resemble Alzheimer's disease; however, they stem from a B-cell mediated immune response against small cell lung cancer[5]. Even if cancer has already been diagnosed, the rapid onset of seemingly unrelated symptoms can be alarming. The most common PNS to develop from thymoma, for example, is myasthenia gravis, where muscle weakness and general motor impairment symptoms may seem inexplicable in the context of the cancer[5,6]. Adding further to the challenge of diagnosis, the same cancer can generate several different PNSs, each with a diverse array of symptoms. Melanoma alone has 8 documented paraneoplastic complications that affect everything from vision to muscle function[7].

The fundamental cause of PNSs is tumor cell expression of protein antigens that are also present in other tissues[8–10]. While B and T cells undergo rigorous training to prevent them from recognizing the body's own proteins, dysregulation of normal cell functions in cancerous cells alters protein structure or expression patterns in a manner that causes the immune cells to disregard their tutelage[10]. Because immune cell strategies for destroying cancer cells are grounded in the recognition of a specific protein, they will see all cells expressing that protein as a threat, even non-cancerous ones. This issue is exemplified by ovarian cancer cells that express NMDA receptors, a glutamate sensing membrane protein critical for neurotransmission in the brain[11].

When B cells attack NMDA receptors on malignant ovarian cells, they produce antibodies against the receptors that reach the brain and disrupt neurotransmission[12].

As PNS symptoms are ultimately caused by the immune response to a tumor, the most effective – although non-trivial – treatment is the eradication of the underlying cancer[8]. With the cancer neutralized, the immune response wanes and ceases to antagonize the healthy tissue. In some PNSs, such as melanoma-associated retinopathy (MAR), the damage to the healthy tissue is reversible, as the immune response only inhibits non-vital molecular machinery of the cell. The near complete reversal of symptoms in the successful treatment of MAR is evidence of this fact, as recovery would not be possible if targeted neurons were killed[13,14]. In other PNSs (cancer-associated retinopathy, cerebellar ataxia, autoimmune encephalitis), however, the immune response causes irreparable damage or cell death in non-dividing neurons, and the degeneration is permanent[15,16]. Transient symptom relief can often be accomplished through therapies like IVIG and plasmapheresis that temporarily eliminate or neutralize humoral components of the immune response (such as antibodies) in the blood stream[17]. However, consistent treatment is required to maintain a therapeutic effect[3]. Since some antibody subclasses are associated with improved cancer prognosis[18,19], elimination of all antibodies from the blood stream may also have a negative impact on the anti-cancer immune responses.

Checkpoint inhibitors have become a mainstay in frontline treatment for many cancers and operate by reinvigorating the immune response which many cancers adeptly repress[20,21]. While this approach has enjoyed laudable success in mitigating tumor growth, many studies now recognize an increase in autoimmunity called immune-related adverse events (irAEs) as a side effect of the reanimated immune response[22–24]. Balancing effective immunotherapy with toxicity and unwanted side effects remains an exigent issue in the development of cancer therapeutics.

❖ 1.2: Melanoma-Associated Retinopathy ❖

Melanoma-associated retinopathy (MAR) is the most common PNS to arise from cutaneous melanoma (CM), an aggressive form of skin cancer that originates in the pigment producing cells of the skin called melanocytes[25]. Unlike uveal melanoma, which impairs vision

because of cancer within the eye[26], the source of MAR vision complications is not the cancer itself, but the immune response against it. The primary melanoma often forms at remote sites such as the arm, leg, or trunk, yet the antibodies produced against the distal tumor eventually mediate PNS symptoms in the eye. Specifically, the pathogenic antibodies in MAR target an ion channel expressed in both the retina and melanocytes called transient receptor potential melastatin 1 (TRPM1). In melanocytes, TRPM1 activity regulates intracellular calcium levels and is involved in the production of melanin[27–29]. In the retina, TRPM1 is expressed by neurons called ON-bipolar cells (ON-BCs) which require the channel for depolarization during the light response[30].

While MAR pathogenesis can be explained by autoantibody inhibition of TRPM1, some understanding of the molecular machinery at the photoreceptor-bipolar cell synapse is useful for appreciating the nature of this antagonism. The open/closed state of TRPM1 is negatively regulated by a G-protein coupled receptor (GPCR) called mGluR6, which responds to changes in glutamate released by the photoreceptors on stimulation by light[30,31]. In darkness, the photoreceptors tonically release glutamate onto mGluR6 in the dendrites of ON-BCs. In turn, mGluR6 is activated and its G-proteins dissociate, whereupon they bind intracellular domains on TRPM1 to hold the channel in its closed state[32]. In response to light, photoreceptors release less glutamate, which deactivates mGluR6 and its G-proteins, relieving their inhibition of TRPM1 to allow channel opening and the influx of cations which depolarizes the cell[33]. With this critical role in the ON-BC light response, TRPM1 is essential for normal vision in both dim and bright lighting conditions. Thus, when TRPM1 autoantibodies bind and inhibit the channel in MAR they cause an array of symptoms associated with ON-BC dysfunction, including nyctalopia (night blindness), photopsia (flashing lights), visual field constriction, and contrast sensitivity issues.

Changes to ON-BC function can be quantified using a visual diagnostic test called electroretinography (ERG), which records the electrical response of the retina to standardized intensities of light flash stimuli under different ambient light conditions. The individual components of the resulting ERG waveform represent the composite electrical activity of different groups of retinal neurons, allowing physicians and researchers to determine the retinal etiology of visual dysfunction. The initial negative inflection of the waveform is the a-wave, which represents photoreceptor activation by the light stimulus. The upward positive inflection of the ERG, termed

the b-wave, is produced predominantly by ON-BCs during their depolarization (**Figure 1-1**). Compared to healthy retina, the MAR b-wave is attenuated ("electronegative"), especially with respect to a relatively normal a-wave in MAR. Isolated attenuation of the b-wave is highly indicative of ON-BC dysfunction, which in the setting of metastatic melanoma is associated with TRPM1 autoantibodies[34–36].

Figure[1-1]

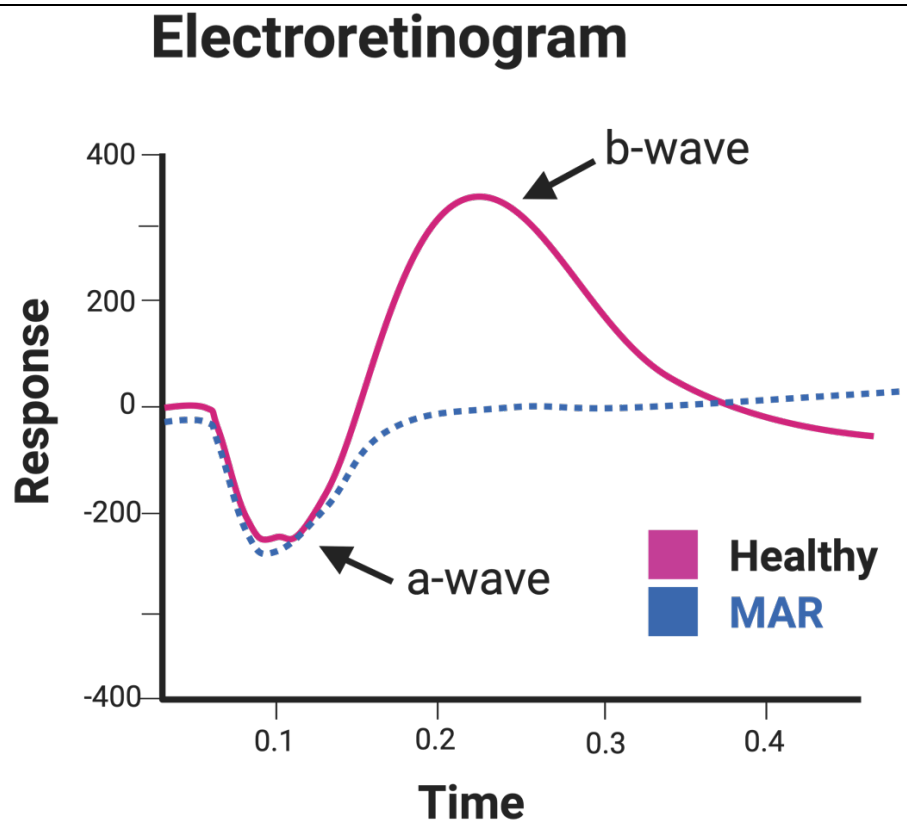

[1-1] **Components of the electroretinogram.** A schematic of mock ERG recordings from healthy (pink) and MAR (blue) eyes. The negative inflection of the ERG waveform, called the a-wave, is produced by the activity of the photoreceptors. The positive inflection that follows, called the b-wave, is produced primarily by the depolarization of ON-BCs. In MAR, an electronegative waveform (attenuated b-wave, out of proportion to the a-wave) is observed indicating ON-BC dysfunction caused by TRPM1 inhibition by autoantibodies.

Previous studies mapping the epitope of TRPM1 autoantibodies in MAR revealed that individual patients generate autoantibodies to different regions of the protein. One group has identified a region of the TPRM1 N-terminus that appears to be a common epitope between all individuals screened to date[1,13,37]. Another group identified patients with serum reactivity against C-terminal epitopes and found that individual patients can have polyclonal reactivity to TRPM1[38].

Curiously, both studies agree that all patient autoantibodies bind exclusively to intracellular epitopes on TRPM1. While intracellular epitopes are not uncommon in PNSs, it was historically accepted that only antibodies targeting extracellular epitopes could directly mediate disease[39]. Only recently have studies presented evidence that antibodies targeting intracellular proteins can be directly pathogenic[40]. For autoantibodies targeting *intracellular* antigens to bind their target and cause disease, they would first have to cross the cell's plasma membrane. This implicates a prerequisite event for the development of symptoms: ON-BCs must internalize TRPM1 autoantibodies for MAR to manifest.

❖ 1.3: Antibody Internalization in Neurons ❖

The internalization of antibodies is a commonly observed phenomenon in certain specialized cell types. Phagocytic cells like macrophages use membrane proteins called Fc receptors to bind antibody-opsonized pathogens and initiate internalization of the antibody-pathogen complex[41]. Intestinal epithelia use the Fc neonatal receptor (FcRn) to bind and internalize IgG before shuttling them through the cell and releasing them into the gut lumen[42]. While commonplace in these scenarios, antibody internalization is not a universal cell behavior. In fact, significant research efforts are focused on understanding the requirements for antibody uptake to improve therapeutic delivery of antibody-drug conjugates[43–46]. Interestingly, some neurons appear to be intrinsically capable of antibody internalization; observations of intracellular IgG in Purkinje cells and motor neurons date back to 1985[47], when it was first hypothesized that antibodies targeting intracellular proteins may be pathogenic[48,49]. Confirmation of this theory surfaced in 1997, when one group reported retinal photoreceptor cell death in response to treatment with antibodies targeting an intracellular calcium binding protein, recoverin[15]. In 2009, additional experiments conducted on living Purkinje cells proved that neuronal antibody internalization was not an artifact caused by cell death or compromised cell membranes[50]. Remarkably, the group established that Purkinje cells could internalize much larger IgM antibodies (950 kDa) as well. Antibody clearance from cells was evident within 24-48 hours and uptake alone did not appear to have negative consequences on cell viability. Shortly afterward, however, another study demonstrated that internalized antibodies targeting the intracellular protein Yo caused cell death in Purkinje cells[16]. These mixed results suggest that pathogenicity results from the specific effects

of antibody-target binding rather than antibody internalization itself. For some intracellular targets, antibody binding leads to less extreme phenotypes. Geis *et al.* demonstrated that internalized anti-amphiphysin antibodies suppressed GABAergic inhibition of motor neuron activity[51]. Similarly, TRPM1 autoantibodies in MAR impair ON-BC depolarization without killing the neurons[13,52].

While the notion that antibodies against intracellular antigens can directly impact neuronal activity has become more widely appreciated, mechanistic explanations of uptake remain sparse[40,53–57]. In 2013, Congdon *et al.* published the first thorough study of antibody internalization mechanisms in which they examined anti-tau uptake in primary neuron cultures and brain slices[53]. They demonstrated reduced uptake at low temperatures, indicating an energy dependent process drives the behavior. Furthermore, blocking FcγR II/III, and inhibiting clathrin-mediated endocytosis independently impaired antibody uptake, suggesting that both components are required for uptake in neurons. The same mechanism was suggested by Rocchi *et al.* for uptake of anti-synapsin I antibodies in hippocampal neurons, despite a different antibody target[57]. However, several reports on retinal endothelial cells propose that antibody internalization requires the Fc neonatal receptor (FcRn)[58–60]. Collectively, these findings suggest that internalization mechanisms may vary by cell type.

While our knowledge of basic endocytosis mechanisms has grown enormously in recent years[61–65], antibodies are a poorly understood cargo, and very little is known about their entry into neurons. Discoveries in this field have the potential for substantial therapeutic impact, yet no new studies addressing this mechanism in any disease have been published since 2019. This includes MAR, for which the postulation of TRPM1 autoantibody internalization was made in 2011[66]. Further experimentation across additional neuronal subtypes and intracellular targets will be critical for understanding the extent of mechanism variability. The outcome may eventually enable cell-specific therapies tailored to either enhance or inhibit antibody entry into neurons for drug delivery or disease prevention, respectively.

❖ 1.4: The Blood-Retinal Barrier in MAR ❖

In MAR and other PNS with autoantibodies against central nervous system (CNS) proteins, the neuronal cell membrane is not the only barrier that antibodies must circumvent to mediate disease. The brain, spinal cord, and retina each have structurally homologous cellular barriers that restrict the passage of macromolecules from the circulation into CNS tissue (**Figure 1-2**)[67]. Endothelial cells (ECs) that line the vessel wall confer the first layer of obstruction; tight junctions between ECs block molecules that would otherwise pass between cells (paracellular transport)[68]. Select molecules that are permitted to cross the barrier do so via transcytosis (vesicular transport) mediated by surface receptors, pumps, transporters, or lipophilic diffusion across the membrane[69]. Pericytes contribute the second layer of fortification to these blood barriers through a combination of structural and chemical support. Pericytes, which surround ECs, physically reinforce the blood vessel and provide critical regulatory signaling to maintain tight junction integrity and regulation of proper blood flow[68]. The end feet of Müller glia in the retina or astrocytes in the brain/spinal cord provide a final layer of reinforcement to the blood vessel. Additionally, these cells secrete signals onto ECs that regulate barrier function and permeability.

Figure[1-2]

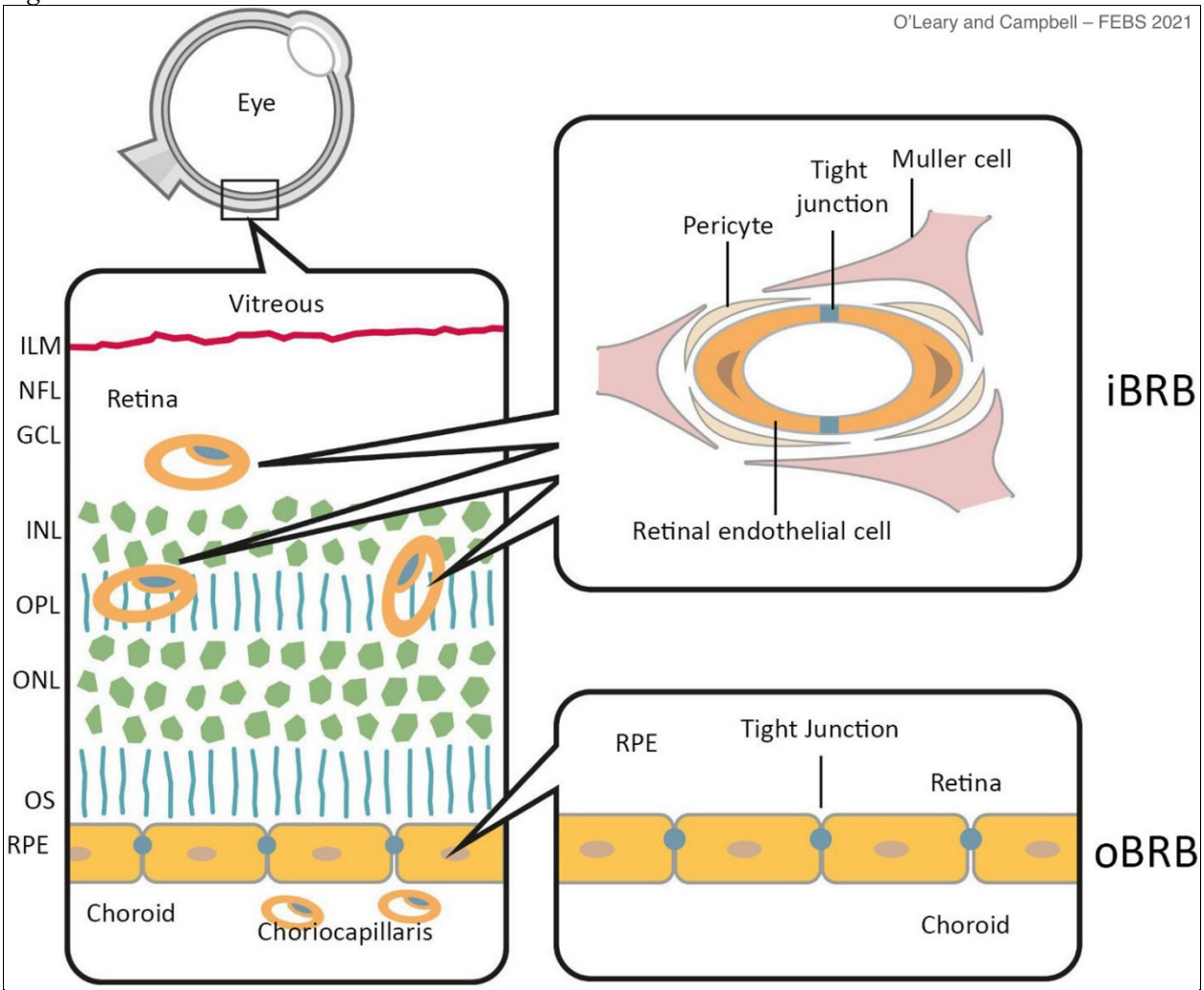

[1-2]**Anatomy of the blood retinal barrier.** Schematic of the outer (oBRB) and inner (iBRB) blood-retinal barriers depicting their cellular composition and location within the retina. The iBRB surrounds blood vessels traversing the outer plexiform layer, inner plexiform layer, and ganglion cell layers. Like the structurally homologous blood-brain barrier and blood-spinal cord-barrier, the iBRB is comprised of endothelial cells, pericytes, and Müller glia that surround the vessel in layers. In the barriers of the brain and spinal cord, astrocytes are found in place of Müller glia. The oBRB is formed by tight junctions between retinal pigment epithelium (RPE) at the interface with the choroid. ILM = inner limiting membrane; NFL = nerve fiber layer; GCL = ganglion cell layer; INL = inner nuclear layer; OPL = outer plexiform layer; ONL = outer nuclear layer; OS = outer segments. *Reproduced with permission from John Wiley and Sons; license attached.*

The regulation of BRB integrity in healthy and disease states is complex and multifactorial (reviewed in Bicker *et al.*[70], O'Leary and Campbell[68]). Inflammation has been identified as a key regulator of BRB integrity, as certain inflammatory cytokines affect the integrity of tight junction

proteins such as Claudin-5[71–76]. Many diseases are characterized by BRB damage or degradation, which could provide autoantibodies with unmitigated access to the retina[77,78]. A study by Mosavi-Hecht *et al.* in 2024 identified vascular leakage and elevated inflammatory cytokine levels in the eyes of a MAR patient, lending credibility to this hypothesis[13] (see **Chapter 2**). Damage is not necessarily required for antibodies to bypass the BRB. While originally considered to be "immune privileged" sites, CNS tissues such as the brain and the retina are regularly patrolled by immune cells. In multiple sclerosis, B cells are known to extravasate directly across the blood-brain barrier using surface adhesion molecules such as VFA-4 and ICAM-1[79]. Similar observations of leukocyte migration into the retina have been made in healthy and disease states[80,81], suggesting that B cells could produce anti-TRPM1 antibodies locally from within the retina. Despite the presence of leukocytes in the eye, Finally, it is possible that antibodies could be trafficked across the BRB into the retina through EC transcytosis, mediated by either Fc receptor shuttling[82] or non-specific, fluid phase endocytosis[83]. Additional studies are required to investigate the contribution of these mechanisms to autoantibody infiltration of the retina. A deeper understanding of these mechanisms may provide the basis for therapies aimed at excluding autoantibodies from the retina to prevent MAR and other inflammatory CNS diseases.

Chapter 1 Bibliography

1. Duvoisin, R. M., Ren, G., Haley, T. L., Taylor, M. H. & Morgans, C. W. TRPM1 Autoantibodies in Melanoma Patients Without Self-Reported Visual Symptoms. *Invest. Ophthalmol. Vis. Sci.* **60**, 2330 (2019).

2. Sculier, C. *et al.* Autoimmune paraneoplastic syndromes associated to lung cancer: A systematic review of the literature: Part 5: Neurological auto-antibodies, discussion, flow chart, conclusions. *Lung Cancer* **111**, 164–175 (2017).

3. Pelosof, L. C. & Gerber, D. E. Paraneoplastic Syndromes: An Approach to Diagnosis and Treatment. *Mayo Clin Proc* **85**, 838–854 (2010).

4. Maverakis, E., Goodarzi, H., Wehrli, L. N., Ono, Y. & Garcia, M. S. The Etiology of Paraneoplastic Autoimmunity. *Clinic Rev Allerg Immunol* **42**, 135–144 (2012).

5. Thapa, B., Mahendraker, N. & Ramphul, K. Paraneoplastic Syndromes. in *StatPearls* (StatPearls Publishing, Treasure Island (FL), 2024).

6. Tormoehlen, L. M. & Pascuzzi, R. M. Thymoma, Myasthenia Gravis, and Other Paraneoplastic Syndromes. *Hematology/Oncology Clinics of North America* **22**, 509–526 (2008).

7. Dec, M. & Arasiewicz, H. Paraneoplastic syndromes in patients with melanoma. *Postepy Dermatol Alergol* **41**, 251–261 (2024).

8. Zekeridou, A. Paraneoplastic Neurologic Disorders. *Autoimmune Neurology* **30**, 1021–1051 (2024).

9. Badawy, M. *et al.* Paraneoplastic Syndromes from Head to Toe: Pathophysiology, Imaging Features, and Workup. *RadioGraphics* **43**, e220085 (2023).

10. Backes, C. *et al.* Immunogenicity of autoantigens. *BMC Genomics* **12**, 340 (2011).

11. Dalmau, J., Geis, C. & Graus, F. Autoantibodies to Synaptic Receptors and Neuronal Cell Surface Proteins in Autoimmune Diseases of the Central Nervous System. *Physiol Rev* **97**, 839–887 (2017).

12. Dalmau, J. *et al.* Anti-NMDA-receptor encephalitis: case series and analysis of the effects of antibodies. *Lancet neurology* **7**, 1091 (2008).

13. Mosavi-Hecht, R. M. *et al.* Case report: Longitudinal evaluation and treatment of a melanoma-associated retinopathy patient. *Front. Med.* **11**, (2024).

14. Abou, Samra Abdullah, Tzekov, R., Yannuzzi, N. A. & Tarabishy, A. B. Electroretinographic Findings in Melanoma-Associated Retinopathy Treated by Intravitreal Dexamethasone Implant. *Ophthalmic Surgery, Lasers and Imaging Retina* **52**, 454–456 (2021).

15. Adamus, G. & Seigel, G. Apoptotic Retinal Cell Death Induced by Antirecoverin Autoandbodies of Cancer-Associated Retinopathy. 9 (1997).

16. Greenlee, J. E. *et al.* Purkinje Cell Death After Uptake of Anti-Yo Antibodies in Cerebellar Slice Cultures. *Journal of Neuropathology & Experimental Neurology* **69**, 997–1007 (2010).

17. Arumugham, V. B. & Rayi, A. Intravenous Immunoglobulin (IVIG). in *StatPearls* (StatPearls Publishing, Treasure Island (FL), 2024).

18. Crescioli, S. *et al.* B cell profiles, antibody repertoire and reactivity reveal dysregulated responses with autoimmune features in melanoma. *Nat Commun* **14**, 3378 (2023).

19. Bolotin, D. A. *et al.* Antigen receptor repertoire profiling from RNA-seq data. *Nat Biotechnol* **35**, 908–911 (2017).

20. Ghemrawi, R. *et al.* Revolutionizing Cancer Treatment: Recent Advances in Immunotherapy. *Biomedicines* **12**, 2158 (2024).

21. Hossain, S. M., Ly, K., Sung, Y. J., Braithwaite, A. & Li, K. Immune Checkpoint Inhibitor Therapy for Metastatic Melanoma: What Should We Focus on to Improve the Clinical Outcomes? *International Journal of Molecular Sciences* **25**, 10120 (2024).

22. Graus, F. & Dalmau, J. Paraneoplastic neurological syndromes in the era of immune-checkpoint inhibitors. *Nat Rev Clin Oncol* **16**, 535–548 (2019).

23. Stavropoulou De Lorenzo, S. *et al.* Neurological Immune-Related Adverse Events Induced by Immune Checkpoint Inhibitors. *Biomedicines* **12**, 1319 (2024).

24. Martens, A., Schauwvlieghe, P. P., Madoe, A., Casteels, I. & Aspeslagh, S. Ocular adverse events associated with immune checkpoint inhibitors, a scoping review. *Journal of Ophthalmic Inflammation and Infection* **13**, 5 (2023).

25. Leonardi, G. C. *et al.* Cutaneous melanoma: From pathogenesis to therapy (Review). *International Journal of Oncology* **52**, 1071–1080 (2018).

26. Kulbay, M. *et al.* Uveal Melanoma: Comprehensive Review of Its Pathophysiology, Diagnosis, Treatment, and Future Perspectives. *Biomedicines* **12**, 1758 (2024).

27. Devi, S. *et al.* Calcium homeostasis in human melanocytes: role of transient receptor potential melastatin 1 (TRPM1) and its regulation by ultraviolet light. *American Journal of Physiology-Cell Physiology* **297**, C679–C687 (2009).

28. Oancea, E. *et al.* TRPM1 Forms Ion Channels Associated with Melanin Content in Melanocytes. *Science Signaling* **2**, ra21–ra21 (2009).

29. Devi, S. *et al.* Metabotropic glutamate receptor 6 signaling enhances TRPM1 calcium channel function and increases melanin content in human melanocytes. *Pigment Cell & Melanoma Research* **26**, 348–356 (2013).

30. Morgans, C. W. *et al.* TRPM1 is required for the depolarizing light response in retinal ON-bipolar cells. *PNAS* **106**, 19174–19178 (2009).

31. Koike, C. *et al.* TRPM1 is a component of the retinal ON bipolar cell transduction channel in the mGluR6 cascade. *Proc Natl Acad Sci U S A* **107**, 332–337 (2010).

32. Xu, Y. *et al.* The TRPM1 channel in ON-bipolar cells is gated by both the α and the βγ subunits of the G-protein Go. *Sci Rep* **6**, 20940 (2016).

33. Morgans, C. W., Brown, R. L. & Duvoisin, R. M. TRPM1: The endpoint of the mGluR6 signal transduction cascade in retinal ON-bipolar cells. *Bioessays* **32**, 609–614 (2010).

34. Berson, E. L. & Lessell, S. Paraneoplastic night blindness with malignant melanoma. *Am J Ophthalmol* **106**, 307–311 (1988).

35. Alexander, K. R. & Fishman, G. A. AOn' Response Defect in Paraneoplastic Night Blindness With Cutaneous Malignant Melanoma. *Invest Ophthalmol Vis Sci* **33**, 7 (1992).

36. Ripps, H. Functional Abnormalities in Vincristine-lnduced Night Blindness. *Invest Ophthalmol Vis Sci* **25**, 8 (1984).

37. Duvoisin, R. M. *et al.* Autoantibodies in Melanoma-Associated Retinopathy Recognize an Epitope Conserved Between TRPM1 and TRPM3. *Invest. Ophthalmol. Vis. Sci.* **58**, 2732 (2017).

38. Gyoten, D. *et al.* Broad locations of antigenic regions for anti-TRPM1 autoantibodies in paraneoplastic retinopathy with retinal ON bipolar cell dysfunction. *Exp Eye Res* **212**, 108770 (2021).

39. Binks, S., Uy, C., Honnorat, J. & Irani, S. R. Paraneoplastic neurological syndromes: a practical approach to diagnosis and management. *Practical Neurology* **22**, 19–31 (2022).

40. Williams, J. P., Carlson, N. G. & Greenlee, J. E. Antibodies in Autoimmune Human Neurological Disease: Pathogenesis and Immunopathology. *Semin Neurol* **38**, 267–277 (2018).

41. Bournazos, S., Gupta, A. & Ravetch, J. V. The role of IgG Fc receptors in antibody-dependent enhancement. *Nat Rev Immunol* **20**, 633–643 (2020).

42. Junker, F., Gordon, J. & Qureshi, O. Fc Gamma Receptors and Their Role in Antigen Uptake, Presentation, and T Cell Activation. *Front Immunol* **11**, (2020).

43. Opaliński, Ł. *et al.* High Affinity Promotes Internalization of Engineered Antibodies Targeting FGFR1. *Int J Mol Sci* **19**, 1435 (2018).

44. Mahalingaiah, P. K. *et al.* Potential mechanisms of target-independent uptake and toxicity of antibody-drug conjugates. *Pharmacology & Therapeutics* **200**, 110–125 (2019).

45. Hammood, M., Craig, A. W. & Leyton, J. V. Impact of Endocytosis Mechanisms for the Receptors Targeted by the Currently Approved Antibody-Drug Conjugates (ADCs)—A Necessity for Future ADC Research and Development. *Pharmaceuticals (Basel)* **14**, 674 (2021).

46. Lv, W. & Champion, J. A. Demonstration of intracellular trafficking, cytosolic bioavailability, and target manipulation of an antibody delivery platform. *Nanomedicine: Nanotechnology, Biology and Medicine* **32**, 102315 (2021).

47. Ritchie, T. C., Fabian, R. H. & Coulter, J. D. Axonal transport of antibodies to subcellular and protein fractions of rat brain. *Brain Research* **343**, 252–261 (1985).

48. Fabian, R. H. & Ritchie, T. C. Intraneuronal IgG in the central nervous system. *Journal of the Neurological Sciences* **73**, 257–267 (1986).

49. Karpiak, S. E. & Mahadik, S. P. Selective uptake by Purkinje neurons of antibodies to S-100 protein. *Experimental Neurology* **98**, 453–457 (1987).

50. Hill, K. E., Clawson, S. A., Rose, J. W., Carlson, N. G. & Greenlee, J. E. Cerebellar Purkinje cells incorporate immunoglobulins and immunotoxins in vitro: implications for human neurological disease and immunotherapeutics. *Journal of Neuroinflammation* **6**, 31 (2009).

51. Geis, C. *et al.* Stiff person syndrome-associated autoantibodies to amphiphysin mediate reduced GABAergic inhibition. *Brain* **133**, 3166–3180 (2010).

52. Kondo, M. *et al.* Identification of Autoantibodies against TRPM1 in Patients with Paraneoplastic Retinopathy Associated with ON Bipolar Cell Dysfunction. *PLoS ONE* **6**, e19911 (2011).

53. Congdon, E. E., Gu, J., Sait, H. B. R. & Sigurdsson, E. M. Antibody Uptake into Neurons Occurs Primarily via Clathrin-dependent Fcγ Receptor Endocytosis and Is a Prerequisite for Acute Tau Protein Clearance. *J. Biol. Chem.* **288**, 35452–35465 (2013).

54. Gu, J., Congdon, E. E. & Sigurdsson, E. M. Two Novel Tau Antibodies Targeting the 396/404 Region Are Primarily Taken Up by Neurons and Reduce Tau Protein Pathology *. *Journal of Biological Chemistry* **288**, 33081–33095 (2013).

55. Schubert, M., Panja, D., Haugen, M., Bramham, C. R. & Vedeler, C. A. Paraneoplastic CDR2 and CDR2L antibodies affect Purkinje cell calcium homeostasis. *Acta Neuropathol* **128**, 835–852 (2014).

56. Greenlee, J. E. *et al.* Anti-Yo Antibody Uptake and Interaction with Its Intracellular Target Antigen Causes Purkinje Cell Death in Rat Cerebellar Slice Cultures: A Possible Mechanism for Paraneoplastic Cerebellar Degeneration in Humans with Gynecological or Breast Cancers. *PLoS ONE* **10**, e0123446 (2015).

57. Rocchi, A. *et al.* Autoantibodies to synapsin I sequestrate synapsin I and alter synaptic function. *Cell Death Dis* **10**, 1–16 (2019).

58. Deissler, H. L., Lang, G. K. & Lang, G. E. Neonatal Fc receptor FcRn is involved in intracellular transport of the Fc fusion protein aflibercept and its transition through retinal endothelial cells. *Exp Eye Res* **154**, 39–46 (2017).

59. Dithmer, M. *et al.* The role of Fc-receptors in the uptake and transport of therapeutic antibodies in the retinal pigment epithelium. *Exp Eye Res* **145**, 187–205 (2016).

60. Deissler, H. L., Lang, G. K. & Lang, G. E. Internalization of bevacizumab by retinal endothelial cells and its intracellular fate: Evidence for an involvement of the neonatal Fc receptor. *Exp Eye Res* **143**, 49–59 (2016).

61. Parton, R. G., Taraska, J. W. & Lundmark, R. Is endocytosis by caveolae dependent on dynamin? *Nat Rev Mol Cell Biol* 1–2 (2024) doi:10.1038/s41580-024-00735-x.

62. Lin, X. P., Mintern, J. D. & Gleeson, P. A. Macropinocytosis in Different Cell Types: Similarities and Differences. *Membranes (Basel)* **10**, 177 (2020).

63. Rennick, J. J., Johnston, A. P. R. & Parton, R. G. Key principles and methods for studying the endocytosis of biological and nanoparticle therapeutics. *Nat. Nanotechnol.* **16**, 266–276 (2021).

64. Kate L. Prichard *et al.* Role of Clathrin and Dynamin in Clathrin Mediated Endocytosis/Synaptic Vesicle Recycling and Implications in Neurological Diseases. *Frontiers in Cellular Neuroscience* **15**, (2022).

65. Szewczyk-Roszczenko, O. K. *et al.* The Chemical Inhibitors of Endocytosis: From Mechanisms to Potential Clinical Applications. *Cells* **12**, 2312 (2023).

66. Dhingra, A. *et al.* Autoantibodies in Melanoma-Associated Retinopathy Target TRPM1 Cation Channels of Retinal ON Bipolar Cells. *J Neurosci* **31**, 3962–3967 (2011).

67. Goncalves, A. & Antonetti, D. A. Transgenic animal models to explore and modulate the blood brain and blood retinal barriers of the CNS. *Fluids and Barriers of the CNS* **19**, 86 (2022).

68. O'Leary, F. & Campbell, M. The blood–retina barrier in health and disease. *The FEBS Journal* **290**, 878–891 (2023).

69. Wu, D. *et al.* The blood–brain barrier: structure, regulation, and drug delivery. *Sig Transduct Target Ther* **8**, 1–27 (2023).

70. Bicker, J., Alves, G., Fonseca, C., Falcão, A. & Fortuna, A. Repairing blood-CNS barriers: Future therapeutic approaches for neuropsychiatric disorders. *Pharmacological Research* **162**, 105226 (2020).

71. Frank, P. G. & Lisanti, M. P. ICAM-1: role in inflammation and in the regulation of vascular permeability. *Am J Physiol Heart Circ Physiol* **295**, H926–H927 (2008).

72. Capaldo, C. T. & Nusrat, A. Cytokine regulation of tight junctions. *Biochimica et Biophysica Acta (BBA) - Biomembranes* **1788**, 864–871 (2009).

73. Vinores, S. A. Breakdown of the Blood–Retinal Barrier. in *Encyclopedia of the Eye* 216–222 (Elsevier, 2010). doi:10.1016/B978-0-12-374203-2.00137-8.

74. Capaldo, C. T. *et al.* Proinflammatory cytokine-induced tight junction remodeling through dynamic self-assembly of claudins. *Mol Biol Cell* **25**, 2710–2719 (2014).

75. Greene, C., Hanley, N. & Campbell, M. Claudin-5: gatekeeper of neurological function. *Fluids and Barriers of the CNS* **16**, 3 (2019).

76. Byrne, E. M. *et al.* IL-17A Damages the Blood–Retinal Barrier through Activating the Janus Kinase 1 Pathway. *Biomedicines* **9**, 831 (2021).

77. Ivanova, E., Alam, N. M., Prusky, G. T. & Sagdullaev, B. T. Blood-retina barrier failure and vision loss in neuron-specific degeneration. *JCI Insight* **4**, e126747.

78. Platt, M. P., Agalliu, D. & Cutforth, T. Hello from the Other Side: How Autoantibodies Circumvent the Blood–Brain Barrier in Autoimmune Encephalitis. *Frontiers in Immunology* **8**, (2017).

79. Alter, A. *et al.* Determinants of Human B Cell Migration Across Brain Endothelial Cells1. *The Journal of Immunology* **170**, 4497–4505 (2003).

80. Crane, I. J. & Liversidge, J. Mechanisms of leukocyte migration across the blood–retina barrier. *Semin Immunopathol* **30**, 165–177 (2008).

81. Xu, H., Dawson, R., Crane, I. J. & Liversidge, J. Leukocyte Diapedesis In Vivo Induces Transient Loss of Tight Junction Protein at the Blood–Retina Barrier. *Investigative Ophthalmology & Visual Science* **46**, 2487–2494 (2005).

82. Tien, J. *et al.* Modifying antibody-FcRn interactions to increase the transport of antibodies through the blood-brain barrier. *mAbs* **15**, 2229098 (2023).

83. Ruano-Salguero, J. S. & Lee, K. H. Antibody transcytosis across brain endothelial-like cells occurs nonspecifically and independent of FcRn. *Scientific Reports* **10**, 3685 (2020).

Chapter 2

Case Report: Longitudinal Evaluation and Treatment of a Melanoma-Associated Retinopathy Patient

Ryan M. Hecht[1], Paul Yang[2], Barrett Heyer[1], Christopher R. Rosenberg[2], Elizabeth White[2], Elizabeth Berry[3], Robert Duvoisin[1,2], and Catherine Morgans[1,2]

[1]Oregon Health and Science University, Department of Chemical Physiology and Biochemistry, Portland, OR, USA

[2]Oregon Health and Science University, Casey Eye Institute, Portland, OR, USA

[3]Oregon Health and Science University, Department of Dermatology, Portland, OR, USA

Frontiers in Medicine

DOI: 10.3389/fmed.2024.1445180

2.0: Preface

To introduce the reader to some of MAR's most salient clinical features, this dissertation opens with a detailed case study that elaborates certain key facets of the disease which become increasingly relevant in subsequent chapters. Importantly, this chapter will acquaint the reader with the causative agent of MAR: autoantibodies targeting TRPM1, an essential ion channel in the retina's neural circuitry. By analyzing the same patient over years, the study below examines changes to TRPM1 autoantibody levels in the blood and how this may be influenced by melanoma progression and cancer treatment. Over the same timeline, we assessed changes to the patient's vision with electroretinogram recordings, which can precisely identify the activity of ON-BCs and how they are impacted by TPRM1 autoantibodies and intraocular corticosteroid treatment. As alluded to in **Chapter 1**, this study also reveals a potential avenue by which TRPM1 autoantibodies gain access to the retina. Vascular leakage identified in the patient's retina represents a hole in the blood-retinal barrier through which autoantibodies or immune cells could pass. Evaluation of BRB integrity in future MAR patients will reveal whether this is a tenet of the disease or unique feature of this patient's presentation. Although the study describes a single patient, we gain valuable insight into MAR pathology that may influence how future patients are examined and treated.

2.1: Abstract

Melanoma-associated retinopathy (MAR) is a paraneoplastic syndrome associated with cutaneous metastatic melanoma in which patients develop vision deficits that include reduced night vision, poor contrast sensitivity, and photopsia. MAR is caused by autoantibodies targeting TRPM1, an ion channel found in melanocytes and retinal ON-bipolar cells (ON-BCs). The visual symptoms arise when TRPM1 autoantibodies enter ON-BCs and block the function of TRPM1, thus detection of TRPM1 autoantibodies in patient serum is a key criterion in diagnosing MAR. Electroretinograms are used to measure the impact of TRPM1 autoantibodies on ON-BC function and represent another important diagnostic tool for MAR. To date, MAR case reports have included one or both diagnostic components, but only for a single time point in the course of a patient's disease. Here, we report a case of MAR supported by longitudinal analysis of serum autoantibody detection, visual function, ocular inflammation, vascular integrity, and response to slow-release intraocular corticosteroids. Integrating these data with the patient's oncological and ophthalmological records reveals novel insights regarding MAR pathogenesis, progression, and

treatment, which may inform new research and expand our collective understanding of the disease. In brief, we find TRPM1 autoantibodies can disrupt vision even when serum levels are barely detectable by western blot and immunohistochemistry; intraocular dexamethasone treatment alleviates MAR visual symptoms despite high levels of circulating TRPM1 autoantibodies, implicating antibody access to the retina as a key factor in MAR pathogenesis. Elevated inflammatory cytokine levels in the patient's eyes may be responsible for the observed damage to the blood-retinal barrier and subsequent entry of autoantibodies into the retina.

2.2: Introduction and Case Description

Melanoma-associated retinopathy (MAR) is a paraneoplastic syndrome affecting patients with cutaneous melanoma (CM) and is characterized by impairment of rod-mediated vision and the ON retinal pathway [1–4]. The visual symptoms of MAR include photopsia, reduced contrast sensitivity, and progressive nyctalopia, all of which are caused by autoantibodies that bind and inhibit an essential ON-bipolar cell (ON-BC) ion channel known as TRPM1 [5,6]. This inhibition prevents ON-BC depolarization during the light response, a phenomenon that can be identified as a reduction in the b-wave amplitude of the full-field electroretinogram (ffERG) [1,5,7].

Melanocytes, the pigment-producing cells of the skin that become cancerous in CM, are one of few cell types outside the eye that express TRPM1 [8–11]. In MAR patients, B cells produce antibodies against melanocyte antigens, including TRPM1 [6,12,13]. Consequently, these circulating autoantibodies disrupt vision when they infiltrate the retina and bind TRPM1 in ON-BCs [5,14]. Serum screening for TRPM1 autoantibodies and ffERG testing serve as the most reliable combination of diagnostic tools for confirming MAR. However, melanoma treatment may influence the presence of serum autoantibodies or the progression of a patient's visual symptoms over time, complicating diagnosis and prognosis [15–17]. Several studies report ffERG recordings or serum autoantibody titers from a single timepoint in a patient's disease, yet none correlate treatment data with diagnostic testing over time to assess MAR progression and resolution. Here, we describe a case of bilateral MAR in a 79-year-old male with stage IV CM. In August 2021, the patient presented with unilateral vision impairment and a relative afferent pupillary defect (RAPD), prompting further ophthalmic testing and treatment for optic neuritis (**Supplementary Table 2-1**). The patient was receiving pembrolizumab treatment without evidence of active disease

when he developed MAR visual symptoms. After observing no response to systemic corticosteroids and severe loss of inner-retinal function on ffERG without evidence of retinal degeneration on multi-modal retinal imaging (optical coherence tomography, fundus autofluorescence), the patient was suspected of having MAR. The diagnosis was supported by the patient's symptoms (nyctalopia, photopsia, blue-tinted vision, and "squiggles" in his vision) and later confirmed with a positive test for anti-ON-BC autoantibodies in the serum. Unlike previous reports, we integrated the patient's treatment history with a longitudinal evaluation of the ocular and humoral components of their disease to gain a more complete understanding of MAR pathology.

2.3: Diagnostic Assessment and Results

2.3.1 Intraocular corticosteroids restore visual function and alleviate MAR visual symptoms

The patient presented with BCVA of 20/40 in the right eye and 20/50 in the left eye. Fundus examination was unremarkable, optical coherence tomography showed normal retinal architecture (data not shown), and wide-field autofluorescence was normal (**Figure 2-1A**). However, wide-field fluorescence angiography (FA) showed a few focal areas of subtle vascular leakage in both eyes (**Figure 2-1A**). Wide-field static perimetry revealed severely constricted visual fields in both eyes (**Supplementary Figure 2-1**). The ffERG showed non-recordable dim scotopic waveforms, electronegative bright scotopic waveforms, and squared a-waves of the photopic single flash and normal 30 Hz flicker (**Figure 2-2A**). Because several studies have reported an improvement of MAR symptoms following intraocular delivery of slow-release corticosteroids [18–20], we administered intraocular slow-release dexamethasone via an intravitreal implant (0.7 mg; AbbVie, North Chicago, IL, USA) to both eyes in October 2021. By February 2022, the patient reported significant improvements to sight, including a reduction in the appearance of "squiggles and stars" in his vision in both eyes, although he felt the left eye had started regressing. Indeed, the ffERG results indicated that the right eye dim scotopic b-wave amplitude had been restored to 116% of the normal range (from 6% at baseline), the electronegative character of the bright scotopic waveform had normalized, and the squared a-wave of the photopic waveform had resolved (**Figure 2-2,** for timelines see **Supplementary Tables 2-1 and 2-2**). The FA also showed resolution of the leakage in the right eye (**Figure 2-1A**). In the left eye, the ffERGs resembled the baseline (**Figure**

2-2) and the FA showed recurrence of leakage in the superior arcade, confirming regression of the left eye (**Figure 2-1A**). Dexamethasone injections were repeated in both eyes in February of 2022. To potentially reduce the frequency of intraocular dexamethasone injections (every ~3 months), intravitreal fluocinolone acetonide implants (0.18 mg, EyePoint Pharmaceuticals; Watertown, MA USA), which have a 2–3-year efficacy period, were injected in both eyes in April 2022. Results from the ffERG in June 2022 demonstrated restoration of the dim scotopic b-wave amplitude to 136% and 156% of normal range for the right and left eyes, respectively, and resolution of the bright scotopic electronegative waveform and photopic squared a-wave in the left eye (**Figure 2-2, Supplementary Table 2-2**). Moreover, widefield static perimetry revealed significant expansion and improvement of visual sensitivity in both eyes (**Supplemental Figure 2-1**). However, these benefits regressed 2-3 months later. In August 2022, an ffERG revealed that b-wave amplitudes in the right and left eye had fallen to 1% and 2% of the normal range, respectively. Unfortunately, fluocinolone acetonide implant monotherapy was not effective and dexamethasone treatment was reinitiated with repeat injections for both eyes in August of 2022. Two months later in October of 2022, the b-wave in the left eye was restored to 122% of the normal range, while the right eye remained at 6% (**Figure 2-2, Supplementary Tables 2-1 and 2-2**). With continued routine dexamethasone implants every 16 weeks, there was a sustained effect of improved visual symptoms, visual fields, and normalization of the ffERG in both eyes. During the course of treatment, steroid-induced elevated intraocular pressures of 32 and 28 mmHg were observed in the right and left eye, respectively, which normalized with pressure-lowering eye drops (dorzolamide/timolol) twice per day. The patient also developed cataract in both eyes, but with cataract surgery and sustained intravitreal steroids, his BCVA stabilized to 20/30 in both eyes.

Figure[2-1]

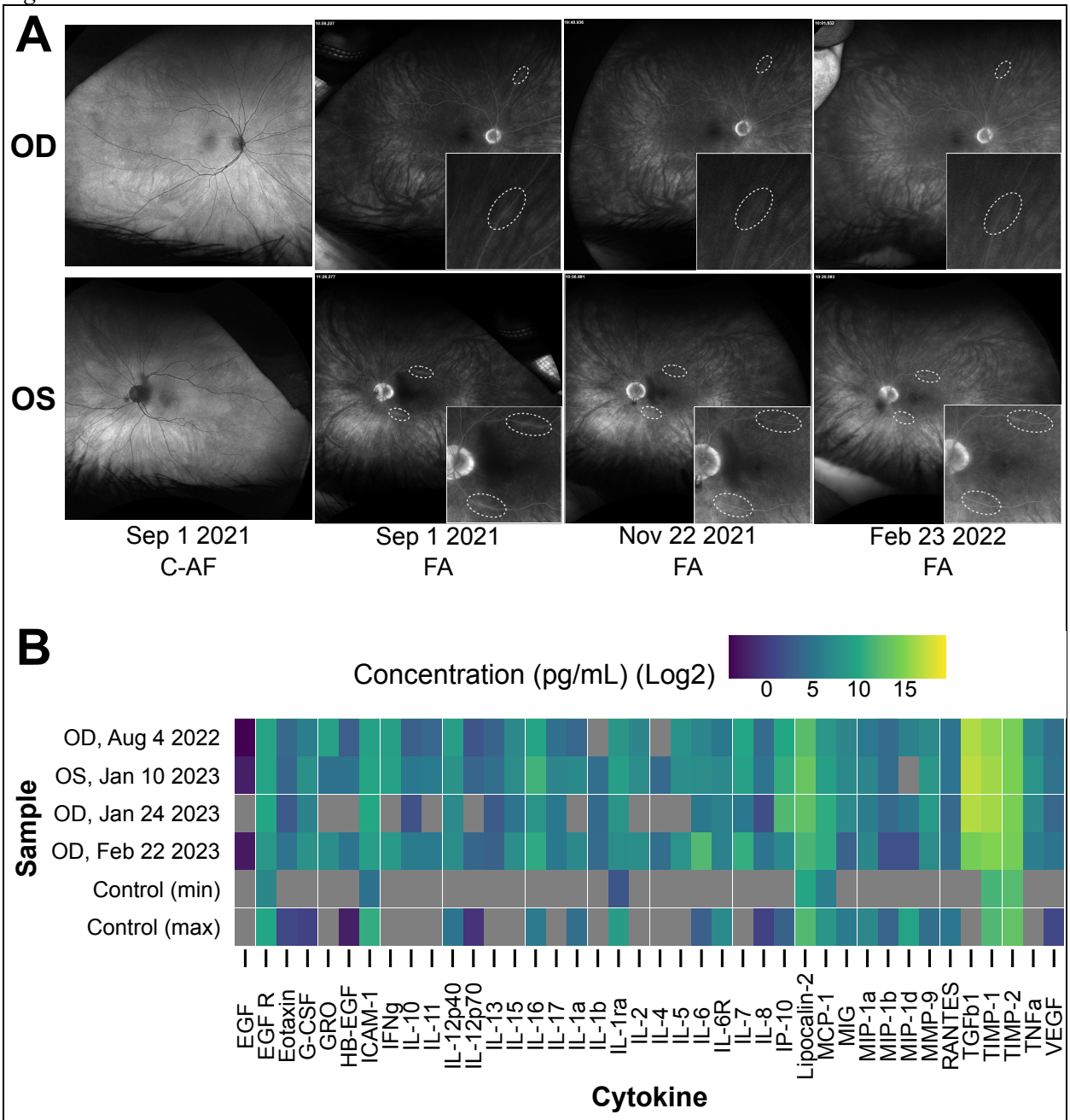

[2-1]Augmented inflammatory cytokine levels and retinal vascular leakage are detected in the MAR eye. (**A**) Baseline images of the patient's retina (first column) show no evidence of abnormalities in color or autofluorescence (C-AF). Fluorescein angiogram images (FA) on September 1, 2021 reveal subtle focal venous vascular leakage of the superior and inferior temporal arcade in the left eye, and in one of the superior arcades in the right eye. Treatment with intravitreal dexamethasone in both eyes showed rapid resolution of leakage in 1 month by November 2021. Three months later (February 2022), there was regression of leakage of the superior temporal arcade in the left eye. (**B**) A heat map displaying the results of a cytokine array that measured the concentration of forty inflammatory cytokines in patient aqueous humor samples collected at multiple points during corticosteroid

treatment. Concentrations are plotted on a log2 scale in pg/mL. Grey bars represent concentrations below the threshold of detection. The four MAR samples are shown alongside a non-MAR control cohort (n = 10) where the maximum and minimum concentration observed across the cohort are displayed for each cytokine. The detection of the following cytokines in the MAR sample but not in the control cohort suggests a heightened inflammatory state in the MAR patient eye: EGF, GRO, IFNγ, IL-10, IL-11, IL-13, IL-15, IL-17, IL-1β, IL-2, IL-4, IL-5, IL-7, TGFβ1, TNFα. OD oculus dexter; OS = oculus sinister.

2.3.2 Inflammatory cytokine levels are augmented within the aqueous humor

To cause MAR symptoms, TRPM1 autoantibodies must bind and inhibit the TRPM1 ion channel in the membrane of ON-BCs [5,6]. Yet to reach the ON-BCs, the autoantibodies must first breach the blood-retinal barrier (BRB), which, under healthy conditions, restricts the passage of macromolecules from the circulation into the retinal tissue [21,22]. Currently, it is not understood how TRPM1 autoantibodies cross the BRB to reach the retina. Several studies report that inflammation in or near the eye can negatively impact the integrity of the BRB [23–29], which may present an avenue for circulating proteins, such as autoantibodies, to access this restricted space. To assess the inflammatory status of the patient's eyes at several stages of treatment, the concentrations of forty inflammatory cytokines were examined in aqueous humor samples using a cytokine array (**Figure 2-1B**). Fifteen cytokines, which were undetectable in a non-MAR control cohort, appear elevated in the MAR patient, several of which have been implicated in regulating BRB integrity, including IL-1β, IL-17A, TNFα , and VEGF-A (**Figure 2-1B**) [23,25,27,29,30]. In accordance with the heightened inflammatory state, evidence of vascular leakage indicative of a compromised BRB was visible in the patient's fluorescein angiograms on September 1, 2021 (**Figure 2-1A**). Over two months later in November 2021, the vascular leakage appeared resolved, following the initiation of dexamethasone treatment on October 6, 2021. By February 23, 2022, leakage reappeared at one site in the left eye within the superior arcade, which correlated with regression of symptoms and abnormal ffERG in the left eye.

Figure[2-2]

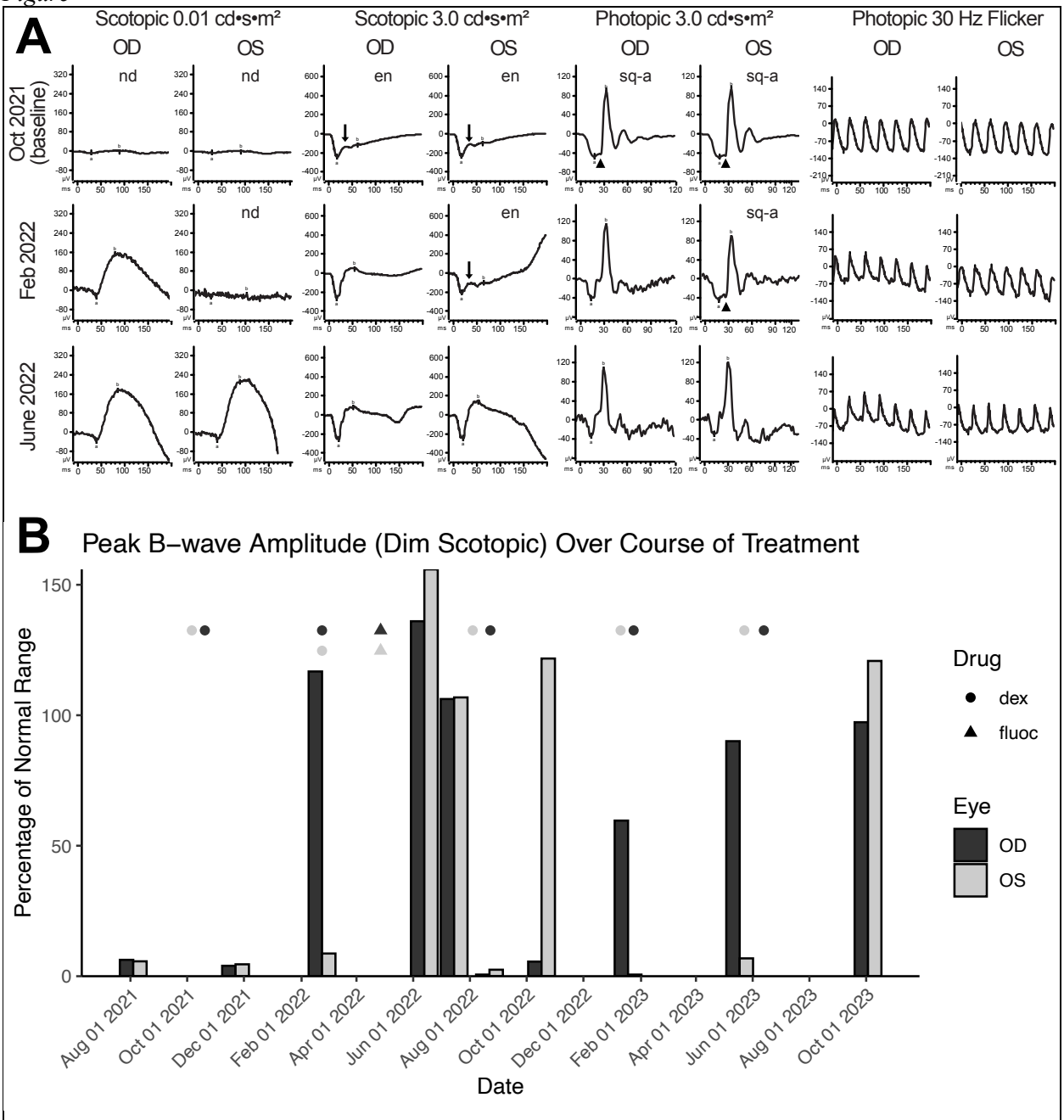

[2-2] Intraocular corticosteroids restore visual function and alleviate MAR visual symptoms. (**A**) The ffERG waveforms in response to each stimuli of the ISCEV standard are shown at baseline on October 2021, illustrating non-detectable rod-dependent response to the dim scotopic stimuli (0.01 cd•s•m^{-2}), electronegative waveform (arrow; b wave amplitude less than a wave amplitude) to the bright scotopic stimuli (3.0 cd•s•m^{-2}), squaring of the a wave (arrow head; widening of the a wave peak) response to the photopic single flash (3.0 cd•s•m^{-2}), and normal appearing 30 Hz flicker. Treatment with intravitreal dexamethasone every 16 weeks normalized the right eye by February 2022 and both eyes by June 2022. OD, oculus dexter; OS, oculus sinister; nd, not detectable; en, electronegative; sq-a, squared a-wave. (**B**) Peak b-wave amplitudes from ffERGs collected during corticosteroid

implant treatment, shown as a percentage of normal range (lower bound). Eyes were dark adapted for ≥ 20 minutes prior to exposure to a 0.01 cd•s•m^{-2} light stimulus. Points mark the dates for intraocular delivery of either dexamethasone (circles) or fluocinolone (triangles) into the left (dark grey) and right (light grey) eyes; stacked points indicate injection to both eyes on the same day. From the first round of dexamethasone delivery, it takes ~3 months to observe the benefit on ffERG b-wave recovery. At baseline, OD and OS achieve only ~6% of the normal range on average. Dex = dexamethasone; fluoc = fluocinolone; OD, oculus dexter; OS, oculus sinister.

2.3.3 TRPM1 autoantibodies persist in patient serum throughout immunotherapy and vision treatment

To detect retinal autoantibodies circulating in the patient's blood, diluted serum from three separate blood draws was applied to cryosections of mouse retina and bound antibodies were detected with a fluorescent anti-human secondary antibody. Retinal bipolar cells were labeled with all three serum draws, with much brighter labeling produced by the sera from the two later collection dates (**Figure 2-3**). This increase in signal strength may be explained by an increase in autoantibody titer, an increase in antibody affinity for retinal autoantigens, or both. When applied to retinal cryosections from TRPM1-KO mice, bipolar cell labeling with the MAR serum was dramatically reduced, indicating that anti-TRPM1 autoantibodies comprise the majority of anti-retinal autoantibodies in the patient's serum (**Figure 2-3**). Further supporting that anti-TRPM1 autoantibodies dominate the composition of retinal autoantibodies, the bipolar cell staining pattern produced by this patient's serum closely resembles that of an anti-TRPM1 mouse monoclonal antibody (**Figure 2-3**). Despite an obvious reduction in immunofluorescence intensity on retina sections from the TRPM1 KO mouse compared to the wild type, anti-retinal labeling is not entirely absent, implicating the presence of autoantibodies against additional retinal antigens in the patient's serum (**Figure 2-3**). Furthermore, the immunofluorescence on the TRPM1-KO retina sections is brighter for the later blood draws indicating an increase in titer and/or affinity of these additional anti-retinal autoantibodies over time. **Supplementary Figure 2-2** shows the ffERG recorded on the same dates as the serum draws.

Figure[2-3]

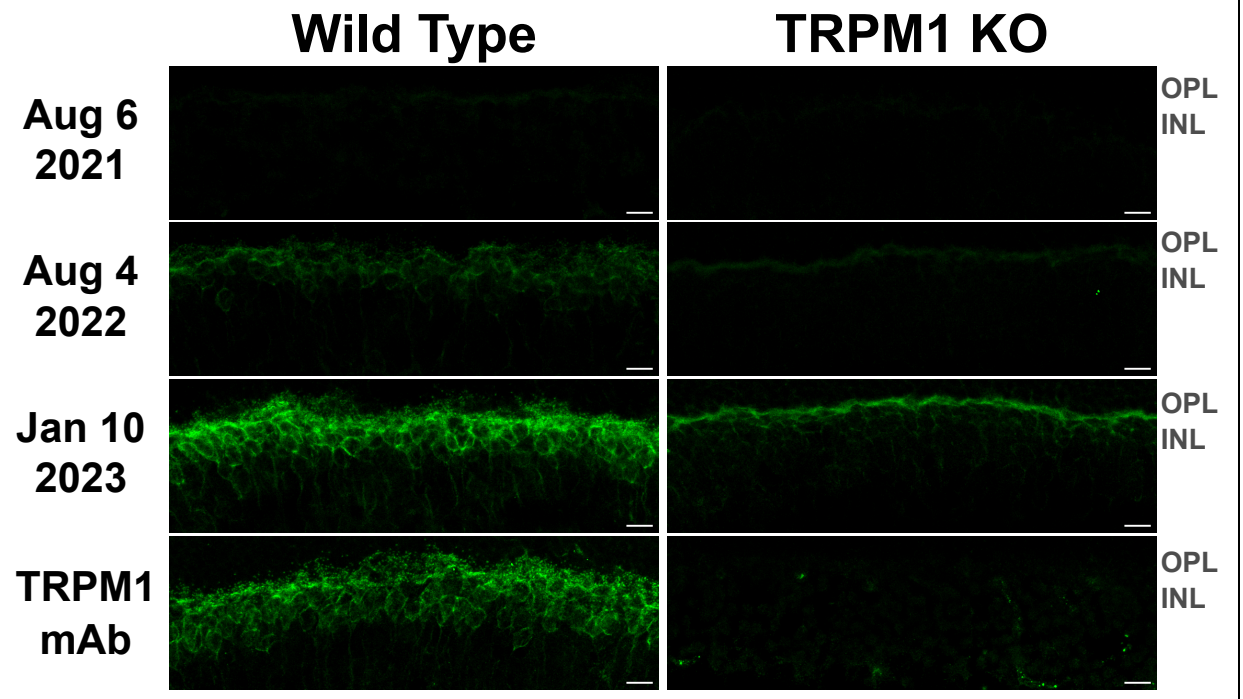

[2-3] **TRPM1 autoantibodies persist in patient serum throughout immunotherapy and vision treatment**. Retina sections from WT and TRPM1 knockout mice were incubated with patient serum (diluted 1:1000) collected on three different dates or with an anti-TRPM1 mouse monoclonal antibody (diluted 1:2000). Anti-retinal autoantibodies in the sera were then visualized by incubating the tissue with an Alexa Fluor 488-conjugated anti-human secondary antibody (green). The anti-TRPM1 monoclonal antibody was visualized using an Alexa Fluor 488-conjugated anti-mouse secondary antibody (green). In all three serum draws, autoantibodies were seen to label bipolar cells. However, the intensity of anti-bipolar cell staining was noticeably higher on sections labeled with the sera from 08/04/22 and 01/10/23. The ON-BC labeling visible in the WT retina is significantly reduced in the TRPM1 KO retina, indicating the majority of ON-BC labeling in the WT retina is caused by autoantibodies against TRPM1. Residual bipolar cell staining in the TRPM1 KO retina is likely caused by additional anti-retinal autoantibodies against other antigens. The similarity in the staining pattern between the anti-TRPM1 monoclonal antibody and the MAR serum on the WT retina is further evidence that the retinal autoantibodies in the MAR patient serum primarily target TRPM1. Scale bars = 10μ; ONL = outer nuclear layer; OPL = outer plexiform layer; INL = inner nuclear layer.

2.3.4 Patient autoantibodies target a region of TRPM1 encoded by exons 8-10

In characterizing previous MAR patient sera, we mapped the immunoreactive epitope targeted by TRPM1 autoantibodies to a region in the N-terminal, cytoplasmic domain of TRPM1, amino acids 337-380 (encoded by exons 8-10) (**Supplementary Figure 2-3**) [31]. Using a slot immunoblot assay in which patient serum is reacted with purified TRPM1 polypeptides, we found that autoantibodies

in the serum of the current patient also bind to this region of TRPM1. Sera from both the current patient and a previous MAR patient gave nearly identical results on the slot immunoblot, reacting with a TRPM1 polypeptide encoded by exons 6-10, but not with a polypeptide encoded by exons 2-7 (**Figure 2-4A**). In agreement with the retinal immunofluorescence results, sera from August 4, 2022 and January 10, 2023 reacted more strongly with the purified TRPM1 polypeptide than the serum from August 6, 2021 (**Figure 2-4B**). Despite the comparatively low titer/affinity of anti-TRPM1 autoantibodies in the August 6, 2021 serum, the patient began reporting vision changes as early as April 2021. Consistent with the slot immunoblot results, the patient's serum labels TRPM1 exons 6-10 but not TRPM1 exons 2-7 when both polypeptides are heterologously expressed by HEK293T cells (**Supplementary Figure 2-4**).

Figure[2-4]

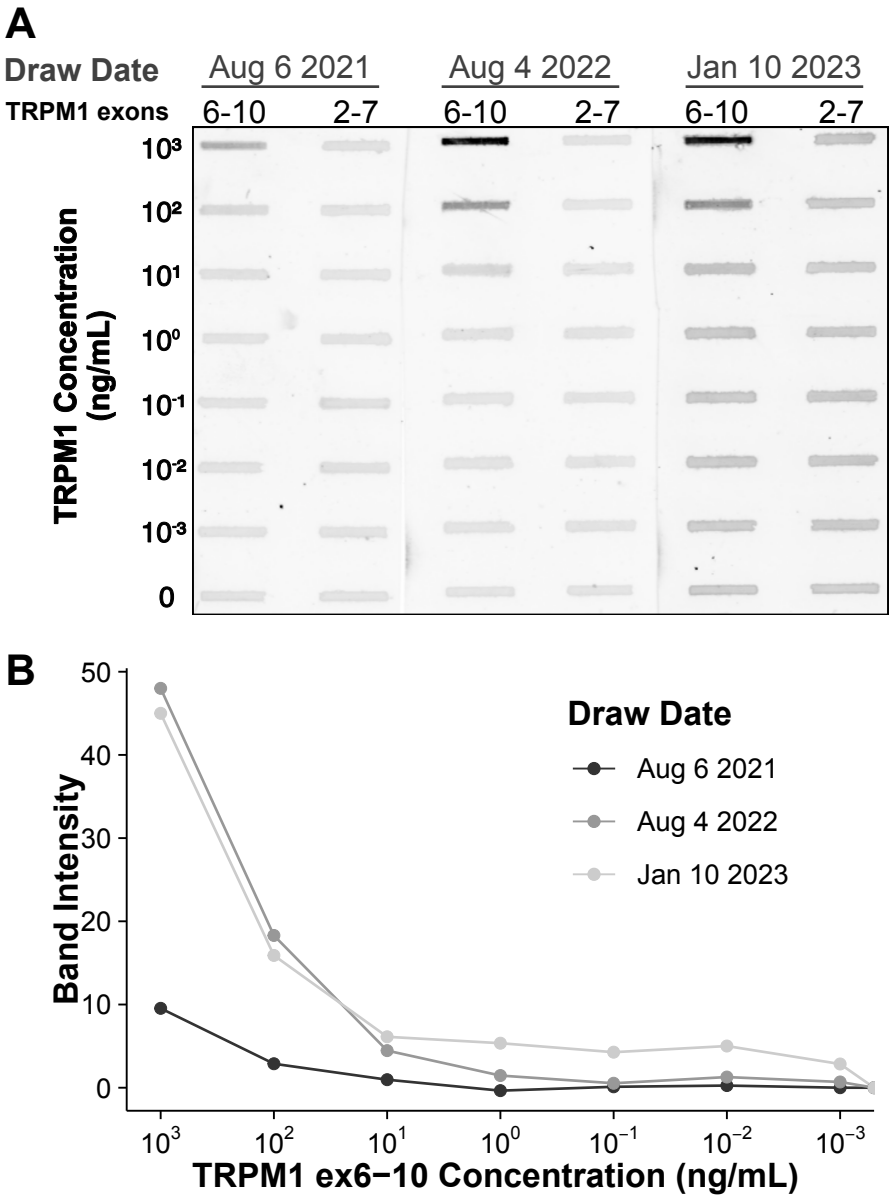

[2-4] **Patient autoantibodies target a region of TRPM1 encoded by exons 8-10**. (**A**) Decreasing concentrations of two recombinant TRPM1 polypeptides were applied to a PVDF membrane in triplicate. The two polypeptides, encoded by exons 6-10 and exons 2-7 of TRPM1, respectively, share two exons of sequence overlap. Diluted patient sera from three different collection dates were then applied to the PVDF, and reactivity with the recombinant polypeptides was visualized with an anti-human secondary antibody conjugated to a near-infrared fluorophore. The signal intensities of the slot immunoblot bands are quantified in **B**. Autoantibodies in the patient sera exclusively react with the TRPM1 polypeptide encoded by exons 6-10. Sera collected on August 4, 2022 and January 10, 2023 yield more intense staining, either due to higher autoantibody concentration, higher autoantibody affinity, or both.

2.4: Discussion

Melanoma-associated retinopathy is a rare paraneoplastic syndrome that affects individuals with cutaneous melanoma, causing visual impairment due to a humoral immune response against ON-BC neurons in the retina. A definitive MAR diagnosis requires assessment of visual dysfunction and autoimmune activity. The bright scotopic ffERG b-wave amplitude provides a useful assessment of ON-BC function and serves as a proxy for the degree of visual impairment. To complement the ffERG, immunofluorescent detection of anti-TRPM1 autoantibodies in the serum indicates the presence and intensity of the immune response against ON-BCs. Together, these tests can be used to monitor disease progression and response to ocular or systemic treatment, such as intraocular corticosteroids or cancer immunotherapy. Here we present the first longitudinal case report of a MAR patient that integrates ffERG recordings, serum autoantibody measurements, aqueous humor cytokine profiling, and the patient's treatment record. The synthesis and integration of these data shed new light on poorly understood aspects of MAR pathogenesis which may prove useful to the greater community of autoimmune retinopathy researchers and clinicians.

First, although the patient developed symptoms in April 2021 (**Supplementary Table 2-1**), we note that ON-BC autoantibodies were barely detectable by immunohistochemistry or immunoblot in the first serum draw from August 6, 2021 (**Figure 2-3, Figure 2-4A**). Consistent with the patient's symptoms, the ffERG recorded on August 4, 2021 revealed an undetectable dim scotopic waveform and electronegative bright scotopic waveform in both eyes, indicating severe bipolar cell dysfunction (see **Supplementary Figure 2-2**). Together, these findings indicate that even low levels of circulating ON-BC autoantibodies can profoundly impact vision. Next, between August 6, 2021 and August 4, 2022, there was a substantial increase in detectable TRPM1 autoantibodies in the patient's serum (**Figure 2-3, Figure 2-4**), which preceded a melanoma relapse (leptomeningeal disease) in September 2022. This spike in retinal autoantibodies occurred in the absence of cancer immunotherapy, though other reports suggest immunotherapy potentiates autoimmune retinopathy [17,32,33]. Our patient underwent ~17 months of nivolumab and pembrolizumab therapy before reporting visual symptoms (**Supplementary Table 2-1**), whereas other studies report the onset of visual dysfunction after 3-6 weeks of immunotherapy. Therefore, any direct effect of the immunotherapy on visual function appears unlikely in this case. However, in one previous study, a patient who developed MAR visual symptoms after 18 months of

pembrolizumab reported greatly improved vision 5 days after stopping treatment. Our patient reported no such improvement to vision after stopping pembrolizumab in August 2021; however, visual function improved after dexamethasone treatment two months later. One possible explanation for the autoantibody surge is that the melanoma relapse reinvigorated the immune response against the cancer, leading to increased production of autoantibodies. A progressive increase in the immunofluorescent labeling intensity on the TRPM1 KO retina sections across serum draws demonstrates the development of additional anti-retinal autoantibodies, consistent with a reinvigorated immune response (**Figure 2-3**). Increased autoantibody levels in the serum may therefore serve as useful predictors for the progression of cancer prior to PET or CT imaging but are not necessarily linked to cancer immunotherapy.

In agreement with previous case reports on MAR, our patient responded positively to intraocular dexamethasone implants, which restored the normal ffERG and correlated with significant improvement in visual fields (**Figure 2-2, Supplementary Figure 2-1**) [18–20]. While ffERG b-wave amplitudes appeared maximally restored during June through August 2022 (**Figure 2-2**), high levels of TRPM1 autoantibodies remained detectable in the patient's serum during this same period (**Figure 2-3, Figure 2-4**), confirming that circulating TRPM1 autoantibodies alone are not sufficient to cause visual impairment [34]. Instead, these data suggest additional pathological factors may be required for autoantibodies to inhibit retinal function. Given that the blood-retinal barrier (BRB) typically prevents antibodies and other macromolecules from accessing the retina, anti-retinal autoantibodies could circulate through the blood yet be restricted from ON-BCs, in which case no visual impairment would occur [26,34]. This concept is supported by a previous study demonstrating the presence of TRPM1 autoantibodies in patients without self-reported visual symptoms [34]. Anti-retinal autoantibodies must first circumvent this barrier before reaching the retina, suggesting that BRB damage or malfunction may be a prerequisite for the development of MAR symptoms.

As inflammation is a known modulator of BRB integrity [23,25,28–30], we sought to examine the inflammatory state of the eye to assess the potential for BRB damage in this MAR patient. Our cytokine array detected a heightened inflammatory state in the patient's aqueous humor on all three collection dates when compared to a non-MAR control cohort (**Figure 2-1B**). Furthermore, several

cytokines linked to BRB or blood-brain barrier (BBB) damage appeared elevated in this patient and their persistence could potentially have reduced the integrity of the BRB and enabled autoantibody access to the retina [26]. Coinciding with the heightened risk of BRB damage caused by inflammation, fluorescein angiograms taken on September 1, 2021 revealed multiple sites of vascular leakage to indicate the loss of BRB integrity (**Supplementary Figure 2-2**). In response to treatment with intraocular dexamethasone, these leakage sites resolved and the patient's vision improved, supporting the hypothesis that inflammation damages the BRB, allowing for the passage of autoantibodies and the onset of MAR symptoms. The reappearance of vascular leakage on fluorescein angiograms February 23, 2022 may reflect the wanning efficacy of the previous dexamethasone implants (left: October 6, 2022, right: October 20, 2022) and the delayed effect of the recently injected implants (left: February 23, 2022, right: February 23, 2022).

The success of intravitreal dexamethasone treatment in restoring the patient's retinal function, visual fields, and visual acuity is consistent with the notion that inflammation regulates BRB integrity. Intraocular dexamethasone reduces inflammation in the eye, which could allow for the restoration of BRB integrity and the exclusion of autoantibodies from the retina, leading to symptom resolution as seen in our patient. Studies that directly evaluate the effects of inflammation on BRB permeability to antibodies are needed to give credence to this hypothesis. Clinicians and researchers should consider collecting these data to compare results in patients with MAR and other autoimmune retinopathies. In doing so, we approach a deeper understanding of the transition from cancer to autoimmunity, the influence of immunotherapy on MAR progression, and the role of the BRB in autoimmune retinopathy.

2.5: Materials & Methods

This study was performed in accordance with the Declaration of Helsinki and protection of the patient's identity. The patient was provided with written informed consent for the use of personal medical data for scientific purposes and publication. IRB00009765.

MAR sample tissue collection

Aqueous humor samples were taken from the front of the patient's eye and were promptly frozen at -80º until use. Whole blood samples were collected in tubes coated with a clotting factor and allowed to clot overnight at 4 ºC. The following day, serum was collected from the surface of the

clot and centrifuged at 1,500 x g for 10 minutes. The supernatant was then transferred to a new tube and aliquots kept at 4 ºC for short term use and at -80 ºC for long term storage.

Slot immunoblotting

Sequences from the TRPM1 N-terminal cytoplasmic domain were cloned from M14 melanoma cells, expressed in *E. coli,* and purified to produce two polypeptides with partially overlapping sequences (**Supplementary Table 2-1**). All references to amino acid and exon positions are given relative to NCBI reference sequence NM_001252020.2. The polypeptides were diluted into phosphate buffered saline (PBS) with 0.5% horse serum and 0.05% NaN_3, then applied to a polyvinylidene difluoride (PVDF) membrane using a Bio-Rad Bio-Dot apparatus. The membrane was blocked in Tris-buffered saline with 0.2% Tween-20 (TBST) and 0.5% horse serum for 1 hr at room temperature, then probed with human MAR serum diluted 1:2000 in the same blocking buffer for 1 hr at room temperature. After three, five-minute washes in TBST, the membrane was incubated with an anti-human IRDye 800CW secondary antibody (1:10K). The membrane was washed thrice more, and results were visualized on a Licor Odyssey infrared imaging system (LI-COR; Lincoln, NE, USA).

Tissue preparation for immunofluorescence

The cornea and lens were removed from freshly dissected mouse eyes and the remaining eyecups (retina and sclera) were immediately fixed by immersion in ice-cold 4% paraformaldehyde for 30 min. Following fixation, the eyecups were washed in ice-cold PBS, then cryoprotected by successive incubation in 10%, 20%, and 30% sucrose for 1 hr each at 4 ºC. Cryoprotected eyecups were embedded in optimum cutting temperature (OCT) medium (Sakura Finetek; Tokyo, Japan) and stored at -80 ºC until sectioning, at which point 20 µm transverse sections were cut using a cryostat. Retinal sections were mounted on Superfrost slides (Thermo Fisher Scientific; Waltham MA, USA), air dried, and stored at -20 ºC or -80 ºC until use.

Retina section immunostaining

Frozen cryosections were thawed, then incubated in antibody incubation solution (AIS; 3% horse serum, 0.5% Triton X-100, 0.025% NaN3 in PBS) for 30 min at room temperature to hydrate, permeabilize, and block the tissue. Sections were then incubated with MAR serum or a mouse TRPM1 antibody (Agosto et al., 2014) diluted in AIS for 1 hr at room temperature. After 3 washes in room temperature PBS, the sections were incubated for 1 hr with secondary antibodies

conjugated to Alexa Fluor 488 (1:1000) and washed three more times. Finally, mounting medium was applied to the samples, followed by coverslips, and the results were visualized by confocal microscopy.

Confocal imaging

Confocal micrographs were taken with a Leica TCS SP8 X confocal microscope (Leica; Wetzlar, Germany) using Leica HC PL APO CS2 40X/1.3 and HC PL APO CS2 63X/1.40 oil immersion objectives (Leica; Cat# 506358, Cat# 15506350). FIJI was used to adjust brightness and contrast and generate Z-projections from image stacks.

Cell culture, transfection, and immunocytochemistry

HEK293T cells (RRID: CVCL_0063) cultured in DMEM with 10% fetal bovine serum were seeded onto polylysine-coated coverslips contained in 24-well tissue culture plates. Using Effectene (Qiagen, Valencia, CA, USA), cells were transfected with pEGFP-C3 plasmids encoding TRPM1 isoforms with EGFP fused to their N-termini. The following day, the cells were fixed for 5 minutes in 4% paraformaldehyde at room temperature, then permeabilized and blocked with AIS for 30 minutes at room temperature. The cells were then incubated with diluted patient serum for 1 hour at room temperature, washed 3 times in PBS, and incubated with an Alexa Fluor 594-conjugated anti-human secondary antibody for 1 hour at room temperature. After 3 additional PBS washes, the coverslips were mounted onto Superfrost slides and imaged.

Visual diagnostics

At regular intervals, the patient underwent ophthalmic examination and testing, which included best-corrected visual acuity, spectral-domain optical coherence tomography (Heidelberg, Franklin, MA, USA), wide-field fundus photography, wide-field fundus autofluorescence (AF), wide-field fluorescein angiography (FA; Optos, Marlborough, MA, USA), wide-field static perimetry (Octopus 900, Haag-Streit, Switzerland), and full-field electroretinography (Diagnosys LLC, Lowell, MA, USA) in accordance with the International Society for Clinical Electrophysiology of Vision [35]. Data were collected with either Burien Allen (BA) or Espion DTL electrodes; data collected on BA electrodes were multiplied by the median ratio of the peak b-wave amplitudes (BA/DTL) measured in a control cohort (n=9) to transform them for comparison with data collected on DTL electrodes. From dark adapted ffERGs with a 0.01 $cd \bullet s \bullet m^{-2}$ stimulus intensity,

peak b-wave amplitudes were divided by the 2.5th percentile (161 μV) of the empirically determined normal range to yield "percentage of normal range."

Cytokine array preparation and quantification

MAR serum and aqueous humor samples were diluted 2X in incubation buffer, then applied to a commercial slide array (Ray Biotech; Cat# QAH-DED-1-1; Corners, GA, USA). The array was prepared and incubated with MAR samples and cytokine standards according to the manufacturer's protocol. Upon completion of the protocol, the array was shipped to Ray Biotech for quantification. Raw data was processed and analyzed using Ray Biotech's QAH-DED-1 Array Analysis Tool.

2.6: Acknowledgements

We thank Drs. Aimee Kohn and Phoebe Lin for providing patient care and acquiring the aqueous humor samples. We also thank Tammie Haley and Gaoying Ren for their technical support in preparing retina sections.

2.7: Supplemental Information

Supplementary Table 2-1 – Patient examination and treatment history

Date	Diagnosis, Treatment, or Exam	Clinical Notes
February 22, 2019	Detection of metastatic melanoma	FNA + metastatic melanoma. PET shows left groin mass, 2 enlarged L inguinal nodes, 0.7cm LUL nodule
April 2019	Dabrafenib and Trametinib	Neoadjuvant therapy; BRAF V600E inhibitors
July 2019	Resection to NED	Primary found on lower back. WLE of primary and resection of metastatic lymph nodes
October 16, 2019	Brain MRI; PET scan	Brain MRI shows 2 cerebellar legions. PET shows 2 new left pulmonary nodes and right inguinal LN
October 11, 2019	SRS and Nivolumab (PD-1 inhibitor)	Stopped Dabrafenib and Trametinib targeted therapies and transitioned to Nivolumab with stereotactic radiosurgery (SRS).
December 2019	Skin biopsy	Left groin biopsy showed metastatic melanoma

January 14, 2020	Pembrolizumab + PV-10 injections	PV-10 = 10% Rose Bengal, selectively destroys tumor cells. Pembrolizumab = PD-1 inhibitor
July 2, 2020	Pembrolizumab + PV-10 injection	Regressed cutaneous metastases, stopped PV-10, continued pembrolizumab
April 2021	First report of visual symptoms	Symptoms include photopsia, nyctalopia, blue vision, and squiggly lines in the visual field.
May 13, 2021	Immunotherapy on hold	Concerns of optical neuritis or possible vision change as result of immunotherapy
June 8, 2021	Prednisone 1 mg/kg	Treatment for optic neuritis. Completed taper 2 weeks later on 6/22/21. Reported no impact on vision
June 24, 2021	Resumed Pembrolizumab	
August 4, 2021	MAR diagnosis ffERG	Baseline ffERG with electronegative dim scotopic b-wave; suspected MAR.
August 5, 2021	Discontinued Pembrolizumab	Persistently worsening vision, concerns that immunotherapy is potentiating MAR
August 6, 2021	Serum draw	Retinal autoantibodies are extremely faint but detectable.
October 2021	Syncopal Event	Thought to be due to myocarditis. Transitioned to surveillance. Followed by extensive cardiac workup: Ziopatch, CTA coronay, cardiac MRI reveal non-obstructive CAD but no evidence of myocarditis. Cleared to resume immunotherapy.
October 6, 2021	Ozurdex (Dexamethasone), OS	Lasts ~3 months
October 20, 2021	Ozurdex (Dexamethasone), OD	Lasts ~3 months
November 22, 2021	ffERG	
February 23, 2022	Ozurdex (Dexamethasone), OU ffERG	Lasts 2-3 months. Compared to the 11/21 Espion DTL baseline, OD demonstrates notable improvements in amplitudes of rod-driven response and no longer demonstrates electronegative pattern. OS rod driven responses remain unchanged/similar to prior, including non-detectable responses to dim flash and an electronegative pattern to bright

		flash. Photopic con-driven responses were stable versus mild fluctuations OU compared to 11/21.
March 1, 2022	Checkup	ffERG on 2/23/22 reveals significant improvement OD. Patient reports significant improvement to vision in both eyes after about 3 months post-Ozurdex, with a reduction in "squiggles and stars" in the left eye and restoration of night vision
April 27, 2022	Yutiq (Fluocinolone acetonide), OU	Lasts 3 years
June 13, 2022	ffERG	Compared to 02/23/22, OD stable and OS has improved significantly.
July 15, 2022	ffERG	Compared to 06/21/22, there was diffuse mild worsening of responses OU, but still better than 02/23/22.
August 4, 2022	Ozurdex (Dexamethasone), OS Serum draw	Indication: states his OS is "going back the way it was." Retinal autoantibodies are easily detectable.
August 22, 2022	Detection of steroid-induced cataracts OU. Begins Cosopt BID OU ffERG	Cosopt = carbonic anhydrase inhibitor with a beta-adrenergic receptor blocking agent intended to reduce intraocular pressure. BID = "twice daily". Compared with 07/15/22, rod responses were flat with reversion to electronegative scotopic waveforms and squaring of photopic a waves OU.
August 23, 2022	Ozurdex (Dexamethasone), OD	Indication: return of symptoms
September 1, 2022	MRI brain and spine	Enlargement of inferior right cerebellar mass (3mm to 10mm). Small adjacent mass 4mm. Previously demonstrated enhancing masses in the superior cerebellum not seen. Leptomeningeal disease in lumbar spine and thoracic spine. Lumbar mass = 4cm, thoracic mass = 10mm, causing severe narrowing of spinal canal
September 4, 2022	T6-T7 thoracic laminectomy with resection of intradural extramedullary mass	confirmed metastatic melanoma

October 3, 2022	Complete radiation to T4-T7, L2-L5, and right sided cerebral metastases	
October 7, 2022	CT PET	FDG avid left iliac nodal involvement and osseous involvement of the left scapula and left interior first rib. Low level FDG uptake within left level 1B cervical lymph node, likely reactive. FDG = radiotracer
October 10, 2022	Ipilimumab 3 mg/kg + nivolumab 1 mg/kg	administered every 21 days x 4 cycles
October 17, 2022	ffERG	OS responses have normalized but OD remains abnormal.
December 19, 2022	MRI thoracic and lumbar spine	Nodular enhancement dorsal to L4, less prominent than in 09/01/22. L2-L3 focal moderately severe spinal canal stenosis
December 26, 2022	Brain MRI	2 small cerebral metastases that appear unchanged since 09/01/22.
December 30, 2022	CT PET	Multiple pleural and peripheral nodules and masses that are hypermetabolic
January 10, 2023	Ozurdex (Dexamethasone), OS Serum draw	Lasts ~3 months Retinal autoantibodies are prominent
January 18, 2023	ffERG	Improved responses OD, but worsening OS.
January 24, 2023	Ozurdex (Dexamethasone), OD	Lasts 2-3 months
February 27, 2023	Chest CT	Improvement in pulmonary consolidation
April 17, 2023	MRI Brain; Thoracic/lumbar spine MRI	Increasing size of 2 enhancing right cerebellar metastases. No new lesions in brain or thoracic/lumbar
April, 2023	Cataract extraction and intraocular lens implant	First impacted eye
May 18, 2023	ffERG	Improved responses OD, but no improvements OS.
May 22, 2023	Nivolumab	480 mg every 28 days
May 23, 2023	Ozurdex (Dexamethasone), OS	Lasts ~3 months
May 24, 2023	Cataract extraction and intraocular lens implant	Second impacted eye

June 13, 2023	Ozurdex, OD	Lasts ~3 months
October 3, 2023	ffERG	Huge improvement to OS. OD improved as well

Supplementary Table 2-2 – Plotted peak electroretinogram b-wave amplitudes and percentage of normal range values for Figure 2.

Date	Eye	Amplitude (µV)	Percent Normal
August 4, 2021	R	10.098	6.27204969
August 4, 2021	L	9.18	5.70186335
November 22 2021	R	6.426	3.99130435
November 22 2021	L	7.344	4.56149068
February 23, 2022	R	188	116.770186
February 23, 2022	L	14	8.69565217
June 13, 2022	R	219	136.024845
June 13, 2022	L	251	155.900621
July 15, 2022	R	171	106.21118
July 15, 2022	L	172	106.832298
August 22, 2022	R	1	0.62111801
August 22, 2022	L	4	2.48447205
October 17, 2022	R	9	5.59006211
October 17, 2022	L	196	121.73913
January 18, 2023	R	96	59.6273292
January 18, 2023	L	1	0.62111801
May 18, 2023	R	145	90.0621118
May 18, 2023	L	11	6.83229814
October 3, 2023	R	156.7	97.3291925
October 3, 2023	L	194.5	120.807453

Supplementary Table 2-3 – Amino acid sequences of the two human TRPM1 recombinant proteins cloned from M14 cells (Figure 3) and the previously mapped MAR epitope. All references to amino acid and exon positions are given relative to NCBI reference sequence NM_001252020.2

Sequence Name	Amino Acid Sequence
TRPM1ex2-7	MGSSHHHHHHSSGLVPRGSHMARNMKDSNRCCCGQFTNQHIPPLPSATPSKNE EESKQVETQPEKWSVAKHTQSYPTDSYGVLEFQGGGYSNKAMYIRVSYDTKPD SLLHLMVKDWQLELPKLLISVHGGLQNFEMQPKLKQVFGKGLIKAAMTTGAWI FTGGVSTGVISHVGDALKDHSSKSRGRVCAIGIAPWGIVENKEDLVGKDVTRVY QTMSNPLSKLSVLNNSHTHFILADNGTLGKYGAEVKLRRLLEKHISLQKINTRLG QGVPLVGLVVEGGPNVVSIVLEYLQEEPPIPVVICDGSGRASDILSFAHKYCEEG G
TRPM1ex6-10	MGSSHHHHHHSSGLVPRGSHMARNVTRVYQTMSNPLSKLSVLNNSHTHFILAD NGTLGKYGAEVKLRRLLEKHISLQKINTRLGQGVPLVGLVVEGGPNVVSIVLEY LQEEPPIPVVICDGSGRASDILSFAHKYCEEGGIINESLREQLLVTIQKTFNYNKA QSHQLFAIIMECMKKKELVTVFRMGSEGQQDIEMAILTALLKGTNVSAPDQLSL ALAWNRVDIARSQIFVFGPH
MAR epitope	EGGIINESLREQLLVTIQKTFNYNKAQSHQLFAIIMECMKKKEL

Supplementary Figure [2-S1]

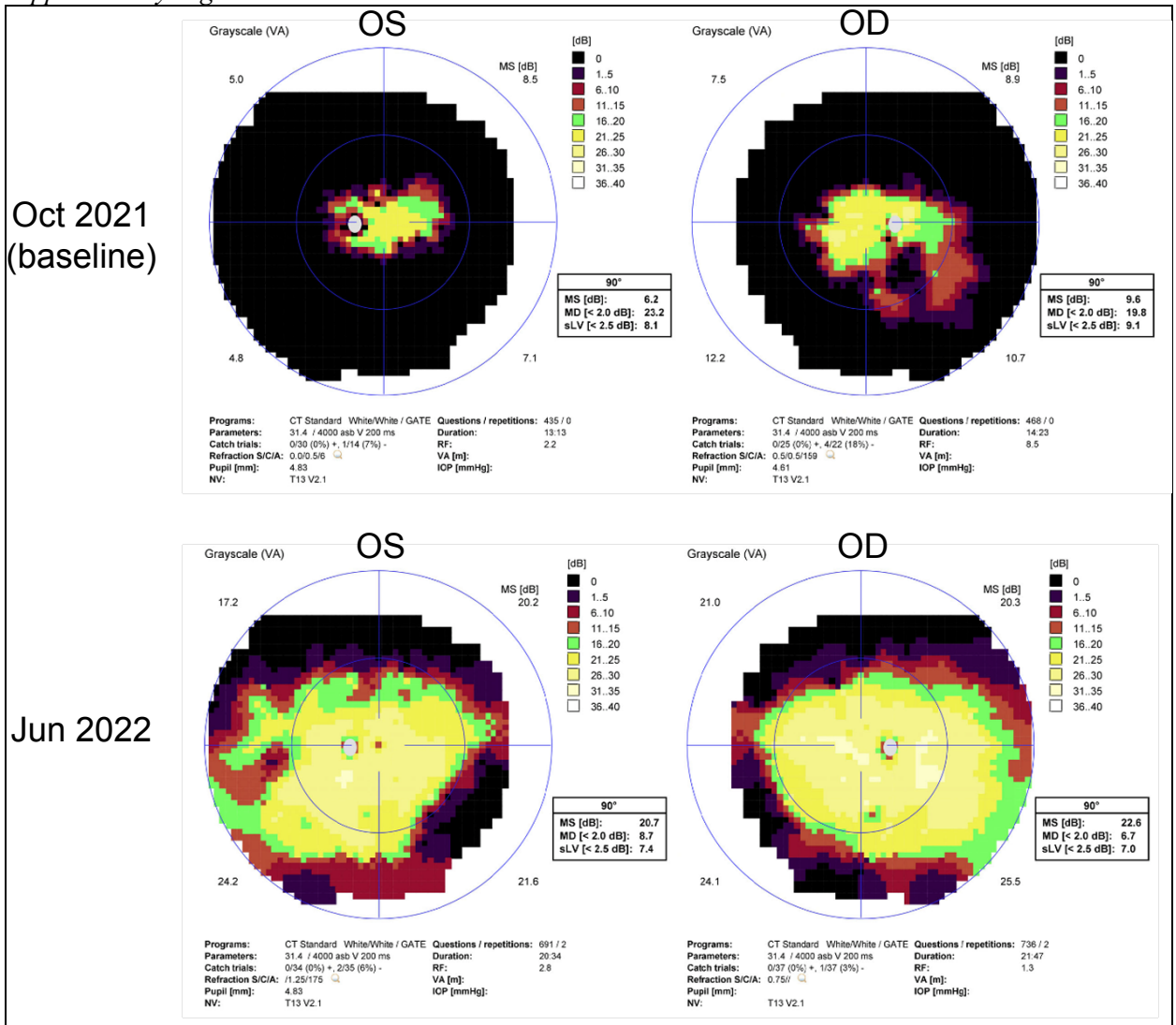

[2-S1] **Effect of intravitreal corticosteroids on static perimetry.** The full field static perimetry results are shown at baseline in October of 2021, illustrating severely constricted field of sensitivity down to a central field of <45 degrees diameter in both eyes. Treatment with intravitreal dexamethasone every 16 weeks significantly improves the sensitivity of the central field and expands the fields to >90 degrees diameter in both eyes by June of 2022. OD, oculus dexter; OS, oculus sinister.

Supplementary Figure [2-S2]

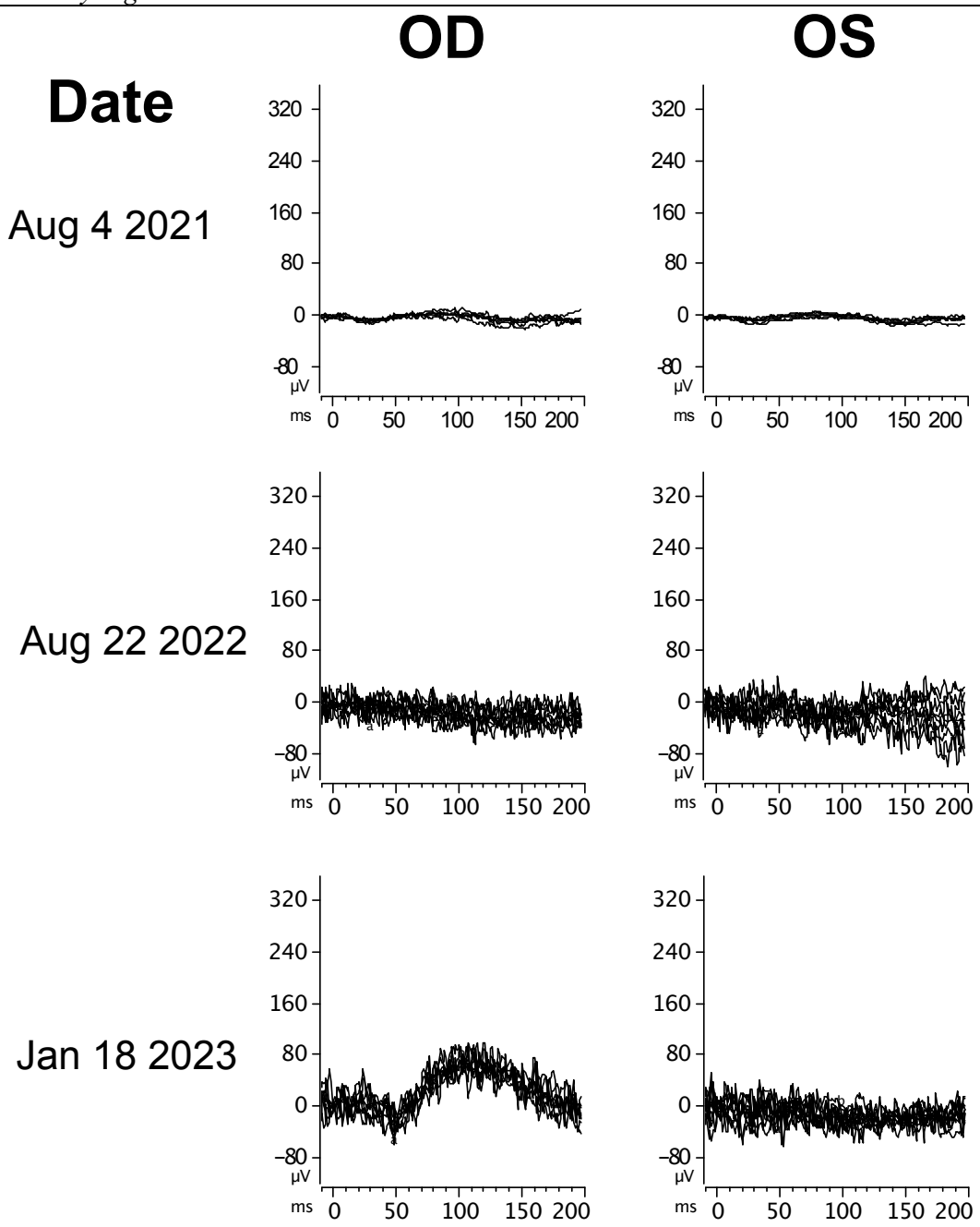

[2-S2] Dark adapted ffERG recordings taken on the same dates as the serum draws. Examples of raw traces from dark adapted ffERG recordings in the left and right eye used to calculate the peak b-wave amplitudes shown in **Figure 2-1**. The recordings shown here correspond to the dates of the serum draws shown in **Figures 2-2** and **2-3**. Multiple recordings are overlayed in each panel.

Supplementary Figure [2-S3]

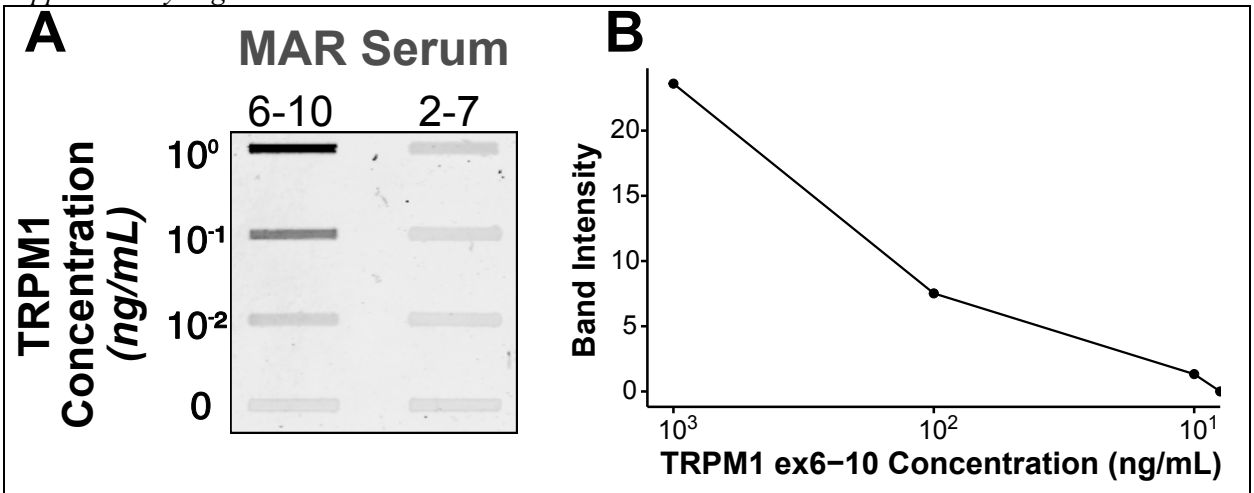

[2-S3] **Serum autoantibodies from the current patient target the same TRPM1 epitope as those from a previous MAR patient**. A slot immunoblot in which serial dilutions of two recombinant TRPM1 polypeptides were applied to a PVDF membrane and reacted with diluted serum from a previous MAR patient. The two polypeptides, encoded by exons 6-10 and exons 2-7 of TRPM1, respectively, share two exons of sequence overlap. Serum autoantibody reactivity with the recombinant polypeptides was visualized with an anti-human secondary antibody conjugated to a near-infrared fluorophore. The signal intensities of the slot immunoblot bands are quantified in **B**.

Supplementary Figure [2-S4]

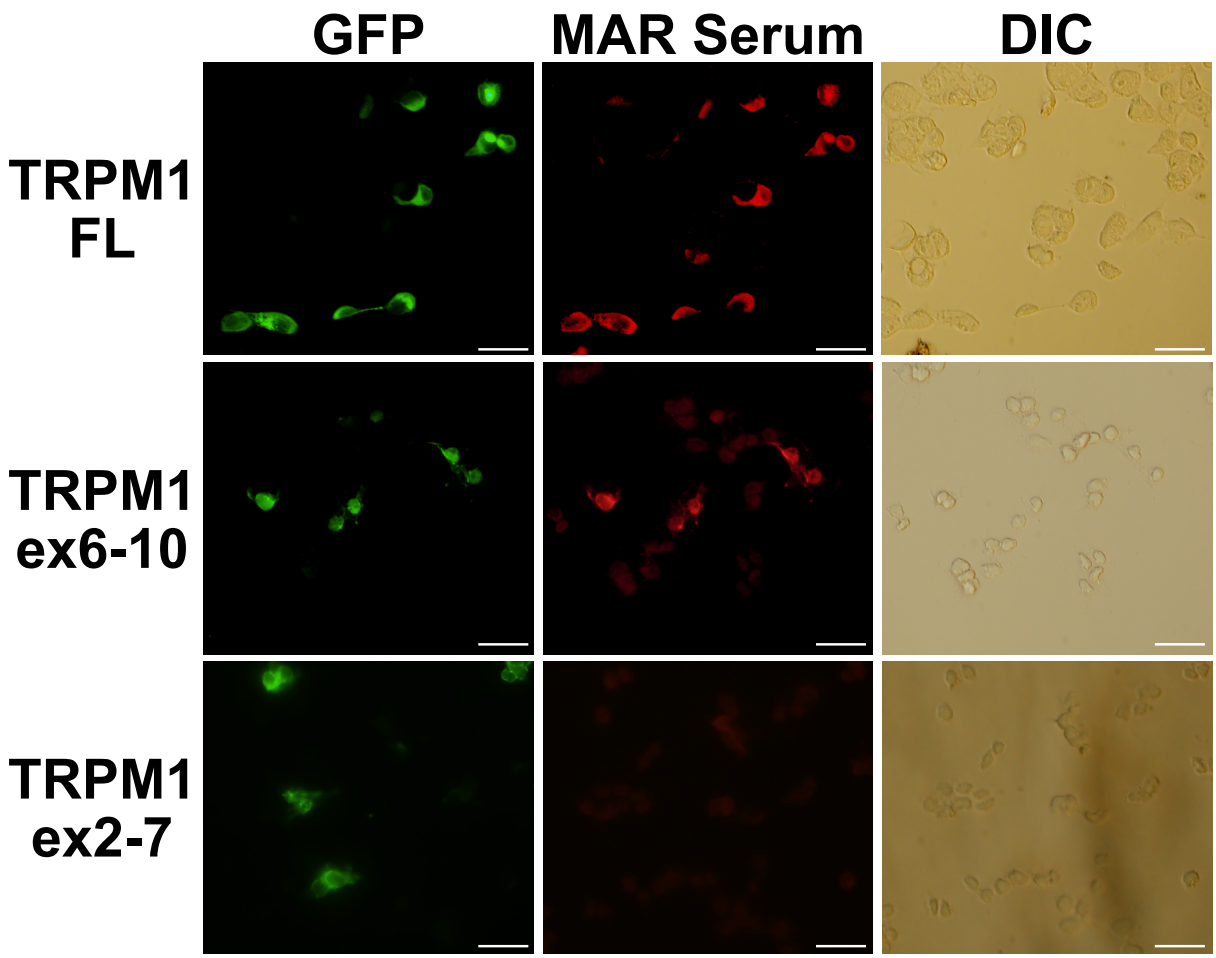

[2-S4] **Serum autoantibodies bind recombinant TRPM1 expressed in HEK293T cells**. HEK293 T cells were transfected with one of three GFP-tagged human TRPM1 isoforms encoding the full-length channel (TRPM1 FL), the region encoded by exons 6-10 (TRPM1 ex6-10), or the region encoded by exons 2-7 (TRPM1 ex2-7). Cells were fixed, then incubated with MAR patient serum and TRPM1-reactive autoantibodies were identified using an Alexa Fluor 594-conjugated anti-human secondary antibody. Patient autoantibodies react with the full length TRPM1 and ex6-10 isoforms, but not the ex2-7 isoform, consistent with the slot immunoblot and retina IHC results.

Chapter 2 Bibliography

1. Milam, A. H. *et al.* Autoantibodies against retinal bipolar cells in cutaneous melanoma-associated retinopathy. *Invest. Ophthalmol. Vis. Sci.* **34**, 91–100 (1993).

2. Keltner, J. L., Thirkill, C. E. & Yip, P. T. Clinical and Immunologic Characteristics of Melanoma-Associated Retinopathy Syndrome: Eleven New Cases and a Review of 51 Previously Published Cases: *Journal of Neuro-Ophthalmology* **21**, 173–187 (2001).

3. Lu, Y. Melanoma-Associated Retinopathy: A Paraneoplastic Autoimmune Complication. *Arch Ophthalmol* **127**, 1572 (2009).

4. Elsheikh, S., Gurney, S. P. & Burdon, M. A. Melanoma-associated retinopathy. *Clin Exp Dermatol* **45**, 147–152 (2020).

5. Xiong, W.-H. *et al.* Serum TRPM1 Autoantibodies from Melanoma Associated Retinopathy Patients Enter Retinal ON-Bipolar Cells and Attenuate the Electroretinogram in Mice. *PLoS ONE* **8**, e69506 (2013).

6. Dhingra, A. *et al.* Autoantibodies in Melanoma-Associated Retinopathy Target TRPM1 Cation Channels of Retinal ON Bipolar Cells. *Journal of Neuroscience* **31**, 3962–3967 (2011).

7. Alexander, K. R. & Fishman, G. A. AOn' Response Defect in Paraneoplastic Night Blindness With Cutaneous Malignant Melanoma. *INVESTIGATIVE OPHTHALMOLOGY* **33**, 7 (1992).

8. Duncan, L. M. *et al.* Down-Regulation of the Novel Gene Melastatin Correlates with Potential for Melanoma Metastasis. *Cancer Res* **58**, 1515–1520 (1998).

9. Duncan, L. M. *et al.* Melastatin Expression and Prognosis in Cutaneous Malignant Melanoma. *JCO* **19**, 568–576 (2001).

10. Deeds, J., Cronin, F. & Duncan, L. M. Patterns of melastatin mRNA expression in melanocytic tumors. *Human Pathology* **31**, 1346–1356 (2000).

11. Fang, D. & Setaluri, V. Expression and Up-Regulation of Alternatively Spliced Transcripts of Melastatin, a Melanoma Metastasis-Related Gene, in Human Melanoma Cells. *Biochemical and Biophysical Research Communications* **279**, 53–61 (2000).

12. Kinker, G. S. *et al.* B Cell Orchestration of Anti-tumor Immune Responses: A Matter of Cell Localization and Communication. *Frontiers in Cell and Developmental Biology* **9**, (2021).

13. Rodgers, C. B., Mustard, C. J., McLean, R. T., Hutchison, S. & Pritchard, A. L. A B-cell or a key player? The different roles of B-cells and antibodies in melanoma. *Pigment Cell & Melanoma Research* **35**, 303–319 (2022).

14. Lei, B., Bush, R. A., Milam, A. H. & Sieving, P. A. Human Melanoma-Associated Retinopathy (MAR) Antibodies Alter the Retinal ON-Response of the Monkey ERG In Vivo. *Investigative Ophthalmology & Visual Science* **41**, 262–266 (2000).

15. Kim, J. M. *et al.* Ophthalmic Immune-Related Adverse Events of Immunotherapy: A Single-Site Case Series. *Ophthalmology* **126**, 1058–1062 (2019).

16. Casselman, P., Jacob, J. & Schauwvlieghe, P.-P. Relation between ocular paraneoplastic syndromes and Immune Checkpoint Inhibitors (ICI): review of literature. *Journal of Ophthalmic Inflammation and Infection* **13**, 16 (2023).

17. Heng, J. S. *et al.* Autoimmune retinopathy with associated anti-retinal antibodies as a potential immune-related adverse event associated with immunotherapy in patients with advanced cutaneous melanoma: case series and systematic review. *BMJ Open Ophthalmology* **7**, e000889 (2022).

18. Chaves, L. J. *et al.* A slow-release dexamethasone implant for cancer-associated retinopathy. *Arq. Bras. Oftalmol.* **86**, 171–174 (2022).

19. Patel, S. R. *et al.* Is it melanoma-associated retinopathy or drug toxicity? Bilateral cystoid macular edema posing a diagnostic and therapeutic dilemma. *Am J Ophthalmol Case Rep* **10**, 77–80 (2018).

20. Xie, K., Kong, C. & Mehta, M. C. A Case of Melanoma-Associated Retinopathy, Uveitis, and Optic Neuritis Associated With Pembrolizumab, Managed With Topical, Intravitreal, and Intravenous Steroids. *J Vitreoretin Dis* **4**, 220–226 (2019).

21. O'Leary, F. & Campbell, M. The blood–retina barrier in health and disease. *The FEBS Journal* **290**, 878–891 (2023).

22. Yang, H. *et al.* A novel and convenient method to immunize animals: Inclusion bodies from recombinant bacteria as antigen to directly immunize animals. *African Journal of Biotechnology* **10**, 8146–8150 (2011).

23. Ferreira, L. B., Williams, K. A., Best, G., Haydinger, C. D. & Smith, J. R. Inflammatory cytokines as mediators of retinal endothelial barrier dysfunction in non-infectious uveitis. *Clin Transl Immunology* **12**, e1479 (2023).

24. Bora, K. *et al.* Assessment of Inner Blood-Retinal Barrier: Animal Models and Methods. *Cells* **12**, 2443 (2023).

25. Byrne, E. M. *et al.* IL-17A Damages the Blood–Retinal Barrier through Activating the Janus Kinase 1 Pathway. *Biomedicines* **9**, 831 (2021).

26. Platt, M. P., Agalliu, D. & Cutforth, T. Hello from the Other Side: How Autoantibodies Circumvent the Blood–Brain Barrier in Autoimmune Encephalitis. *Frontiers in Immunology* **8**, (2017).

27. Capaldo, C. T. & Nusrat, A. Cytokine regulation of tight junctions. *Biochimica et Biophysica Acta (BBA) - Biomembranes* **1788**, 864–871 (2009).

28. Ogura, S. *et al.* Sustained inflammation after pericyte depletion induces irreversible blood-retina barrier breakdown. *JCI Insight* **2**, (2017).

29. Capaldo, C. T. *et al.* Proinflammatory cytokine-induced tight junction remodeling through dynamic self-assembly of claudins. *Mol Biol Cell* **25**, 2710–2719 (2014).

30. Frank, P. G. & Lisanti, M. P. ICAM-1: role in inflammation and in the regulation of vascular permeability. *Am J Physiol Heart Circ Physiol* **295**, H926–H927 (2008).

31. Duvoisin, R. M. *et al.* Autoantibodies in Melanoma-Associated Retinopathy Recognize an Epitope Conserved Between TRPM1 and TRPM3. *Invest. Ophthalmol. Vis. Sci.* **58**, 2732 (2017).

32. Chauhan, M. Z., Mansour, H. A., Zafar, M. K. & Uwaydat, S. H. Anti-Programmed Death Ligand-1 Induced Acute Vision Loss in a Patient With Cancer-Associated Retinopathy. *Cureus* **14**, e21709 (2022).

33. Chen, Q. *et al.* Cancer-associated retinopathy after anti-programmed death 1 (PD-1) antibody for treating hepatocellular carcinoma——a case report of a Chinese patient. *American Journal of Ophthalmology Case Reports* **25**, 101370 (2022).

34. Duvoisin, R. M., Ren, G., Haley, T. L., Taylor, M. H. & Morgans, C. W. TRPM1 Autoantibodies in Melanoma Patients Without Self-Reported Visual Symptoms. *Invest. Ophthalmol. Vis. Sci.* **60**, 2330 (2019).

35. McCulloch, D. L. *et al.* ISCEV Standard for full-field clinical electroretinography (2015 update). *Doc Ophthalmol* **130**, 1–12 (2015).

Chapter 3

The Split Retina as an Improved Flat Mount Preparation for Studying Inner Nuclear Layer Neurons in the Vertebrate Retina

Ryan M. Hecht[1], Qing Shi[1], Tavita R. Garrett[2], Benjamin Sivyer[2], and Catherine Morgans[1]

[1]Department of Chemical Physiology and Biochemistry, Oregon Health and Science University, Portland, OR 97239, USA

[2]Casey Eye Institute, Oregon Health and Science University, Portland, OR 97239, USA

Journal of Visualized Experiments

DOI: 10.3791/65757

3.0: Preface

Chapters 1 and 2 discuss the primary implication of autoantibodies against intracellular epitopes on TRPM1: autoantibodies must be internalized by ON-BCs to cause MAR symptoms. In MAR and other paraneoplastic syndromes featuring intracellular autoepitopes, very little is known about the mechanisms that neurons employ to traffic antibodies across the plasma membrane. To learn more about this behavior, researchers have applied two main strategies for visualizing and analyzing antibody uptake. The first entails the preparation of primary neuron cultures from animal tissues, most frequently the brain. An advantage of this method is the relative ease by which neurons can be examined and manipulated in culture. Time course microscopy is simple for cultured neurons and offers a convenient strategy for evaluating uptake kinetics. Contrarily, cultured neurons have been removed from the context of their native tissue and their behavior may consequently differ from what occurs *in vivo*. In the second strategy, living tissue slices offer a more physiological preservation of cellular connectivity. However, they are more challenging to prepare reproducibly and severing cell bodies with a blade introduces the potential for antibodies to passively diffuse into the neurons, bypassing endocytosis. Disappointed by both strategies, the search for an improved model was begun…

The split retina method is a retina preparation technique intended for examination of inner retinal neurons by immunohistochemistry and electrophysiology. While the original publication makes no mention of it, the split retina was originally developed as a model system for visualizing antibody internalization in ON-BCs. Through the course of development, it became obvious that the technique would be widely beneficial to the research community, and it was thus refined into a methods paper that we published in the Journal of Visualized Experiments (JoVE). The limitations of our previous model systems inspired us to innovate toward a simpler, more reliable, and more physiological system. Thus, the split retina was born.

3.1: Abstract

Bipolar cells and horizontal cells of the vertebrate retina are the first neurons to process visual information after photons are detected by photoreceptors. They perform fundamental operations such as light adaptation, contrast sensitivity, and spatial and color opponency. A complete understanding of the precise circuitry and biochemical mechanisms that govern their behavior will advance visual neuroscience research and ophthalmological medicine. However, current preparations for examining bipolar and horizontal cells (retinal whole mounts and vertical slices) are limited in their capacity to capture the anatomy and physiology of these cells. In this work, we present a method for removing photoreceptor cell bodies from live, flatmount mouse retinas, providing enhanced access to bipolar and horizontal cells for efficient patch clamping and rapid immunolabeling. Split retinas are prepared by sandwiching an isolated mouse retina between two pieces of nitrocellulose, then gently peeling them apart. The separation splits the retina just above the outer plexiform layer to yield two pieces of nitrocellulose, one containing the photoreceptor cell bodies and another containing the remaining inner retina. Unlike vertical retina slices, the split retina preparation does not sever the dendritic processes of inner retinal neurons, allowing for recordings from bipolar and horizontal cells that integrate the contributions of gap junction-coupled networks and wide-field amacrine cells. This work demonstrates the versatility of this preparation for the study of horizontal and bipolar cells in electrophysiology, immunohistochemistry, and *in situ* hybridization experiments.

3.2: Introduction

The retina is a thin neural tissue located in the posterior eye where light is intercepted and processed into an electrochemical signal that can be interpreted by the brain. At the back of the retina, rod and cone photoreceptors are stimulated by light, which reduces their tonic release rate of the neurotransmitter, glutamate[1]. The first neurons to experience and respond to this light-induced change in glutamate concentration are the bipolar cells (BCs) and horizontal cells (HCs), whose somas reside in the outermost region of the inner nuclear layer (INL). These second order neurons perform the first stage of signal processing in the retina and shape critical features of vision such as light adaptation, contrast sensitivity, and spatial/color opponency[2]. While these functions have been ascribed to BCs and HCs, the circuitry and biochemical mechanisms

underlying these processes are not fully understood[3]. Therefore, the advancement of tools and methods for exploring BC and HC physiology is of paramount importance.

Vertical (transverse) retina sections have long proven the most practical model for studying BCs and HCs; however, certain aspects of BC and HC physiology are inaccessible to the experimenter under this model. Direct recordings from HCs or indirect measurements of their effects on BCs are inaccurate since the lateral processes of these cells are severed during slicing. Wholemount retina preparations circumvent this issue by preserving these lateral processes, but the surrounding retinal layers pose a challenge for accessing these cells[4]. While there are abundant examples of immunostaining[5–8] and patch clamp recordings[9] from INL neurons in wholemount retinas, there is an opportunity to expedite and simplify the collection of these data. The inherent limitations of transverse sections and the challenges of the wholemount model thus inspired the development of this alternative flatmount retina preparation.

The following work describes a protocol for easily removing the photoreceptor layer from live, flatmount retinas to enhance access to BCs and HCs for simplified patch clamping and faster, more efficient immunolabeling. Peeling apart two pieces of nitrocellulose membrane attached to either side of an isolated retina tears the tissue through the photoreceptor axons, leaving a "split retina" that retains the outer plexiform layer (OPL) and all inner retinal layers. While others have described protocols for mechanically separating layers of the retina, these methods are either poorly suited to patch clamping and microscopy applications or require tedious manipulation of the tissue. Several of these methods require frozen or lyophilized tissue for layer separation, making them incompatible with electrophysiology experiments.[10–12] Others are designed for live tissue, but necessitate 5-15 sequential peels with filter paper[4,11] or treatment with trypsin[13] to remove the photoreceptors. The technique described here improves upon its predecessors by simplifying the photoreceptor removal procedure and expanding the repertoire of downstream applications.

3.3: Protocol

NOTE: Eye enucleation, retina dissection, and retina splitting should be performed as quickly as possible to preserve the health of the living tissue. Aim to complete the dissection in <4 min per eye. These three steps are to be performed sequentially.

1. Materials preparation for retina dissection and splitting

1.1 Prepare pieces of nitrocellulose membrane

NOTE: Detaching the split retina from the nitrocellulose membrane reduces background fluorescence in microscopy and simplifies patch clamp recording. Membrane removal can be performed before or after tissue fixation. For fixed split retinas, it is NOT necessary to treat the pieces of nitrocellulose membrane. For *live* split retinas, treat the membrane according to steps 1.1.3 – 1.1.5 to facilitate gentle detachment from the tissue.

1.1.1 Cut 16 pieces (or more) of nitrocellulose membrane in 5 x 5 mm squares. Extra can be prepared in bulk and stored for future use.

1.1.2 Set aside half of the pieces of membrane for later use. These pieces will not be treated with blocking solution.

1.1.3 Incubate the remaining pieces in a detergent-free IHC blocking solution (such as 3% horse serum + 0.025% NaN_3 diluted in PBS) for 10 min at room temperature, shaking gently. CAUTION: Use appropriate PPE when handling NaN_3, as it is a potent toxin.

1.1.4 Wash the membrane pieces thoroughly by incubation in bicarbonate-buffered Ames media for 10 min at room temperature, shaking gently.

1.1.5 Completely air dry the blocked pieces of membrane (~20 min). Label and store the membrane pieces at room temperature, keeping them separate from the untreated pieces of membrane.

1.2 Prepare Ames media

1.2.1 Prepare bicarbonate-buffered Ames media and maintain the solution at room temperature under constant carbogenation (95% O2 and 5% CO2).

2. Mouse eye enucleation

2.1 Euthanize the mouse by any available method according to institutional IACUC guidelines.
2.2 Flip the mouse onto one side and use two fingers to gently press down around the eye socket. This will cause the eye to bulge out from the skull.
2.3 Using curved dissection scissors, snip underneath the bulged eye to sever the optic nerve and to separate the eye from the skull.
2.4 Scoop the eye with the scissors and place it into a petri dish filled with ice-cold Ames media.
2.4.1 NOTE: For downstream applications in which the tissue will be fixed after splitting, ice-cold PBS can be used instead of Ames media.
2.5 Repeat steps 2.1 – 2.4 for the remaining eye.

3. Retina dissection

3.1 Use the custom glass transfer pipette to transfer one eye to a new petri dish containing fresh, ice-cold Ames media.
3.1.1 NOTE: The wide opening of the custom transfer pipette prevents accidental squishing of the tissue, and using glass minimizes adhesion of the tissue to the walls of the pipette. However, a wide-mouth plastic transfer pipette is also acceptable if the experimenter is already proficient at using this tool.
3.1.2. NOTE: For downstream applications in which the tissue will be fixed after splitting, ice-cold PBS can be used instead of Ames media.
3.2 Use forceps to stabilize the eye by pinning its extra connective tissue to the bottom of the petri dish. Then, puncture the eye along the ora serrata line using a 25-gauge needle to create an entry point for the Vannas scissors.
3.3 Use Vannas scissors to cut along the ora serrata line until the cornea comes free from the rest of the eye (**Figure 3-S1A**).
3.4 Remove the lens from the eyecup using forceps (**Figure 3-S1B**).
3.5 Use the custom glass pipette to transfer the eyecup to a large volume (≥100 mL) of carbogenated Ames and repeat steps 3.1 – 3.5 with the remaining eye.
3.5.1 NOTE: Eyecups are placed into carbogenated Ames to maintain tissue health while the dissection is performed on the other eye.

3.6 Transfer one eyecup to a petri dish filled with freshly carbogenated Ames.

3.7 Using Vannas scissors, make a small snip inward from the edge of the sclera, then use two pairs of forceps to peel the sclera away from the retina (**Figure 3-S1C**).

3.7.1 NOTE: Avoid grabbing the retina with the forceps. Instead, pull apart on the flaps of the sclera created by the scissor snip (**Figure 3-S1C**).

3.8 Use the Vannas scissors to snip the optic nerve connecting the sclera and the retina (**Figure 3-S1D**), then gently pry the retina from the sclera using the scissors or forceps to isolate the retina. (**Figure 3-S1E, Figure 3-1A**).

3.8.1 NOTE: While the RPE will typically remain attached to the eyecup, no extra steps are required to remove the RPE in the event it is attached to the retina.

3.8.2 NOTE: At this point, the edges of the retina may be optionally trimmed with a scalpel to prevent curling during the flattening step (**Figure 3-1B**).

3.9 Use a scalpel to cut the retina into halves or quarters (**Figure 3-1C**), then use the custom transfer pipette to return the pieces to a large volume (≥ 100 mL) of continuously carbogenated Ames media.

3.9.1 NOTE: The choice of halves or quarters is subjective. Choose the best option for the desired application.

3.10 Repeat steps 3.6 – 3.9 for the remaining eye before proceeding to retina splitting.

4. Retina splitting

4.1 Discard the Ames media from the petri dishes and replace it with freshly carbogenated Ames.

4.1.1 NOTE: To maintain carbogenation throughout the remainder of the retina splitting procedure, replace the media in the petri dish with freshly carbogenated Ames roughly every 5 minutes.

4.2 Using the custom transfer pipette, place a piece of retina onto a glass slide (7.5 x 5 cm), ganglion cell side up, then flatten it by removing the surrounding liquid with a delicate task wipe (**Figure 3-1D**).

4.2.1 NOTE: If necessary, the retinal edges can be further flattened by gently pulling with a fine tip paintbrush under a dissection microscope.

4.3 Use forceps to lower a dry 5 x 5 mm piece of nitrocellulose membrane onto the retina, causing it to adhere to the ganglion cell side (**Figure 3-1E**).

4.3.1 NOTE: If membrane removal from *live* tissue is required (i.e., for electrophysiology), use a dry piece of serum-treated membrane for this step (see steps 1.1.3 – 1.1.5 for details). This reduces the strength of the adhesion to the ganglion cell layer, making it easier to remove the retina from the nitrocellulose post-split.

4.4 Flip the retina over so that the nitrocellulose is resting on the glass slide and place a dry piece of 5 x 5 mm membrane onto the photoreceptor side of the retina (**Figure 3-1F**).

4.5 Touch the wetted tip of the paintbrush to the space between the two membranes and allow capillary action to suck the Ames into the sandwich (**Figure 3-1G**). This *reduces* the adherence of the membranes to the retina and is *only necessary if the retina has been overly dried with the delicate task wipe.*

4.5.1 NOTE: If the retina has lost its shiny appearance, it has been overly dried, and step 4.5 is necessary.

4.6 To ensure uniform adherence, apply light downward pressure to the upper membrane with a wetted paintbrush (**Figure 3-1H**).

4.7 While pinning the lower membrane to the glass with one pair of forceps, use a slow, steady motion to gently peel the upper membrane away with a second pair of forceps. This will cause the retina to split just above the OPL (**Figure 3-1I**).

4.8 Discard the upper membrane containing the photoreceptors (**Figure 3-1J, left**). The lower membrane contains the inner retina, henceforth referred to as a "split retina" (**Figure 3-1J, right**).

4.9 Immediately return the split retina to carbogenated Ames media.

4.9.1 NOTE: For experiments on living tissue, retinas may benefit from a 15–30-minute recovery period in carbogenated Ames after splitting.

5. Preparation of split retinas for immunofluorescence experiments

NOTE: The split retina will still be attached to the nitrocellulose membrane until step 5.5. Complete either step 5.1, 5.2, 5.3, or 5.4, not all four. CAUTION: Use appropriate PPE and proceed carefully when handling paraformaldehyde (fixative).

5.1 Preparation for flatmount immunofluorescence

5.1.1 Incubate the split retina in 4% paraformaldehyde on ice for 30 min using enough solution to completely cover the retina.
5.1.2 Wash the split retinas 3 times in 5-10 mL of room temperature PBS.
5.1.2.1 Optional Pause: Split retinas may be left in PBS at 4 ºC for up to 24 hrs.

5.2 Preparation for immunofluorescence with vertical sections of split retina

5.2.1 Incubate the split retina in 4% paraformaldehyde on ice for 30 min using enough solution to completely cover the retina.
5.2.2 Wash the split retinas 3 times in 5-10 mL of room temperature PBS.
5.2.2.1 Optional Pause: Split retinas may be left in PBS at 4 ºC for up to 24 hrs.
5.2.3 With the membrane still attached, sequentially immerse the split retina in 10%, 20%, and 30% sucrose at 4 ºC for 1 h each to cryoprotect the tissue.
5.2.4 Embed the cryoprotected split retinas in O.C.T. compound and store them at -80 ºC (up to 6 months) until cryosectioning.
5.2.5 Remove the embedded split retinas from -80 ºC and use a cryostat to cut sections 20 µm thick. Mount the sections onto electrostatically charged glass microscope slides, allow them to air dry, then store them at -20 ºC for up to 6 months.

5.3 Preparation for dual fluorescence in situ hybridization and immunohistochemistry

5.3.1 Incubate the split retina in 4% paraformaldehyde on ice for 2 hrs using enough solution to completely cover the retina.
5.3.2 Wash the split retinas 3 times in 5-10 mL of room temperature PBS.
5.3.2.1 Optional Pause: Split retinas may be left in PBS at 4 ºC for up to 24 hrs.

5.4 Preparation for electrophysiology

5.4.1 Prepare patch pipettes by pulling thick-walled borosilicate glass pipettes with filament using a micropipette puller. Only use pipettes with a measured resistance between 6-10 MΩ.
5.4.2 Back fill the pulled pipettes with internal solution containing (in mM): 125 K-gluconate, 8 KCl, 5 HEPES, 1 $MgCl_2$, 1 $CaCl_2$, 0.2 EGTA, 3 ATP-Mg, and 0.5 GTP-Na.

5.5 Removal of the split retina from the nitrocellulose membrane

5.5.1 Using a hydrophobic barrier pen, prepare circular wells on a microscope slide (~1 cm in diameter) and allow them to air dry for 5-10 min.
5.5.2 Place the split retinas within the prepared hydrophobic barrier pen wells and add enough PBS to completely cover them.
5.5.3 Under a dissection microscope, push the bristles of a fine paintbrush under the edges of the tissue and gently lift upward. In this manner, work around the retina in a circle to lift it away from the membrane.
5.5.4 Use forceps to remove the membrane from underneath the floating piece of retina.
5.5.5 Carefully aspirate away the remaining PBS so that the piece of retina comes to rest on the microscope slide, ganglion cell-side down.
NOTE: The following steps are not to be performed sequentially. Choose the appropriate protocol for the desired application (i.e., immunostaining OR dual fluorescence in situ hybridization [FISH] & immunohistochemistry [IHC] OR electrophysiology).

6. Immunostaining

6.1 If not yet prepared, use a hydrophobic barrier pen to create circular wells on a microscope slide (~1 cm in diameter) and allow them to air dry for 5-10 min. All incubation steps and wash steps will be performed within these pen wells.
6.2 Incubate the split retinas or vertical split retina sections in Antibody Incubation Solution (AIS: 3% horse serum, 0.5% Triton X-100, 0.025% NaN3 in PBS) for 30 min at room temperature.
6.3 Incubate the split retinas or vertical split retina sections with primary antibodies diluted in AIS for 1 h at room temperature.
6.3.1 NOTE: primary antibody incubation time will require optimization for different protein targets and antibodies.
6.4 Wash the tissue 3 times in room temperature PBS.
6.5 Incubate the tissue with secondary antibodies diluted in AIS for 1 h at room temperature.
6.6 Wash the tissue 3 times in room temperature PBS.
6.7 If nuclear staining is desired, incubate the tissue with DAPI diluted in PBS for 30 s at room temperature.

6.8 Wash the tissue once in room temperature PBS.

6.9 Apply a drop of slide mounting media to each piece of tissue and mount a glass coverslip.

6.10 Apply nail polish around the edges of coverslip to seal the sample. Store the slide at 4 ºC.

7. Dual FISH & IHC

7.1 Bake the split retinas at 40 ºC for 30 min in a hybridization oven to increase adherence to the slide.

7.2 Complete the RNAscope FISH protocol according to the manufacturer's protocol with the following exceptions and alterations:

7.2.1 No antigen retrieval step is required.

7.2.2 Use protease III with an incubation time of 18 min at room temperature.

7.2.3 Perform all wash steps on the slide within the wells made by a hydrophobic barrier pen.

7.3 Incubate the samples in primary antibody diluted in PBS for 30 min at 40 ºC in the hybridization oven.

7.4 Wash the samples 3 times in room temperature PBS.

7.5 Incubate the samples in secondary antibody diluted in PBS for 30 min at 40 ºC in the hybridization oven.

7.6 Wash the samples 3 times in room temperature PBS.

7.7 Incubate the samples in 1X DAPI for 30 s at room temperature.

7.8 Wash the samples once in room temperature PBS.

7.9 Apply a drop of anti-fade mounting media to each piece of tissue and mount a glass coverslip.

7.10 Apply nail polish around the edges of coverslip to seal the sample. Store the slide at 4 ºC.

8. Electrophysiology

8.1 After removing the nitrocellulose membrane, transfer a split retina into the patch-clamp recording chamber and gently anchor it in place with a platinum harp.

8.2 Throughout the experiment, continuously perfuse the split retina with Ames solution carbogenated with 95% O_2 and 5% CO_2. Maintain the solution between 32-34 °C.

8.2.1 NOTE: During the experiment, the tissue can be visualized using Dodt gradient contrast microscopy.

8.3 Under room lighting, perform whole-cell voltage-clamping to record from INL neurons.
8.3.1 While recording, simulate light responses using a microcellular injection unit to apply pharmaceutical compounds, or a 470 nm LED to stimulate channelrhodopsin (ChR2).
8.3.1.1 NOTE: Light intensity can be measured using a digital optical power meter.

Confocal microscopy

Confocal immunofluorescence images were taken with a white light laser equipped confocal microscope using a 40X/1.3 or 63×/1.40 oil immersion objective. FIJI was used to adjust brightness and contrast and to generate Z-projections from image stacks.

Animals

Wild-type mice: Adult (>3 months) male and female C57BL/6J mice were used for experiments in Figures 1, 2, 4, 5, and 6. For Figure 3, mice expressing GFP under the Pcp2 promoter (Pcp2-cre/GFP) [14] were used.

Transgenic mice: For horizontal cell visualization with GFP during immunohistochemistry or electrophysiology experiments (**Figure 3-6**), a triple-transgenic mouse was used: vGATFLPo; vGlut2Cre; Ai80d. The vGATFlpo and vGluT2Cre strains are knock-in mice expressing Flpo or Cre recombinase downstream of their respective promoters. The Ai80d mouse is an intersectional reporter mouse (CatCh/EYFP) and will only express Ca2+ permeable channelrhodopsin (ChR2) in cells expressing Cre and Flpo recombinases. Thus, the triple transgenic mouse only expresses ChR2 in cells with a history of both VGAT and vGluT2 expression.

Mice were provided water and food ad libitum and were maintained on a 12-h light/dark cycle. Mice were euthanized by exposure to isoflurane followed by cervical dislocation. All animal procedures were in accordance with the National Institutes of Health guidelines and approved by the Oregon Health and Science University Institutional Animal Care and Use Committee.

3.4: Results

3.4.1 The split retina procedure

The procedure for preparing split retinas is illustrated in **Figure 3-1**. A more detailed demonstration of the technique can be found in the video exhibit accompanying the original publication of this manuscript (DOI: 10.3791/65757).

Figure[3-1]

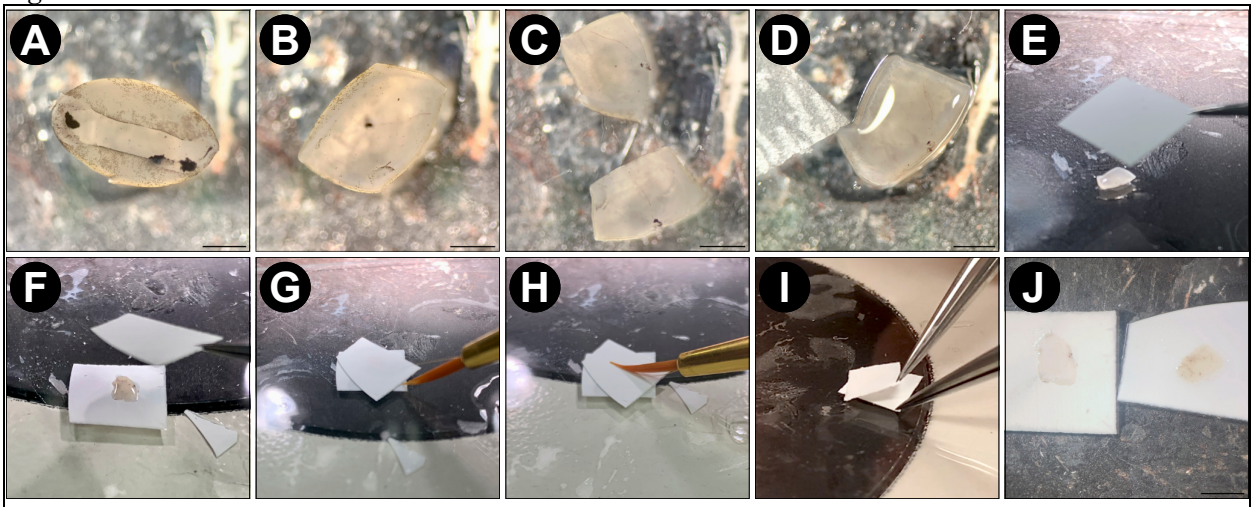

[3-1] **Split retina procedure**. **A**) Following enucleation and eyecup preparation in cold PBS or Ames media, isolate the mouse retina from the eyecup and replace the PBS with room temperature, carbogenated Ames media. **B**) Using a scalpel, trim the edges of the retina away until there are no regions with an inward curl (optional). **C**) Cut the retina into quarters or halves using a scalpel. **D**) Place one piece of retina on a glass slide (ganglion cell side up) using the custom transfer pipette and remove all excess Ames using a delicate task wipe. Ensure that the semi-dry retina is lying flat on the glass before proceeding to the next step. Use an Ames-wetted paintbrush tip to gently unfold regions of the retina that are not flat. **E**) Using forceps, place a pre-cut piece of dry nitrocellulose membrane (5 x 5 mm) onto the flattened retina. **F)** Flip the piece of nitrocellulose so that the photoreceptor side of the retina is now facing up. Then place another dry piece of membrane onto the retina. **G**) Touch the wetted tip of the brush to the space between the two membranes and allow capillary action to suck the Ames into the sandwich. This *reduces* the adherence of the membranes to the retina and is *only necessary if the retina was overly dried with the delicate task wipe*. **H)** Use a wetted paintbrush tip to gently press downward onto the center of the sandwiched retina. **I**) Use one pair of forceps to pin the bottom piece of membrane onto the glass slide, while using another pair of forceps to gently peel the top piece of membrane away from the bottom one. **J**) The inner retina (left) remains on the bottom membrane while the photoreceptors (right) are pulled away with the top membrane. Images A, B, C, D, and J were acquired using a dissection microscope; the scale bar represents approximately 1 mm; images E-I were acquired with a smartphone camera without magnification.

3.4.2 Retina splitting preserves photoreceptor terminals

To confirm that retina splitting does not damage the dendrites of second order neurons in the OPL, vertical sections of split retinas were stained with antibodies against the synaptic vesicle protein synaptophysin (green), and protein kinase C alpha (PKCα) (red). The intense band of synaptophysin labeling across the top of the split retina indicates that the photoreceptor synaptic terminals are retained (**Figure 3-2**). Furthermore, PKCα staining reveals normal morphology of rod bipolar cells (RBCs). No photoreceptor nuclei are visible, indicating that the retina is split between the OPL and innermost row of photoreceptor cell bodies (**Figure 3-2**).

Figure[3-2]

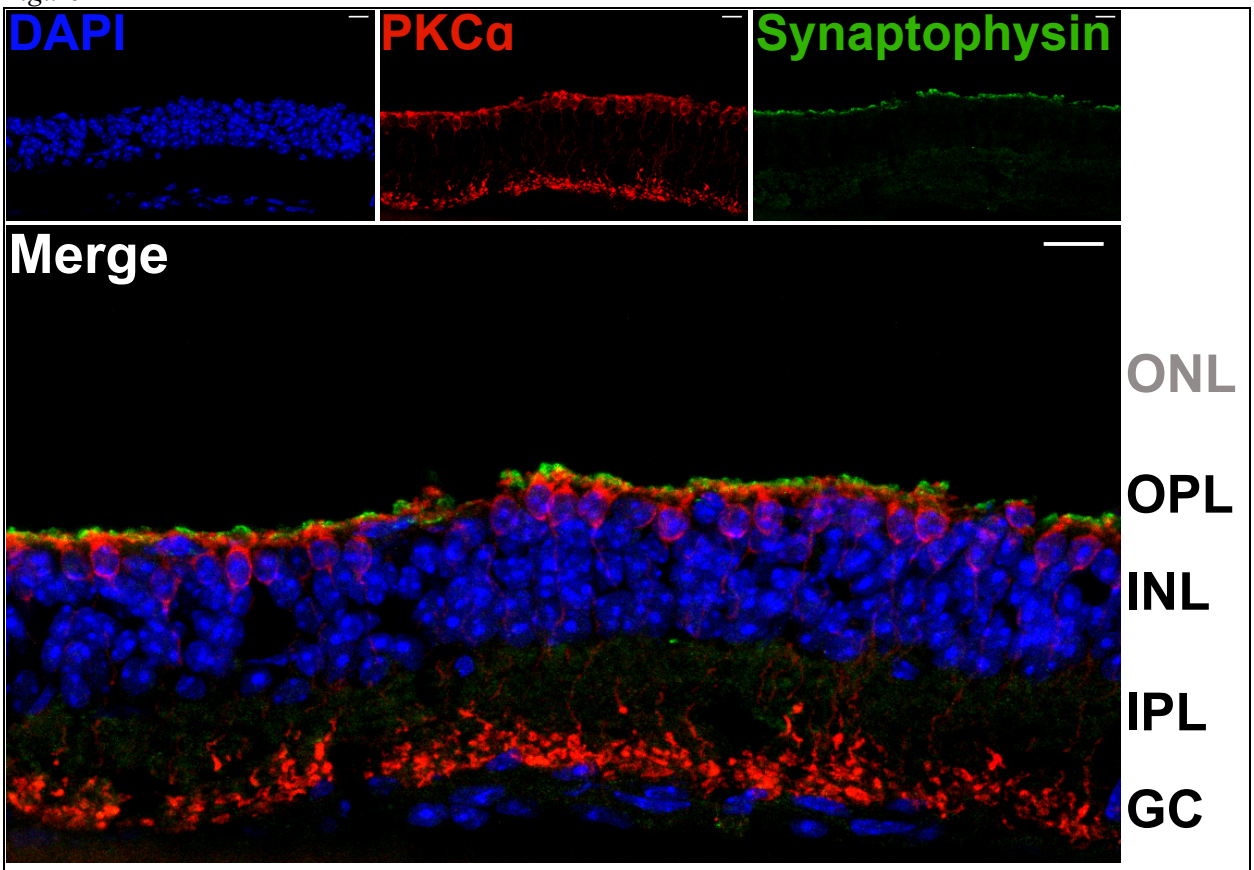

[3-2] **Split retinas retain photoreceptor terminals**. Fluorescent confocal micrographs showing a vertical cross-section of a spit retina that was cryosectioned (20 µm thickness) following the splitting procedure. Each image is a maximum projection of a confocal z-stack. The section was immunolabeled with antibodies against PKCα (top center) and synaptophysin (top right) to visualize RBCs and synaptic vesicles, respectively. The merged image (bottom) shows synaptic vesicles (green), which reside in the photoreceptor terminals, just above the apical processes of the RBCs (red) in the OPL. Cell nuclei are labeled with DAPI (blue). No photoreceptor nuclei are

visible within the ONL. Abbreviations: ONL = outer nuclear layer; OPL = outer plexiform layer; INL = inner nuclear layer; IPL = inner plexiform layer; GC = ganglion cells. Scale bars = 10 μm.

3.4.3 Synapse morphology in the OPL is preserved after retina splitting

Using a mouse that expresses GFP in RBCs under the pcp2 promoter[14] pre- and post-synaptic proteins in the OPL were immunolabeled to assess the integrity of this synaptic layer following a split[14]. Despite the shear forces occurring through the axons of the photoreceptors, splitting does not perturb the morphology of photoreceptor-BC synapses in the OPL, as normal positioning of RBC dendrites, labeled for RGS11, and photoreceptor synaptic ribbons, labeled for CtBP2[15] is observed (**Figure 3-3**). For each synaptic contact between rods and RBCs, RGS11 can be seen as red puncta that lie within the horseshoe shape of the synaptic ribbon (green). In a subsequent experiment, an anti-GPR179 antibody[16] was used to label the post-synaptic ON-BC dendritic tips[16], and an anti-PSD-95 antibody was used to label pre-synaptic rod photoreceptor terminals (**Supplementary Figure 3-S2**). These results again confirm the stability of the OPL in the split retina preparation, as RBC dendrites are shown to closely associate with their pre-synaptic partner, the rod terminals.

Figure[3-3]

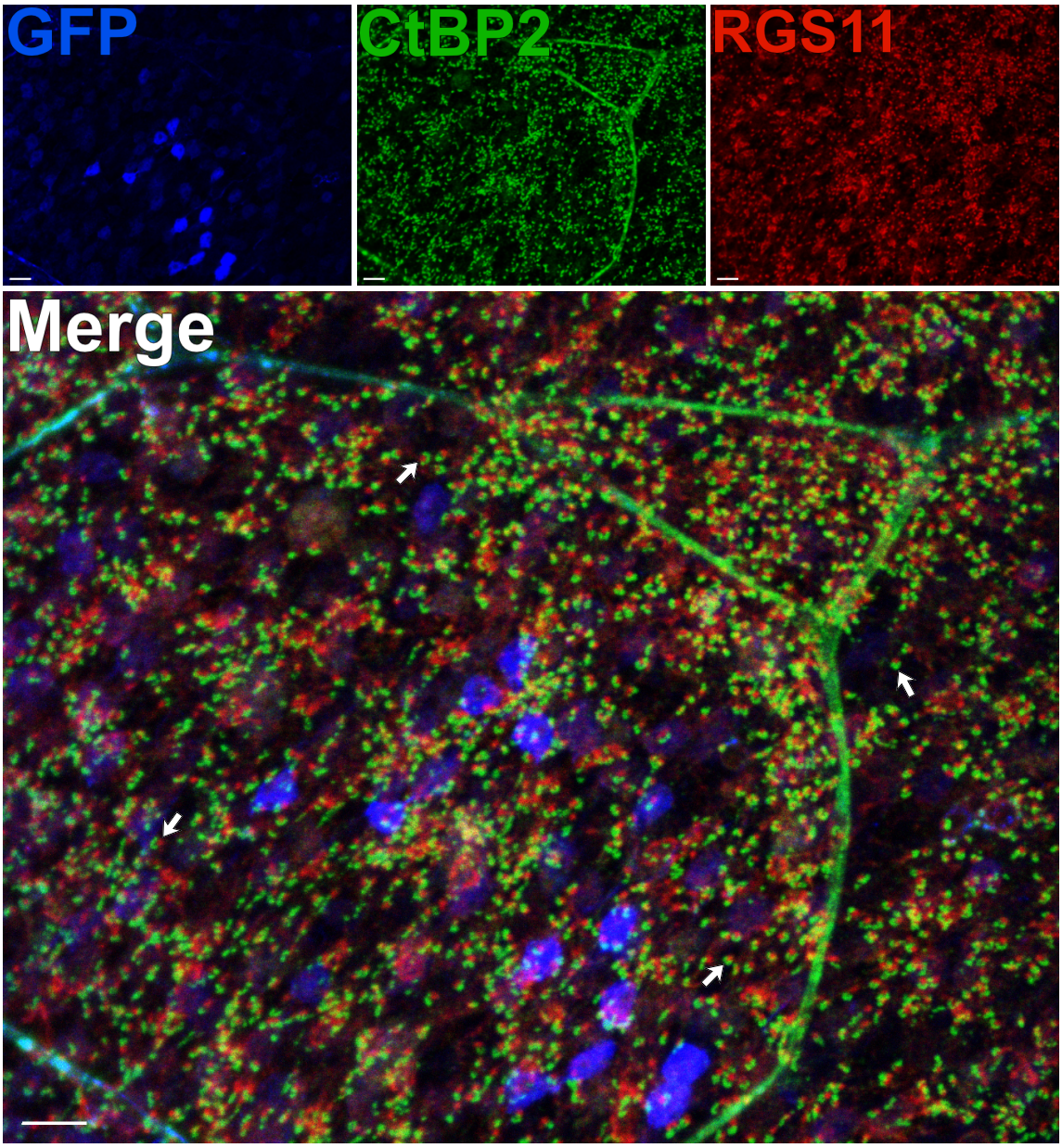

[3-3] **Synapse morphology in the OPL is preserved after retina splitting**. Confocal immunofluorescence images of a split retina from a transgenic mouse expressing GFP in RBCs under the Pcp2 promoter. Levels of GFP expression (blue) vary across RBCs in the retina. Following splitting, the retina was fixed, then incubated with antibodies against CtBP2 (green) and RGS11 (red) to label photoreceptor synaptic ribbons and ON-BC dendritic tips, respectively. Each red-green pair represents a synaptic contact between a rod and an ON-BC. Scale bars = 10 µm.

3.4.4 Retina splitting maintains RBC viability

To assess the viability of the inner-retinal neurons after a split, a membrane impermeable, near-infrared nuclear dye (MI-NIR) was used, which enables the identification of dead cells. After incubation with MI-NIR, split retinas were fixed, then labeled with anti-PKCα to identify RBCs. Confocal micrographs of the split retina reveal regional variability in cell viability across the tissue, with some regions experiencing higher rates of cell death than others. This variability may result from damage inflicted onto certain regions of the retina during the dissection, splitting, or handling procedures. (**Figure 3-4**). Given that the cell bodies of RBCs reside in the outermost region of the INL, close to the site of the split, a careful evaluation of their viability was warranted. Scarce colocalization of PKCα and MI-NIR confirmed that most RBCs remain viable after retina splitting (**Figure 3-4**).

Figure[3-4]

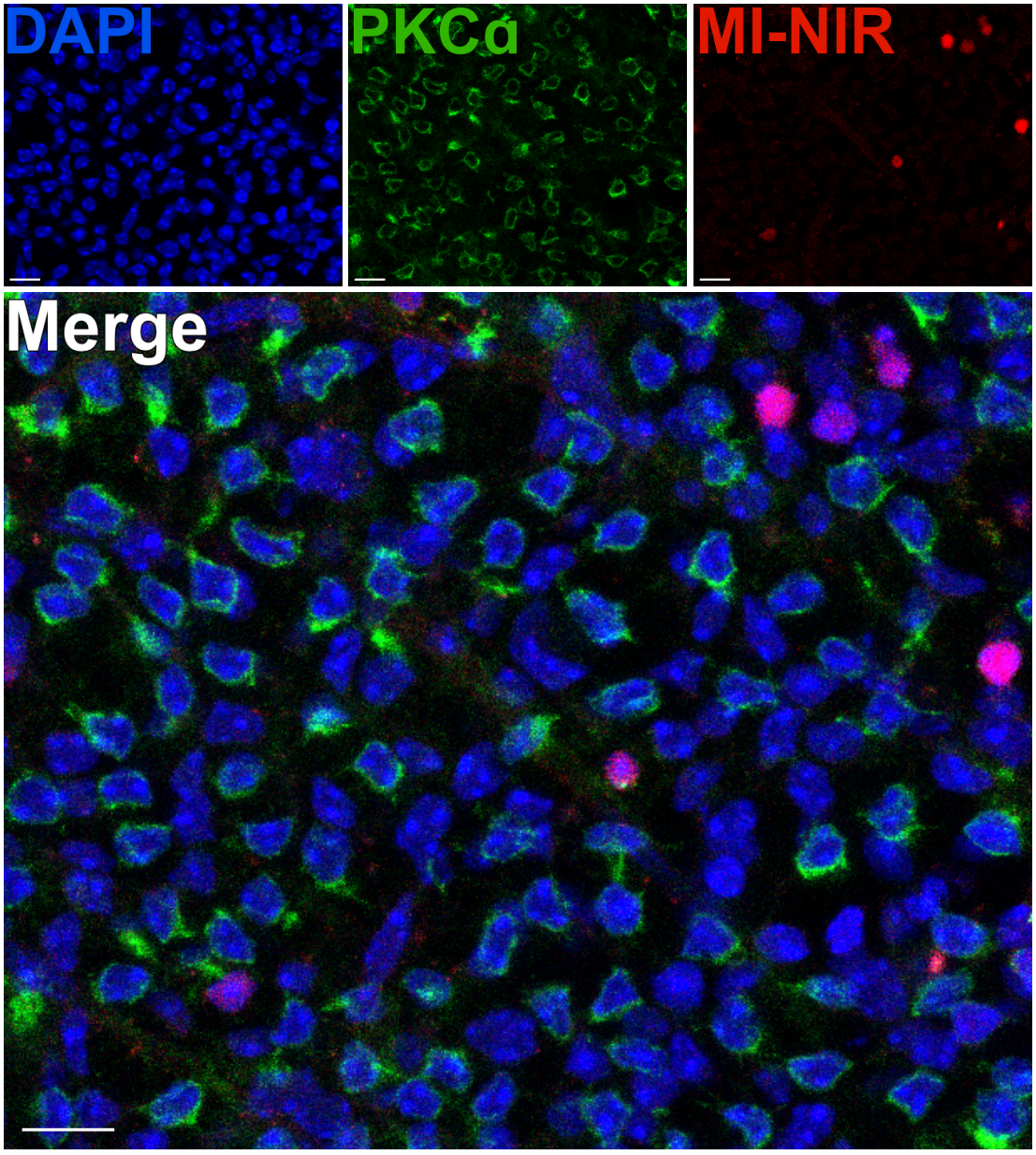

[3-4] **Rod bipolar cells are viable after retina splitting**. Fluorescent confocal micrographs showing a region of a split retina in a flatmount perspective. After splitting, the live retina was incubated with MI-NIR dye (red) for 30 min at 37 °C. The retina was then fixed and immunolabeled with antibodies against PKCα to visualize RBCs. In this region of the retina, colocalization of PKCα and MI-NIR is infrequent. MI-NIR colocalizes with nuclei (blue) that do not belong to RBCs. Abbreviations: MI-NIR = membrane impermeable NIR live/dead stain. Scale bars = 10 µm.

3.4.5 Split retinas are amenable to dual FISH and IHC

By extending the fixation time for standard IHC, split retinas can be sequentially processed by FISH and IHC to label mRNAs and proteins simultaneously[17,18]. Experiments confirmed that a 2-h fixation in 4% PFA yields robust mRNA labeling while still preserving protein epitopes for antibody binding. FISH was performed on split retinas followed by IHC to visualize the expression of the $GABA_A$ receptor subunit δ (GABRD; anti-sense mRNA probes) in relation to the position of RBCs (anti-PKCα antibody) in the outer INL (**Figure 3-5A**). GABRD mRNA expression appears rare in RBCs (**Figure 3-5A**); however, the transcript is abundantly expressed by amacrine cells and ganglion cells as evidenced by the labeling pattern on transverse sections from an intact retina (**Figure 3-5B**). In the outer INL (**Figure 3-5A**), GABRD mRNA is more evenly distributed compared to the inner INL (**Figure 3-5C**) where it is concentrated in distinct cells. Antisense probes targeting other GABA receptor subunits produce distinct labeling patterns, demonstrating the specificity of the probes (data not shown).

Figure[3-5]

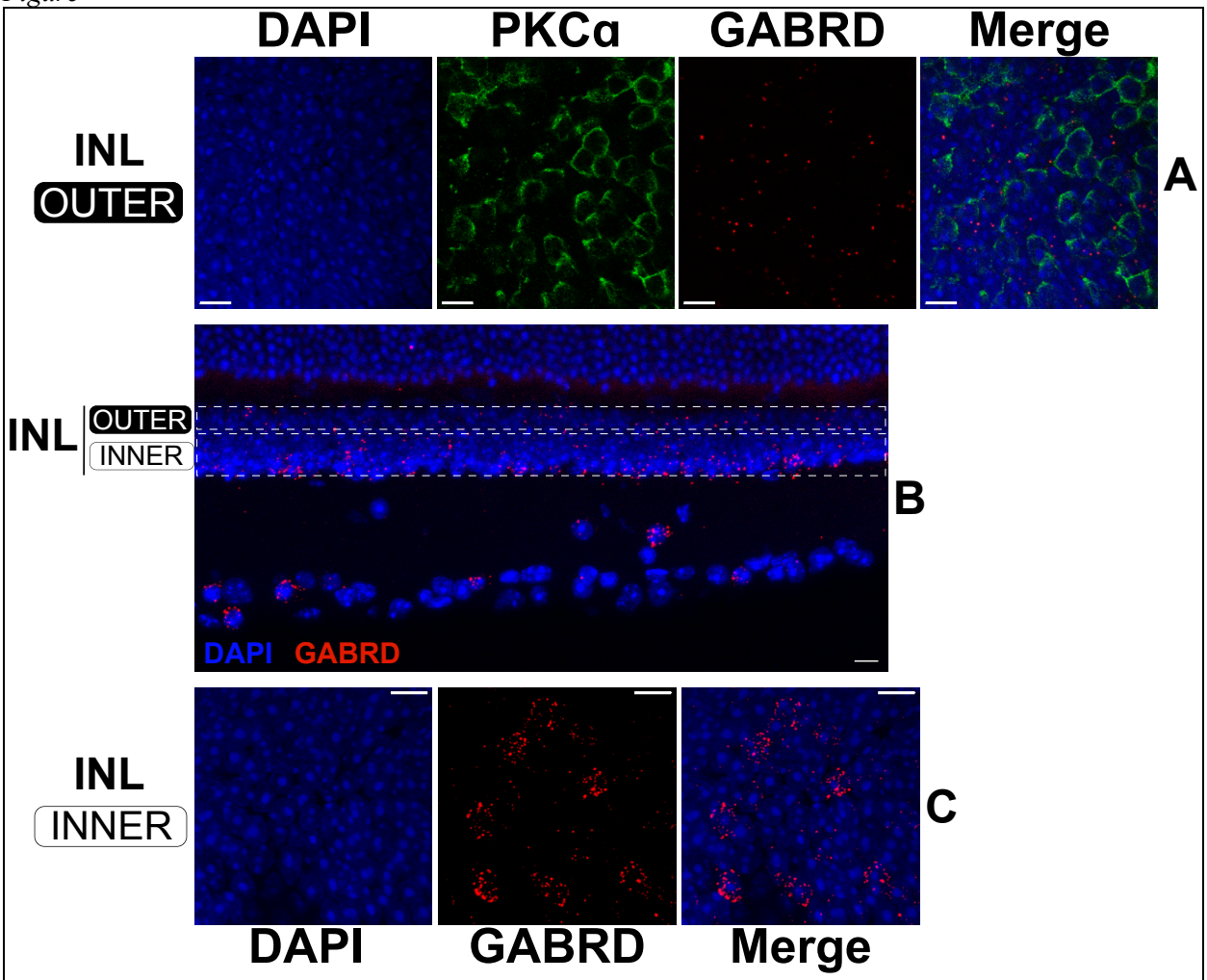

[3-5] **Dual FISH and IHC in a split retina and an intact retina**. Confocal micrographs of a flatmount split retina (**A**, **C**) and a vertical section from an intact retina (**B**). Images in (**A**) and (**C**) are maximum projections of optical sections in the upper and lower regions of the INL respectively. The dotted rectangles in (**B**) represent the approximate boundaries used to create the projections shown in (**A**) and (**C**). The split retina (**A**, **C**) was fixed for 2 h, then labeled with antisense mRNA probes against GABRD (red). Afterward, the split retina was stained with antibodies against PKCα to label RBCs (green). The PKCα channel was omitted from projections of the lower INL for clarity. The intact retina in (**B**) was fixed for 24 h before sectioning. Afterward, the fixed retina was labeled with antisense mRNA probes against GABRD (red). All samples were stained with DAPI (blue) for 20 s prior to coverslip mounting. Abbreviations: INL = inner nuclear layer. Scale bars= 10 µm.

3.4.6 Split retinas are well-suited to patch-clamp electrophysiology recording from BCs and HCs

To patch a BC or HC soma in a traditional wholemount retina, the pipette must approach from either the ganglion cell side or the photoreceptor side. Both approaches require traversing several retinal layers to reach the INL, during which the pipette tip often becomes obstructed by debris. In a vibratome slice preparation, the BC and HC somas are readily accessible, but their dendritic processes may be severed, disrupting their lateral connections. In split retinas, however, the cell bodies of RBCs and HCs sit at the tissue's surface, providing greatly improved access to patch pipettes while preserving the OPL's lateral circuitry.

Figure 3-6 shows chemically simulated light responses recorded from BCs in a split retina. Perfused Ames medium was supplemented with L-AP4 (4 μM), a group III mGluR agonist, to simulate glutamate release from photoreceptors in darkness. The mGluR6 antagonist, CPPG (600 μM, in Ames), was puffed onto the dendrites of the patched cell (held at -60 mV) to simulate a light flash via inhibition of mGluR6. Cells responded to CPPG puffs with two types of inward currents. One type shows a transient current followed by a plateau (**Figure 3-6A**), similar to the canonical light-evoked currents recorded from RBCs in retinal slices [19]. The other type remains sustained throughout the puff duration (**Figure 3-6B**), resembling currents recorded from ON cone bipolar cells (ON-CBC)[19].

A separate experiment was performed to target HCs, a cell type with a wide dendritic field that is often difficult to preserve in slice preparations. A mouse line expressing channelrhodopsin (ChR2) and GFP in HCs was used to facilitate easy identification under a fluorescence microscope. First, currents from HCs were recorded in response to a series of depolarization steps (-100 mV to 50 mV, step size = 15 mV) to which they responded with inward currents followed by outward currents (**Figure 3-6C**). These cells were then stimulated with a brief blue light pulse (200 ms, 470 nm) producing large, ChR2-driven inward currents in two cells (**Figure 3-6D**).

Figure[3-6]

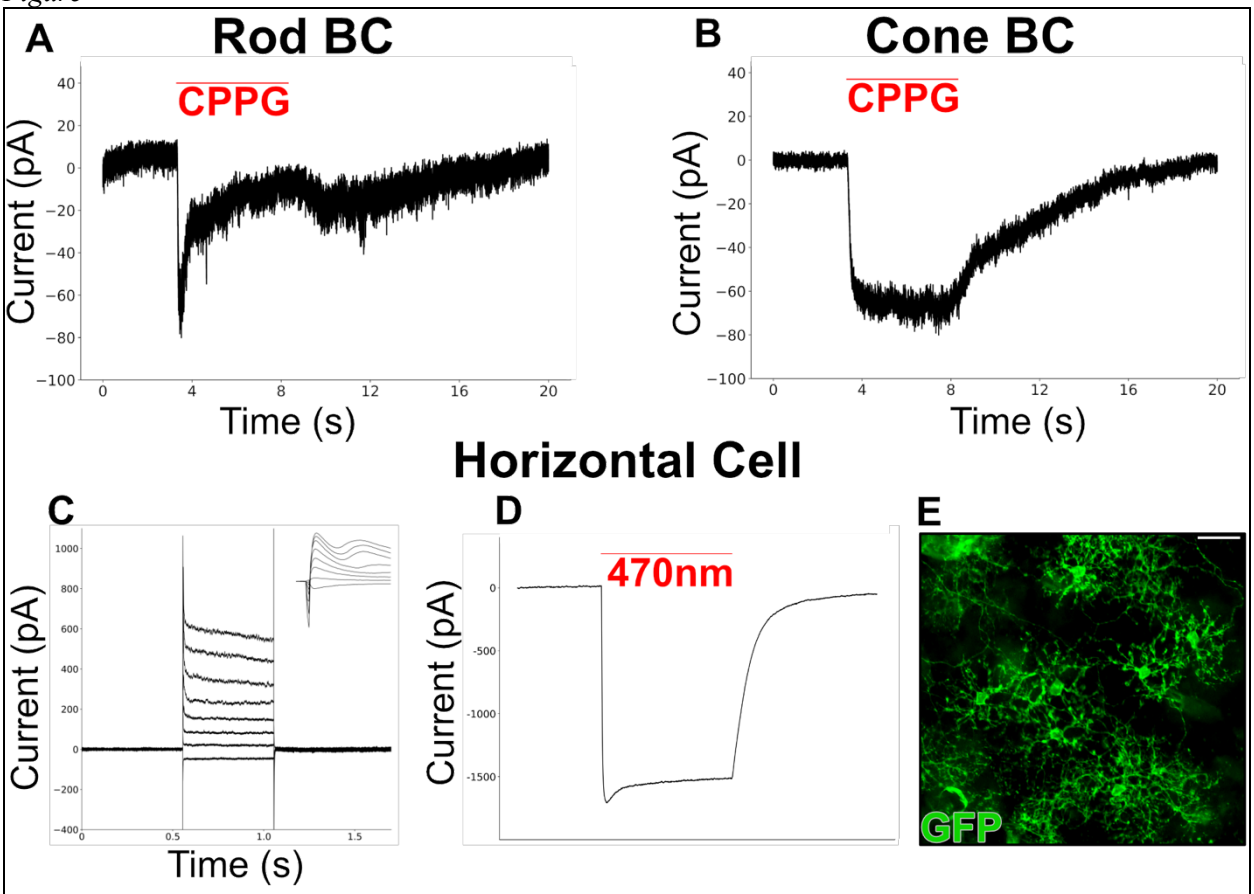

[3-6] Patch clamp recordings from INL neurons in split retinas. A putative RBC (A) and CBC (B) were voltage-clamped at -60 mV in perfused Ames media containing L-AP4 (4 µM). Puffing CPPG (600 µM) onto the dendrites of the clamped cells invoked an inward current which was transient in the RBC but sustained in the CBC. The RBC recording in (A) is a single trace whereas the CBC recording in (B) represents the average of 3 traces. (C) A patch clamp recording from an HC in a vGATFLPo; vGlut2Cre; Ai80d mouse. The red line shows the duration of a 200 ms, 470 nm light pulse used to invoke the large, inward current through ChR2. (D) Injected current responses from an HC that was voltage clamped at -60 mV, then stepped between -70 mV and +35 mV in 15 mV intervals and returned to -60 mV. The inset shows the same traces in a 6 ms window surrounding the start of the voltage step. (E) Immunofluorescent micrograph of a flatmount split retina showing horizontal cells expressing GFP in a vGATFLPo; vGlut2Cre; Ai80d mouse. Scale bar = 20 µm. Electrophysiology data were collected at a 20 kHz sampling rate and filtered with a low-pass Bessel filter at 5 kHz. Data were then exported, and offline visualization and analysis were performed using Python 3.

3.4.7 Retina splitting enables rapid interrogation of INL and OPL anatomy

The retina's external limiting membrane (ELM) and ONL comprise a barrier ~90 μm thick, which impedes the diffusion of antibodies into the inner retina and creates suboptimal immunostaining conditions[20–22]. Therefore, immunolabeling targets in the OPL or INL using a conventional flatmount retina requires time-intensive staining protocols that often necessitate 48-96 h antibody incubations [5–8,20,22].

Removing the photoreceptors allows for rapid antibody penetration of inner retinal neurons. As a result, labeling of inner-retina protein targets can be achieved in as little as 1 h with the use of dye-conjugated primary antibodies. Antibodies against PKCα and Calbindin-D were used to label RBCs and HCs of the INL respectively (**Figure 3-7**). Unlike traditional vertical retina sections that truncate the lateral processes of wide-field neurons, the split retina preparation enables visualization of the full dendritic arbor of wide-field cells such as HCs (**Figure 3-6E, 3-7**).

Figure[3-7]

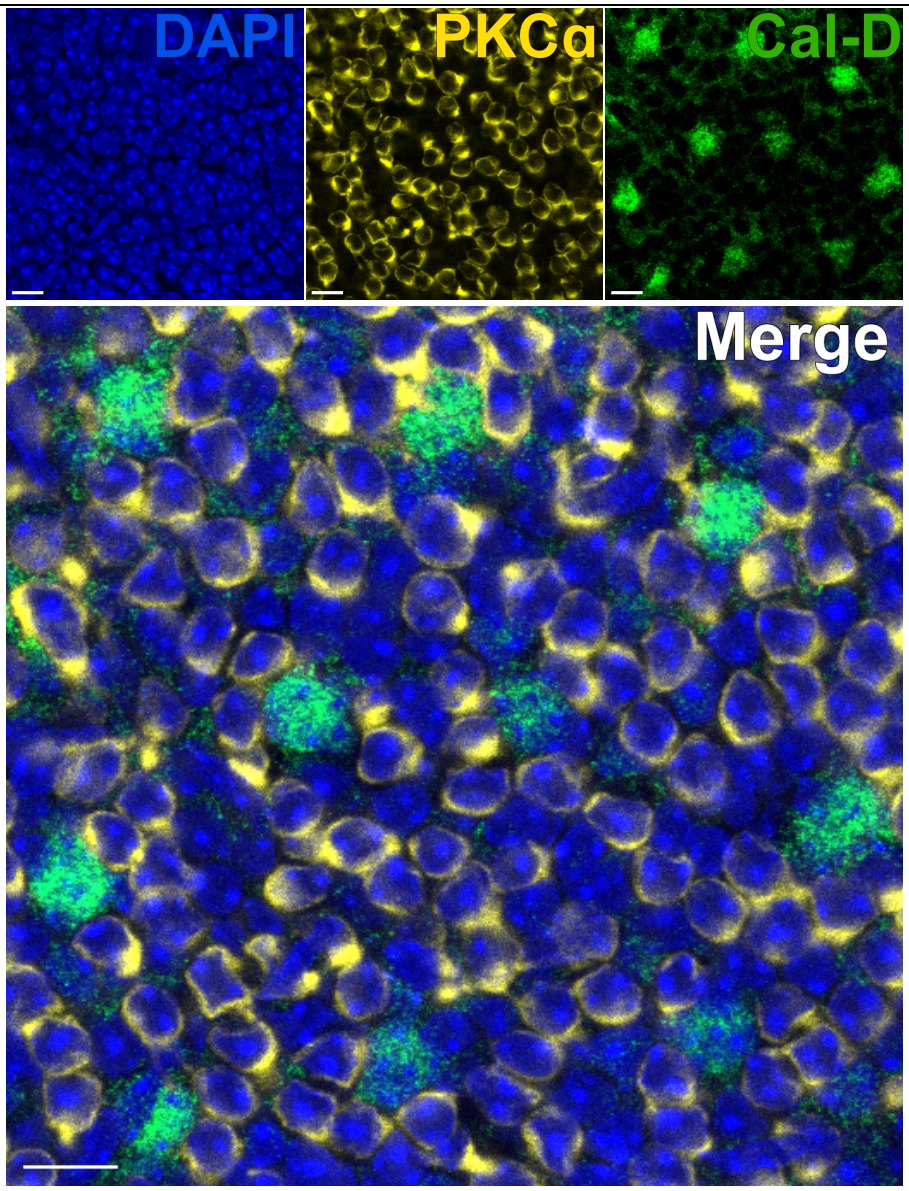

[3-7] **Rapid immunolabeling of inner retina proteins in a split retina**. Confocal immunofluorescence images of a split retina from a flatmount perspective. The split retina was incubated with antibodies against PKCα (yellow) and Calbindin-D (green) for 1 h at room temperature to label ON-BCs and HCs respectively. Each single channel image is an average Z-projection composed of four optical sections: DAPI, Average z10-13; Calbindin-D, Average z11-14; PKCα, Average z11-14. In the merged image, the same projections are superimposed. Scale bars = 10 µm.

3.5: Discussion

After photoreceptors transduce photon absorption into neurotransmitter release, BCs and HCs are the first retinal neurons to process the visual signal[23]. While the importance of these neurons is

well-appreciated, many of their functions are incompletely understood or unexplored altogether. Many BC and HC physiology studies would likely benefit from a flatmount retina preparation that improves access to INL neurons while preserving lateral connectivity. The development of the split retina method represents an effort to provide an easy protocol for acquiring high quality electrophysiological recordings and microscopy data from BCs and HCs in a flatmount orientation. The split retina preparation described here can be performed in about 20 min per mouse (10 min per retina) following retina isolation, without the use of specialized equipment. The method draws inspiration from existing photoreceptor removal procedures but offers significant improvements in simplicity, speed, and versatility[4,10–13]. Unlike previous methods for separating retinal layers, retina splitting does not require freezing, lyophilization, or repeated application of adhesives to the retina. With practice, nearly all photoreceptors can be removed in a single tear with the nitrocellulose membrane. The speed and ease of this approach allows one to minimize the time the retina spends out of carbogenated Ames, enabling high cell viability for long periods; split retinas can be maintained in carbogenated Ames media for several hours post-split. As a testament to the health of INL neurons in this preparation, a live/dead cell stain (**Figure 3-4**) and patch-clamp electrophysiology (**Figure 3-6**) confirm the viability of RBCs and HCs following a split.

The removal of the photoreceptor layer in split retinas conveys a significant advantage during immunolabeling by dramatically reducing the diffusion time for antibodies into the INL. Primary and secondary antibody labeling can be completed within 2 h, a substantial improvement to conventional flatmount staining which can take 72 h or longer depending on the target[5–8,20,22]. As a result, microscopy data can be acquired on the same day as tissue preparation, drastically accelerating the pace of immunofluorescence experiments. To facilitate mRNA probe annealing, FISH experiments typically recommend much longer fixation times (~24 h) than immunolabeling[18]. However, the experiments presented here demonstrate that a 2 h fixation still produces exceptional FISH labeling (**Figure 3-5**). Despite extending the fixation time from 30 min to 2 h, it was not necessary to perform antigen retrieval steps to obtain excellent immunolabeling, but this may vary with the antibody or antigen. The protease treatment in the FISH protocol may interfere with antibody labeling, likely due to the destruction of target epitopes. This issue was circumvented by using polyclonal antibodies that target multiple epitopes, decreasing the likelihood that epitope destruction would hinder immunolabeling. Additionally, a moderate

protease treatment (ACD protease III) was used to prevent excessive epitope alteration while still providing sufficient tissue penetration.

Occasionally, the retina will instead split through the outer nuclear layer (ONL), leaving behind layers of photoreceptor somas with no INL cells visible. To prevent this, one should ensure that the retina lies completely flat on the glass, and that any residual liquid from around the retina has been removed. Pressing more firmly onto the nitrocellulose with the paintbrush may also help prevent splitting through the ONL. If the membrane becomes too wet or the retina is folded over itself, the chances of a successful split will be greatly diminished. Using DAPI to stain cell nuclei is useful for assessing the quality of the split and for determining the coverage of remaining photoreceptors. Photoreceptor nuclei are smaller, brighter, and more superficial (**Supplementary Figure 3-S3A**), whereas BC nuclei are larger, dimmer, and deeper (**Supplementary Figure 3-S3B**). In some cases, the plane of the tear will vary slightly across the piece of retina, resulting in patches where photoreceptors cell bodies have not been completely removed (**Supplementary Figure 3-S3C**). For applications in microscopy and electrophysiology, this does not hinder the ability to collect quality data from regions where photoreceptors have been properly removed; large fields of exposed inner retina can easily be found when imaging or recording with a patch pipette. If more complete photoreceptor removal is desired, a second tear can be performed with an additional piece of nitrocellulose membrane, although 100% photoreceptor removal is not guaranteed. Caution is therefore advised when using split retinas in gene expression or proteomics studies where residual photoreceptor material could influence results. For single cell applications, this concern is unwarranted, as data from photoreceptors can be excluded from analysis.

The advantages of the split retina preparation are perhaps most salient in electrophysiological recordings of wide-field interneurons. Whereas traditional vertical slices sever the extensive processes of wide-field cells, the split retina preparation leaves the OPL and IPL intact, allowing one to capture input from wide-field cells such as HCs[24], A17s[25], TH ACs[26], and NOS-1 ACs[27] that would otherwise be overlooked in vertical slices. Therefore, interpretation of results and comparison with previous data collected from retinal slices requires careful thought. Nonetheless, in experiments using pharmacological mimics of light stimulation, these results resemble data recorded from retinal slices[19]. By expressing ChR2 under cell-specific promoters, one can

stimulate a desired cell population while recording from BCs in the INL to investigate the desired cell's impact on the vertical information pathway. Recording directly from deeper INL neurons, such as amacrine cells, is also feasible in the split retina. While in this case the patch electrode must first travel through the more superficial INL neurons, there is considerably less tissue obstructing its path when compared to a traditional whole mount preparation.

In addition to measuring the influence of wide-field cells on other neurons, this method enables direct single-cell patch clamping from HCs, whose dendrites form an extensive gap-junction coupled network in the OPL[28]. Horizontal cells send critical feedback to photoreceptors which shapes the transmission of vertical information through the retina. However, since the dendritic fields of HCs are truncated in vertical slices, single cell recording data are lacking. This work presents anatomically and physiologically intact HCs from which ChR2-evoked currents are recorded in a triple transgenic mouse line (**Figure 3-6, C-E**). Outside of ChR2 stimulation, the split retina can be used to study endogenous HC currents and gap junction coupling[28]. While the split retina provides a convenient model for studying synaptic connectivity and neuronal activity induced by chemical application or ChR2 stimulation, the lack of photoreceptors precludes any direct exploration of natural light responses or light adaptation mechanisms.

In situ imaging in the retina has made admirable progress in recent years. However, the majority of imaging studies are limited to the ganglion cell layer in whole mount retina preparations[29]. The authors envision that the absence of photoreceptors in the split retina will make it an ideal model for live calcium imaging in the OPL and INL. Beyond calcium imaging, this model has great potential for use with genetically encoded biosensors such as iGluSnFR[30,31], iGABASnFR[32], and pHluorin[33]. Combined with the split retina preparation, these powerful tools may offer an efficient approach to exploring the synaptic interactions and biophysical properties of BCs and HCs that contribute to light processing in the retina.

3.6: Acknowledgements

This work was supported by the following NIH grants: NIH grant R01EY031596 (to C.M.); NIH grant R01EY029985 (to C.M.); NIH grant P30EY010572 (to C.M.); NIH grant R01EY032564 (to

B.S.). We thank Tammie Haley for her technical support in preparing retina sections, and Dr. Charles Allen for generously contributing the mRNA FISH probes used in this work.

3.7: Supplemental Information

Materials list – Description of the materials required to perform the split retina procedure.

Name of Material/ Equipment	Company	Catalog Number	Comments/Description
#1.5 glass coverslips	Fisherbrand	12544E	
2 pairs of Dumont #5 forceps	Ted Pella	38125	
25-gauge needle	Becton Dickenson	305122	
470 nm LED	THORLABS	M470L2	
5-306 curved scissors	Miltex	5-306	
9" disposable Pasteur pipettes	Fisherbrand	13-678-20D	for constructing custom transfer pipette
Ai80d mouse	Jackson Laboratories	25109	RRID: IMSR_JAX:025109
Ames Medium w/L-Glutamate	US Biological	A1372-25	
amplifier control software	Molecular Devices	Clampex 10.3 software	
anti-calbindin D28K antibody	Invitrogen	PA-5 85669	RRID: AB_2792808, host species = rabbit; 1:100 dilution
anti-CtBP2 antibody	BD Biosciences	612044	RRID: AB_399431, host species = mouse; 1:5K dilution
anti-GPR179 antibody	NA	NA	gift from Kirill Martemyanov; Scripps Research Institute, Jupiter, FL; Orlandi et al., 2013; host species = sheep; 1:1K dilution
anti-PKC alpha antibody	Sigma-Aldrich	P4334	RRID: AB_477345, host species = rabbit; 1:5K dilution
anti-PKC alpha antibody	Santa Cruz Biotechnology	sc8393 AF594	RRID: AB_628142, host species = mouse; 1:1K dilution
anti-PSD95 antibody	BD Transduction Laboratories	610495	RRID: AB_397862, host species = mouse; 1:1K dilution
anti-RGS11 antibody	NA	NA	gift from Ted Wensel; Baylor College of Medicine, Houston, TX; Chen et al., 2003; host species = rabbit; between 1:1K and 1:5K dilution
anti-Synaptophysin P38 antibody	Sigma	S-S5768	RRID: AB_477523, host species = mouse; 1:1K dilution
Aquamount mounting media	Epredia	13800	"Slide mounting media"

C57BL/6J mouse	Jackson Laboratories	000664	RRID: IMSR_JAX:000664
carbogen tank	Matheson	NA	95% O_2 and 5% CO_2
custom transfer pipette	custom build	NA	Instructions: use scissors to cut off the tip of a plastic transfer pipette at the point it begins to taper. Use pliers to safely break off the last 2-3 inches of a glass Pasteur pipette. Fit the narrow end of the glass Pasteur pipette into the wide tip of the plastic transfer pipette. Wrap parafilm around the joint of the two pieces to enhance the seal.
Digital optical power meter	THORLABS	PM100D	
dissection microscope	Zeiss	Stemi 2000	
electrophysiology amplifier	Molecular Devices	Axopatch 200B	
electrophysiology microscope	Olympus	OLYMPUS, BX50WI	Dodt gradient contrast microscopy
Fluoromount-G	SouthernBiotech	0100-01	
HC PL APO CS2 40X/1.3	Leica	506358	
HC PL APO CS2 63×/1.40	Leica	15506350	
Hybridization oven	Robbins Scientific	Model 1000	for RNAscope protocol only
Immedge hydrophobic barrier pen	Vector Laboratories	H-4000	
isoflurane	Piramal Critical Care	66794-017-25	
Kimwipe (delicate task wipe)	Kimtech Science	34155	
Leica HC PL APO CS2 40X/1.3 oil immersion objective	Leica	506358	
Leica HC PL APO CS2 63×/1.40 oil immersion objective	Leica	15506350	
Leica TCS SP8 X confocal microscope	Leica	discontinued	
medium 15 mm petri dish	Corning	25060-60	eyes are kept here during retina dissection
Merit 97-275 steel scissors	Merit	97-275	
Micropipette Puller	Sutter Instrument	p-97	
Mm-Gabrd-C2 mRNA probe	ACD	459481-C2	

mouse euthanasia chamber	NA	NA	custom build; glass petri dish covering a small glass jar.
nitrocellulose membrane filters	GE Healthcare Life Sciences; Whatman	7184-005	0.45 µm pore size
Picospritzer	General Valve Corporation	Picospritzer II	referred to in the text as "microcellular injection unit"
plastic transfer pipets	Fisherbrand	13-711-7M	for constructing custom transfer pipette
Plastic tubing	Tygon	R-603	for connection to carbogen tank
platinum harp	custom build	NA	for anchoring split retinas within the electrophysiology recording chamber.
size 0 paint brush	generic	NA	for flattening retina during splitting.
SlowFade Gold antifade reagent	Molecular Probes	S36937	referred to in the text as "anti-fade mounting media"
small 10 mm petri dish	Falcon	353001	eyes are placed here following enucleation
small glass pane (7.5 x 5 cm)	generic	NA	isolated retina pieces are placed onto this for the splitting procedure
Superfrost plus microscope slides	Fisherbrand	12-550-15	electrostatically charged glass microscope slides
Thick-walled borosilicate glass pipettes with filament	Sutter Instrument	BF150-86-10HP	
Vannas Scissors; straight	Titan Medical	TMS121	not brand specific; any comparable scissors will work
vGATFLPo mouse	Jackson Laboratories	29591	RRID: IMSR_JAX:029591
vGlut2Cre mouse	Jackson Laboratories	28863, 016963	RRID: IMSR_JAX:028863, RRID: IMSR_JAX:016963
Zombie NIR Fixable Viability Kit	BioLegend	423105	referred to in the text as "MI-NIR"

Figure[3-S1]

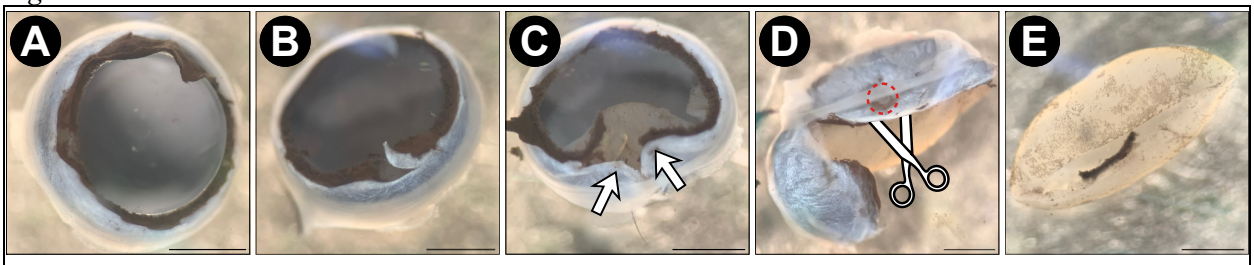

[3-S1] **Key stages of the retina dissection**. All images were taken with a smartphone camera mounted to the ocular lenses of a dissection microscope. (**A**) A top-down image of a mouse eye following removal of the cornea. (**B**) A

top-down image of the mouse eyecup after the lens has been removed. (**C**) A small incision is made in the sclera on the mouse eyecup. Arrows indicate the two flaps of the sclera which are pulled in opposite directions by forceps to begin separating the retina from the sclera. (**D**) After the sclera has been partially pulled away from the retina, Vannas scissors are inserted between the sclera and the retina, and the optic nerve is severed, freeing the retina. The red dotted circle shows the optic nerve head, and the scissors demonstrate the correct cutting trajectory (insert scissors between the sclera and the retina). The isolated retina after the sclera is pried away.

Figure[3-S2]

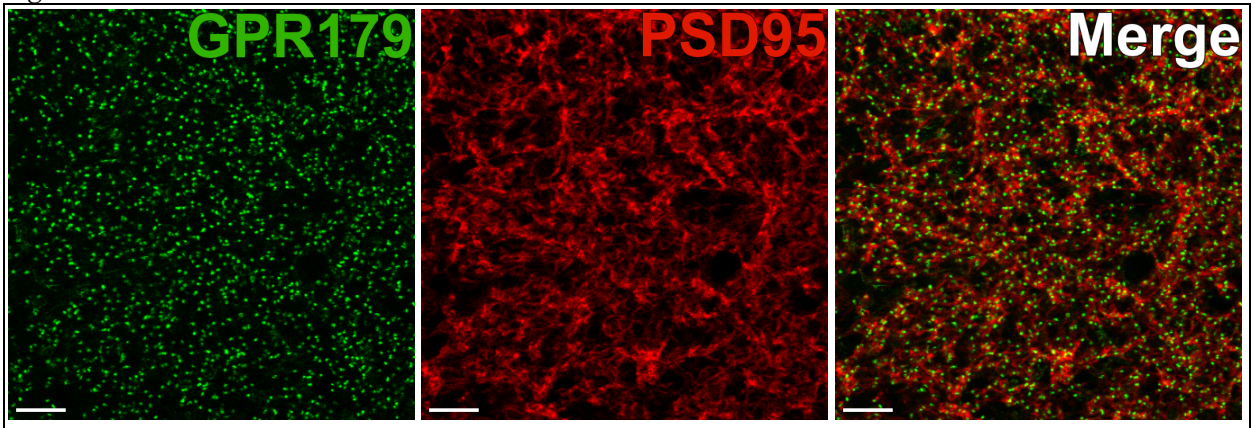

[3-S2] **Characterization of pre- and post-synaptic components of the OPL in the split retina**. Confocal immunofluorescence images from the OPL in a split retina. The split retina was incubated with antibodies against GPR179 and PSD95 for 1 h at room temperature to label to the dendritic tips of ON-BCs and the terminals of rod photoreceptors, respectively. The left and center images are maximum projections of several optical sections; the same projections are superimposed in the rightmost image. GPR179 puncta in the ON-BC dendritic tips are seen to associate closely with the rod photoreceptor terminals, demonstrating intact synaptic contacts within the OPL. Scale bars = 10 μm.

Figure[3-S3]

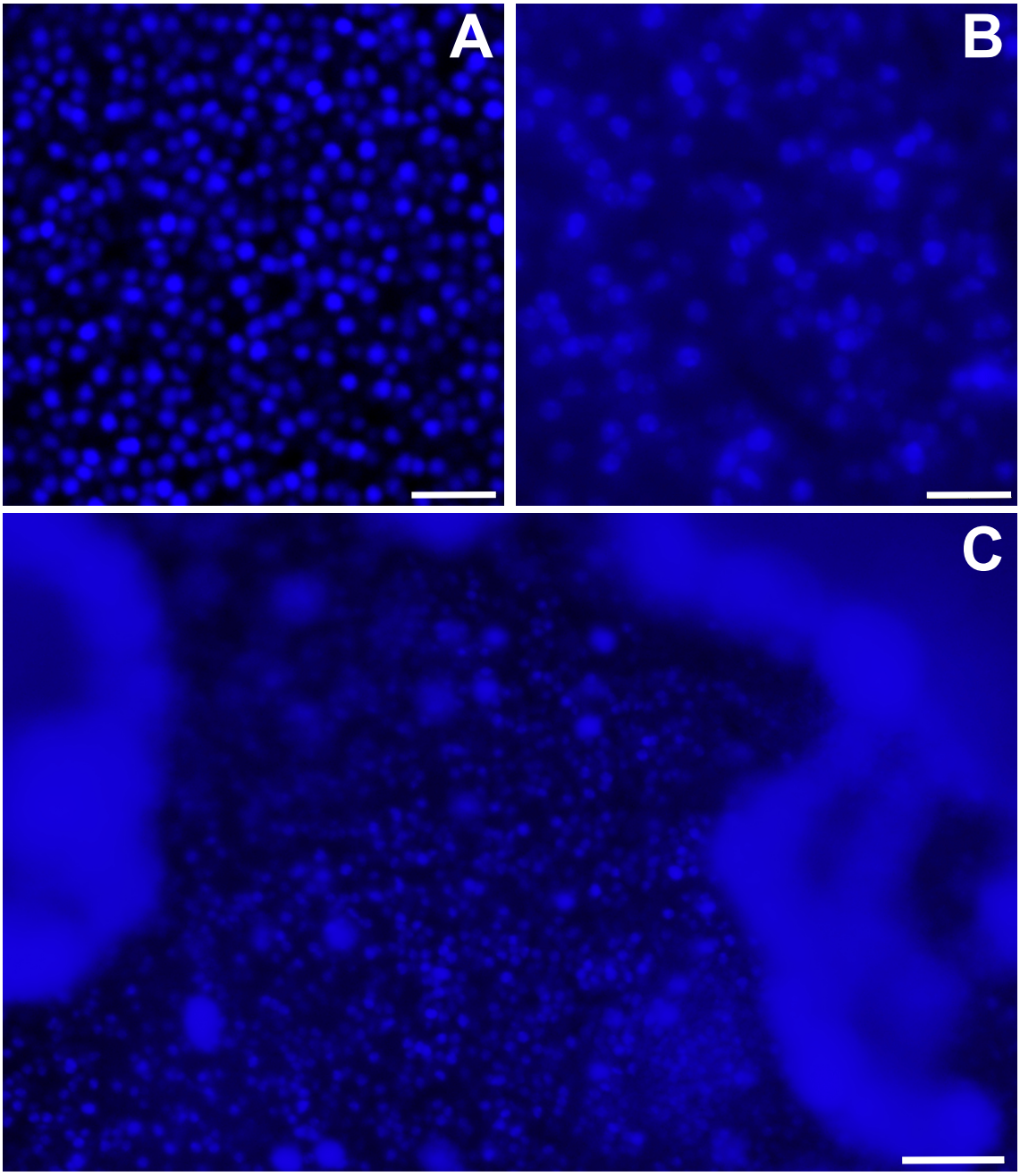

[3-S3] **Troubleshooting: assessing the quality of a split retina**. Fluorescent micrographs of a split retina stained with DAPI to visualize cell nuclei. Cells can be identified based on the diameter and tissue depth of the nucleus. (**A**) Photoreceptor nuclei are smaller, brighter, and more superficial, whereas (**B**) BC nuclei are larger, dimmer, and deeper. (**C**) A low magnification image of a region where photoreceptors were incompletely removed. The nuclei that appear in focus are from BCs, which are deeper than the photoreceptor nuclei on the edges of the image that appear out of focus. Scale bars for (A) and (B) = 20 µm. Scale bar for (C) = 50 µm.

Chapter 3 Bibliography

1. Morgans, C. W. Neurotransmitter release at ribbon synapses in the retina. *Immunology & Cell Biology* **78**, 442–446 (2000).

2. Euler, T., Haverkamp, S., Schubert, T. & Baden, T. Retinal bipolar cells: elementary building blocks of vision. *Nat Rev Neurosci* **15**, 507–519 (2014).

3. Barnes, S., Grove, J. C. R., McHugh, C. F., Hirano, A. A. & Brecha, N. C. Horizontal Cell Feedback to Cone Photoreceptors in Mammalian Retina: Novel Insights From the GABA-pH Hybrid Model. *Frontiers in Cellular Neuroscience* **14**, (2020).

4. Walston, S. T., Chang, Y.-C., Weiland, J. D. & Chow, R. H. Method to remove photoreceptors from whole mount retina in vitro. *Journal of Neurophysiology* **118**, 2763–2769 (2017).

5. Stefanov, A., Novelli, E. & Strettoi, E. Inner retinal preservation in the photoinducible I307N rhodopsin mutant mouse, a model of autosomal dominant retinitis pigmentosa. *Journal of Comparative Neurology* **528**, 1502–1522 (2020).

6. Matsuoka, R. L. *et al.* Transmembrane semaphorin signaling controls laminar stratification in the mammalian retina. *Nature* **470**, 259–263 (2011).

7. Matsuoka, R. L. *et al.* Guidance-Cue Control of Horizontal Cell Morphology, Lamination, and Synapse Formation in the Mammalian Outer Retina. *J. Neurosci.* **32**, 6859–6868 (2012).

8. Wässle, H., Puller, C., Müller, F. & Haverkamp, S. Cone Contacts, Mosaics, and Territories of Bipolar Cells in the Mouse Retina. *J. Neurosci.* **29**, 106–117 (2009).

9. Thoreson, W. B. & Dacey, D. M. Diverse Cell Types, Circuits, and Mechanisms for Color Vision in the Vertebrate Retina. *Physiological Reviews* **99**, 1527–1573 (2019).

10. Guido, M. E. *et al.* A simple method to obtain retinal cell preparations highly enriched in specific cell types. Suitability for lipid metabolism studies. *Brain Research Protocols* **4**, 147–155 (1999).

11. Rose, K., Walston, S. T. & Chen, J. Separation of photoreceptor cell compartments in mouse retina for protein analysis. *Mol Neurodegeneration* **12**, 28 (2017).

12. Todorova, V. *et al.* Retinal Layer Separation (ReLayS) method enables the molecular analysis of photoreceptor segments and cell bodies, as well as the inner retina. *Sci Rep* **12**, 20195 (2022).

13. Shiosaka, S., Kiyama, H. & Tohyama, M. A simple method for the separation of retinal sublayers from the entire retina with special reference to application for cell culture. *Journal of Neuroscience Methods* **10**, 229–235 (1984).

14. Ivanova, E., Hwang, G.-S. & Pan, Z.-H. Characterization of transgenic mouse lines expressing Cre-recombinase in the retina. *Neuroscience* **165**, 233–243 (2010).

15. Sarria, I., Orlandi, C., McCall, M. A., Gregg, R. G. & Martemyanov, K. A. Intermolecular Interaction between Anchoring Subunits Specify Subcellular Targeting and Function of RGS Proteins in Retina ON-Bipolar Neurons. *J Neurosci* **36**, 2915–2925 (2016).

16. Orlandi, C., Cao, Y. & Martemyanov, K. A. Orphan Receptor GPR179 Forms Macromolecular Complexes With Components of Metabotropic Signaling Cascade in Retina ON-Bipolar Neurons. *Invest Ophthalmol Vis Sci* **54**, 7153–7161 (2013).

17. Dikshit, A., Zong, H., Anderson, C., Zhang, B. & Ma, X.-J. Simultaneous Visualization of RNA and Protein Expression in Tissue Using a Combined RNAscope™ In Situ Hybridization and Immunofluorescence Protocol. *Methods Mol Biol* **2148**, 301–312 (2020).

18. Wang, F. *et al.* RNAscope. *J Mol Diagn* **14**, 22–29 (2012).

19. Morgans, C. W. *et al.* TRPM1 is required for the depolarizing light response in retinal ON-bipolar cells. *PNAS* **106**, 19174–19178 (2009).

20. Alessio, E. & Zhang, D.-Q. Immunostaining of whole-mount retinas with the CLARITY tissue clearing method. *Investigative Ophthalmology & Visual Science* **61**, 5054 (2020).

21. Ferguson, L. R., Dominguez II, J. M., Balaiya, S., Grover, S. & Chalam, K. V. Retinal Thickness Normative Data in Wild-Type Mice Using Customized Miniature SD-OCT. *PLoS One* **8**, e67265 (2013).

22. Ivanova, E., Toychiev, A. H., Yee, C. W. & Sagdullaev, B. T. Optimized Protocol for Retinal Wholemount Preparation for Imaging and Immunohistochemistry. *J Vis Exp* 51018 (2013) doi:10.3791/51018.

23. Kolb, H. Neurotransmitters in the Retina. in *Webvision: The Organization of the Retina and Visual System* (eds. Kolb, H., Fernandez, E. & Nelson, R.) (University of Utah Health Sciences Center, Salt Lake City (UT), 1995).

24. Chaya, T. *et al.* Versatile functional roles of horizontal cells in the retinal circuit. *Sci Rep* **7**, 5540 (2017).

25. Egger, V. & Diamond, J. S. A17 Amacrine Cells and Olfactory Granule Cells: Parallel Processors of Early Sensory Information. *Front Cell Neurosci* **14**, 600537 (2020).

26. Dacey, D. M. The dopaminergic amacrine cell. *J Comp Neurol* **301**, 461–489 (1990).

27. Park, S. J. *et al.* Connectomic analysis reveals an interneuron with an integral role in the retinal circuit for night vision. *eLife* **9**, e56077 (2020).

28. Janssen-Bienhold, U. *et al.* Connexin57 is expressed in dendro-dendritic and axo-axonal gap junctions of mouse horizontal cells and its distribution is modulated by light. *J Comp Neurol* **513**, 363–374 (2009).

29. Jain, V. *et al.* The functional organization of excitation and inhibition in the dendrites of mouse direction-selective ganglion cells. *Elife* **9**, e52949 (2020).

30. Marvin, J. S. *et al.* Stability, affinity, and chromatic variants of the glutamate sensor iGluSnFR. *Nat Methods* **15**, 936–939 (2018).

31. Strauss, S. *et al.* Center-surround interactions underlie bipolar cell motion sensitivity in the mouse retina. *Nat Commun* **13**, 5574 (2022).

32. Marvin, J. S. *et al.* A genetically encoded fluorescent sensor for in vivo imaging of GABA. *Nat Methods* **16**, 763–770 (2019).

33. Beckwith-Cohen, B., Holzhausen, L. C., Wang, T.-M., Rajappa, R. & Kramer, R. H. Localizing Proton-Mediated Inhibitory Feedback at the Retinal Horizontal Cell-Cone Synapse with Genetically-Encoded pH Probes. *J Neurosci* **39**, 651–662 (2019).

Chapter 4

A Mechanistic Characterization of Antibody Internalization in Retinal ON-Bipolar Cells

Ryan M. Mosavi-Hecht[1], Robert M. Duvoisin[1], and Catherine W. Morgans[1,2]

[1]Department of Chemical Physiology and Biochemistry, Oregon Health and Science University, Portland, OR 97239, USA

[2]Casey Eye Institute, Oregon Health and Science University, Portland, OR 97239, USA

Pending submission to *Neurology: Neuroimmunology & Neuroinflammation*

DOI: *pending*

4.0: Preface

Like other studies before it, **Chapter 2** presented a case of MAR in which the patient produced autoantibodies against the intracellular N-terminus of TRPM1. This observation insinuates that MAR symptoms can only manifest if TRPM1 autoantibodies first penetrate the cytoplasm of ON-BCs. As **Chapter 1** illustrates, there is an enormous knowledge gap and surprising paucity of experiments aimed at understanding the mechanism of antibody internalization in neurons, despite obvious therapeutic relevance. The chapter that ensues is an attempt to remedy this issue. As the first study to address antibody internalization mechanisms in neurons since 2019, and the very first to do so in MAR, this investigation illuminates novel aspects of ON-BC biology that further our collective understanding of MAR pathogenesis and, more broadly, neuronal antibody uptake.

The split retina model introduced in **Chapter 3** provided the foundation for this study by offering a simple yet physiological platform for studying inner retinal neurons such as ON-BCs. Here, its originally design as a model for antibody internalization is fully realized, enabling an unprecedented glimpse into the behavior of living ON-BCs. By pharmacologically inhibiting endocytic pathways and treating split retinas with antibodies against several intracellular ON-BC proteins, we make valuable progress toward understanding the antibody uptake in MAR. Validating the need for further investigation into antibody uptake mechanisms in neurons, we find that ON-BCs use distinct strategies for internalizing antibodies.

4.1: Abstract

Background and Objectives: Autoantibodies directed against intracellular antigens are a hallmark feature of many paraneoplastic syndromes. While recognized for their diagnostic utility, they are often considered to be non-pathogenic compared to autoantibodies directed against cell surface antigens. However, in some diseases, such as melanoma-associated retinopathy (MAR), autoantibodies against intracellular antigens directly cause disease symptoms. MAR patients experience vision impairment from autoantibodies that target intracellular epitopes on an ion channel called TRPM1, expressed in retinal ON-bipolar cells (ON-BCs). Several studies have reported that TRPM1 autoantibodies become internalized by ON-BCs, enabling them to bind the channel's intracellular domains and inhibit its activity. However, the mechanism by which these

autoantibodies enter ON-BCs remains undiscovered. In this study, we endeavored to characterize the nature of autoantibody entry into ON-BCs.

Methods: Using a freshly isolated split retina mouse preparation, we visualized and characterized the internalization of antibodies in ON-BCs with confocal microscopy. Through the use of pharmacological inhibitors, genetic animal models, and biochemical alteration of antibody structure, we examined the cellular requirements for antibody internalization in ON-BCs.

Results: We found that antibodies targeting multiple intracellular proteins are internalized by ON-BCs using a dynamin-dependent, clathrin-independent endocytic pathway. Robust antibody internalization and target binding is visible after 1 hour of incubation. Additionally, these antibodies do not require engagement with their target antigen or Fc receptors for internalization, suggesting the involvement of a non-specific, bulk endocytosis mechanism. Lastly, we observed antibody internalization in horizontal cells, indicating that ON-BCs are not the only retinal neurons capable of antibody uptake.

Discussion: Our results demonstrate that ON-BCs efficiently internalize antibodies to intracellular antigens using a receptor- and antigen-independent pathway. We propose that internalized antibodies which bind an intracellular antigen are stabilized and protected from rapid degradation. This study provides a useful foundation for determining the antibody internalization mechanisms underlying other paraneoplastic syndromes. Furthermore, the capacity of retinal neurons to internalize antibodies offers novel therapeutic possibilities for the targeted delivery of antibody-drug conjugates to treat retinal diseases and possibly other neurological conditions.

4.2: Introduction

The role of autoantibodies in neurological disorders has recently garnered attention following new findings regarding their contribution to pathological processes[1,2]. In the context of paraneoplastic autoimmunity, the presence of self-protein targeting antibodies in the serum or cerebral spinal fluid is evidence of an anti-cancer immune response, and often precedes the detection of an underlying tumor[3,4]. Beyond their diagnostic value as disease biomarkers, autoantibodies can directly and indirectly disrupt neuronal function through binding to neuronal antigens[5,6]. One such disease

where autoantibodies directly impair neuronal activity is melanoma-associated retinopathy (MAR), a rare paraneoplastic syndrome that causes visual impairment in individuals with cutaneous melanoma (CM)[7,8]. MAR symptoms (nyctalopia, photopsia, and diminished contrast sensitivity) are caused by an antibody-mediated immune response against an ion channel called TRPM1, expressed by retinal ON-bipolar cells (ON-BCs)[9,10]. In the dark, the G-proteins $G\alpha_o$ and $G\beta\gamma$ maintain TRPM1 in the closed state while their upstream metabotropic glutamate receptor, mGluR6, remains activated by the tonic release of glutamate from the photoreceptors. In response to light, the photoreceptors slow their rate of glutamate release, deactivating mGluR6 and the G-proteins, which enables TRPM1 channel opening and subsequent ON-BC depolarization[11,12]. In MAR, TRPM1 autoantibodies bind the channel and block its activity, preventing ON-BC depolarization, which causes MAR's visual symptoms[10,13,14].

Outside of the retina, TRPM1 is expressed in melanocytes, the pigment producing cells of the skin that become cancerous in CM[15,16]. The precise trigger for autoantibody production against TRPM1 is unknown; however, the autoantibodies are believed to form part of the immune response against CM tumors[17,18]. In CM and other cancers, some isotypes of autoantibodies against tumor antigens correlate positively with disease outcomes[19–21], presumably due to the immune effector functions they initiate by engaging malignant cells. However, paraneoplastic syndromes like MAR arise when the autoantibodies reach targets in healthy, peripheral tissues[22,23]. Previous studies examining the target epitopes of MAR autoantibodies revealed that, across all patients tested, the autoantibodies bind exclusively to intracellular domains of TRPM1[24–26]. A notable implication of this discovery is that TRPM1 autoantibodies must cross the plasma membrane of ON-BCs to reach their target and cause MAR symptoms. While antibody uptake induced by binding to surface antigens is well documented[27–29], the mechanism of endocytosis is not fully understood. Furthermore, how antibodies that only recognize *intracellular* antigens could engage the cell and become internalized remains a mystery.

TRPM1 autoantibody internalization by ON-BCs has been reproduced experimentally in mouse retinas, both in transverse slices[10] and dissociated neural cultures[13]. However, previous studies have not investigated the cellular mechanisms responsible for this phenomenon. Furthermore, disadvantages inherent in these model systems limit their usefulness in evaluating the underlying

mechanism. Retinal slices, for example, contain cells that were severed during cutting, enabling antibodies to passively diffuse into the damaged cell and bypass endocytic pathways. Similarly, preparation of dissociated neuronal cultures using proteases and mechanical disruption can amputate cell structures, such as dendrites and axons, that may be critical sites of endocytosis. Even when undamaged, dissociated cells are removed from their endogenous context within the tissue, which may alter their default behavior.

Here, we present a detailed examination of the mechanisms underlying antibody internalization in ON-BCs using the split retina model[30] that boasts high physiological relevance, simple preparation, and minimal perturbation to cellular structures. We demonstrate that ON-BCs internalize antibodies using dynamin-dependent endocytosis, and that uptake is not unique to TRPM1 antibodies. Our evidence points to a dynamin-dependent, clathrin-independent mechanism such as fast endophilin-mediated endocytosis (FEME) for uptake, although more specific pharmacological inhibitors or genetic tools are required to verify a precise mechanism. These findings may provide clues to the pathogenic mechanisms of other paraneoplastic syndromes and autoimmune disorders with autoantibodies directed against intracellular antigens.

4.3: Materials & Methods

Animals

Adult mice (>3 months, male and female) from one transgenic and three knockout strains were used in the live antibody uptake experiments. The Grm6-tdTomato line expresses tdTomato under a ~9 kb fragment of the mGluR6 promoter, resulting in red fluorescence in ON-BCs[31]. The PKCα-KO line contains a neomycin resistance cassette inserted into the ATP-binding region of PKCα, rendering a global knockout[32] (The Jackson Laboratory; Bar Harbor, ME; B6:129-Pkrca (tm1Jmk)/J; RRID:IMSR_JAX:00906). Beta 2 microglobulin (B2M) knockout mice (The Jackson Laboratory; Bar Harbor, ME; RRID: IMSR_JAX:002087) were used to determine the involvement of MHC Class I in antibody internalization. Male and female C57BL6 mice (The Jackson Laboratory; Bar Harbor, ME; RRID: IMSR_JAX:000664) over 3 months of age were used as wild type animals. For the validation of target specificity during anti-TRPM1 monoclonal antibody development, TRPM1 KO mice were used[12]. The animal study was approved by OHSU

Institutional Animal Care and Use Committee. The study was conducted in accordance with the local legislation and institutional requirements.

TRPM1 antibody development

Two overlapping segments of the TRPM1 N-terminus (exons 2-7 and exons 6-10; NM_001252020.2; **Supplemental Table 4-S1**) were cloned from human M14 melanoma cells, then expressed in *E. coli* (Novagen (Sigma-Aldrich); Burlington, MA, USA; *pET-28a(+)*, Cat#: 69864) and the resulting his-tagged polypeptides were purified on a nickel column (Qiagen; Venlo, Netherlands; Ni-NTA Agarose; Cat#: 30210). Mice were immunized four times, three weeks apart, with the purified TRPM1 polypeptides in a Freund's adjuvant mixture. Serum from the immunized animals was used to confirm a positive immune response to TRPM1 by ELISA prior to splenic harvest and generation of hybridomas. Individual hybridoma clones were screened for reactivity with the purified TRPM1 proteins by ELISA. Supernatants from select clones were additionally screened for reactivity with TRPM1 in transfected HEK293T cells and mouse retina sections. Specificity for TRPM1 was confirmed with TRPM1 KO animals. Finally, monoclonal antibodies were isotyped (Thermo Fisher; Waltham, MA; Pro-Detect™ Rapid Antibody Isotyping Assay Kit, mouse; Cat#: A38550) and purified from the hybridoma supernatants with protein G sepharose columns (Cytiva; Marlborough, MA; Cat#: 17040401).

Cell culture, transfection, and immunocytochemistry

HEK293T cells were cultured in Dulbecco's modified eagle medium (DMEM, 10% fetal bovine serum, penicillin, and streptomycin) and maintained at 37 ºC and 5% CO_2 in a tissue culture incubator. Cells were seeded onto acid-washed glass cover slips coated in polylysine (Sigma-Aldrich; Burlington, MA; Cat#: p4707). For transient transfections, the same TRPM1 sequences used for antibody development were subcloned into pEGFP-C3 vectors (Clontech (NovoPro); Mountain View, CA; Cat#: V012022) and delivered to cells using Effectene (Qiagen; Venlo, Netherlands; Cat#: 301425) to produce TRPM1 polypeptides with EGFP fused to their N-termini. Twenty-four hours post transfection, the cells were fixed with 4% paraformaldehyde for 5 minutes at room temperature, then washed 3 times in PBS. The fixed cells were then incubated with B cell hybridoma supernatants for 1 hour at room temperature, followed by another 3 washes in PBS. The cells were next incubated for 1 hour at room temperature with an anti-mouse secondary antibody conjugated to Alexa Fluor 594. All antibodies and B cell hybridoma supernatants were

diluted into antibody incubation solution (AIS; 3% horse serum, 0.5% Triton X-100, 0.025% NaN_3 in PBS). Cell nuclei were stained with DAPI for 30 seconds, and after a final PBS wash the coverslips were placed onto slides (Superfrost Plus; Fisher Scientific; Waltham, MA; Cat#: 1255015) with an aqueous mounting medium (Epredia; Portsmouth, New Hampshire; Cat#: 13800).

Transferrin uptake assay

The assay was modified from the previously described protocol[33]. Briefly, HEK293T cells were seeded onto acid-washed glass cover slips coated in polylysine at a density of ~60% confluence. Prior to the assay, the cells were starved in serum-free DMEM for 16-24 hours to synchronize their cell cycles. Drugs were diluted into DMEM with 1% DMSO and added to cells for 15 minutes in a tissue culture incubator. Alexa Fluor 488-labeled transferrin (Jackson ImmunoResearch; West Grove, PA; Cat#: 015-540-050) was added at a final concentration of 5 µg/mL, and cells were allowed to internalize the compound for 15 minutes in the tissue culture incubator. The cells were washed once in DMEM, then washed again for 15 minutes in ice-cold acid wash buffer (0.2 M acetic acid; 0.5 M NaCl; pH 2.8) for 15 minutes to remove membrane bound transferrin. The cells were then washed once in PBS before fixation with 4% PFA for 5 minutes at room temperature. After three more washes in PBS, cell nuclei were stained with DAPI for 30 seconds, and cells were washed for a final time in PBS before being mounted onto microscope slides with aqueous mounting medium.

Retina section preparation and immunofluorescent labeling

Retinal cryosections were prepared as described previously[12]. Antibodies (IgG or Fabs) were diluted into AIS and incubated with the tissue for 1 hour at room temperature. After three washes in room temperature PBS, the tissue was incubated with secondary antibodies conjugated to Alexa Fluor 488 (Supplemental Table 2) Jackson ImmunoResearch; West Grove, PA; RRID: AB_2338841, AB_2632468) diluted into AIS (1:1000) for 1 hour at room temperature. The tissue was washed thrice more in room temperature PBS, cell nuclei were labeled with DAPI, and the tissue was washed again in PBS. Finally, coverslips were mounted onto the samples and results were visualized using confocal microscopy.

Drug preparation and Fab generation

Drug-induced toxicity was monitored using a viability dye (Zombie Violet; BioLegend; San Diego, CA; Cat#: 423113). Drugs were prepared in DMSO, then diluted to their final concentration in either 0.5% or 1% DMSO in Ames media or DMEM. Solutions were equilibrated to 37 ºC in a tissue culture incubator for ≥ 30 minutes prior to the start of the antibody uptake assay. To produce antigen binding fragments (Fabs) from anti-PKCα polyclonal rabbit IgG, serum proteins were removed (Thermo Fisher Scientific; Waltham, MA; Cat#: 44600) and the remaining IgG were digested with papain, then Fabs were purified over protein A columns (Thermo Fisher Scientific; Waltham, MA; Cat#: 44985). The purity of the Fabs was confirmed by SDS-PAGE, and their activity was validated by labeling PKCα fixed retinal cryosections using a Fab-specific secondary antibody conjugated to Alexa Fluor 488.

Protein gel electrophoresis

To confirm the purity of the Fab fragments, the digested IgG samples were separated by SDS-PAGE under reducing conditions and visualized by Coomassie staining. First, the samples were boiled at 98 ºC for 5 minutes to reduce and denature the IgG and Fabs. Samples were diluted into a loading solution containing a reducing agent (Thermo Fisher Scientific; Waltham, MA; Cat#: NP0009) and separated by electrophoresis on a 4-12% gradient bis-tris gel (Thermo Fisher Scientific; Waltham, MA; Cat#: NP0322BOX) for 75 minutes in MOPS buffer on ice (175V). Afterward, the gel was incubated in Coomassie stain (Coomassie brilliant blue R250, 3.03 mM; MeOH, 50%; acetic acid, 10%, dH_2O, 40%) for 1 hour at room temperature, and destained (MeOH, 40%; acetic acid, 10%; dH_20, 50%) for 2 hours at room temperature.

Retina slice preparation and antibody uptake assay

Freshly dissected mouse retinas were embedded in 3% agarose (in PBS) and 250 μm thick slices were cut on a vibratome. Live retinal slices were added to microfuge tubes containing Ames medium with diluted antibodies for 1 hour on a heat block at 37 ºC. Slices were then washed once in room temperature PBS and fixed in 4% PFA for 5 minutes at room temperature. After 3 washes in room temperature PBS, the slices were incubated with Alexa Fluor-labeled secondary antibodies diluted in AIS. The slices were washed once with room temperature PBS, stained with DAPI for 30 seconds, and washed thrice more in PBS. Finally, coverslips were mounted using an aqueous mounting media.

Split retina live antibody uptake assay

The photoreceptor outer segments and cell bodies were removed from freshly dissected mouse retinas as described previously[30]. The membrane containing the photoreceptor terminals and the inner retinal neurons (henceforth referred to as "split retina") was placed in a beaker of continuously carbogenated, room temperature (95% O_2, 5% CO_2) Ames medium (US Biological; Salem, MA; Cat# A1372-25). Split retinas were allowed to recover in carbogenated, room temperature Ames medium for 15 minutes. To prevent any precipitation of hydrophobic drug compounds upon contacting the aqueous interface of the retinal tissue, split retinas were briefly dipped into 37 ºC Ames medium containing 1% DMSO. The split retinas were then dabbed on a delicate task wipe (contacting only the attached nitrocellulose membrane) to remove excess moisture. Subsequently, the split retinas were placed in wells of a 12-well tissue culture plate and incubated in 1% DMSO in Ames medium, with or without an inhibitor compound, for 15 minutes in a tissue culture incubator (37 ºC, 5% CO_2). The split retinas were again dabbed on delicate task wipes, then transferred to wells containing the same solutions, now spiked with anti-TRPM1 or anti-PKCα antibodies or Fabs (**Supplemental Table 4-S2**), and incubated for 1-2 hours in the tissue culture incubator. Afterward, the split retinas were washed by transfer to new wells containing 37 ºC Ames medium. The pre-warmed Ames medium was aspirated, and the samples were washed twice more with room temperature Ames medium. Next, the samples were incubated for 15 minutes in room temperature Ames medium containing a fixable viability dye diluted 1:2K. The samples were washed 3 times in room temperature PBS, then fixed in 4% paraformaldehyde for 30 minutes at 4 ºC. The samples were washed 3 times in room temperature PBS, then incubated with Alexa Fluor 488-conjugated anti-mouse or anti-rabbit secondary antibodies (**Supplemental Table 4-S2**) for 1 hour at room temperature to visualize the internalized TRPM1 or PKCα antibodies. An antibody incubation solution containing detergent (AIS) was used as the secondary antibody diluent to permeabilize the cell membranes, allowing access to the previously internalized antibodies. After 3 washes in room temperature PBS, the split retinas were removed from the nitrocellulose membranes[30] and mounted onto microscope slides with #1.5 coverglass (Fisherbrand; Waltham, MA; Cat#: 12544E) and an aqueous mounting medium.

Confocal imaging

Images were acquired on a Leica TCS SP8 X or Stellaris 8 white light laser confocal microscope (Leica; Wetzlar, Germany) using HC PL APO CS2 40X/1.3 (Leica; Wetzlar, Germany; Cat#

506358) or HC PL APO CS2 63X/1.40 (Leica; Wetzlar, Germany; Cat# 15506350) objectives. Acquisition regions on split retina tissue were selected based on the following criteria: the tissue is level with no severe sloping; minimal levels of cell death are observed in ON-BCs; dendritic processes of ON-BCs are visible by Td-tomato expression; no remaining photoreceptors obstruct the imaging region; the expected density of ON-BCs is observed; cells appear intact, and morphology is as expected.

Quantification and statistics

Antibody internalization was quantified using a custom Arivis (Zeiss; Oberkochen, Germany) analysis pipeline. A subset of images from split retina antibody internalization experiments was used to train a machine learning model to detect true antibody uptake signal while excluding signal associated with dead cells and antibody aggregation artifacts (**Supplemental Figure 4-S1**). The Cellpose algorithm was used to identify and count the number of ON-BCs in each image[34,35], and the summed pixel intensities in the antibody uptake channel were divided by the average number of ON-BCs to produce an "average uptake per cell." The Shapiro-Wilk test was applied to test for normality within each data set. For comparison of means in normally distributed data with two conditions, Welch's unpaired t-test was applied. Comparison of means in non-parametric data was done using the Mann-Whitney U test followed by a post-hoc pairwise Wilcox test.

4.4: Results

4.4.1 Antibodies targeting intracellular epitopes are internalized by ON-BCs in transverse slices and split retinas

We first used a conventional live retinal slice model to establish that antibodies targeting intracellular epitopes are internalized by ON-BCs. To achieve this, we generated a monoclonal antibody against a region of the intracellular TRPM1 N-terminus. In HEK293T cells transiently transfected with recombinant TRPM1 – the same construct used to produce the antibody immunogen – the antibody specifically labeled transfected cells (**Supplemental Figure 4-S2**). As further validation of its specificity, the antibody selectively labeled bipolar cells in cryosections from wild type mouse retinas (**Supplemental Figure 4-S3A**), but not TRPM1 KO mouse retinas (**Supplemental Figure 4-S3B**). In live slices of mouse retina incubated with the TRPM1

monoclonal antibody, evidence of uptake was visible in the dendrites and cell bodies of rod bipolar cells (RBCs) – the most abundant subtype of ON-BC in the mouse retina (**Figure 4-1A**). To investigate whether antibodies targeting other intracellular ON-BC proteins become internalized, we used an antibody against PKCα, a cytosolic kinase often used as a marker for RBCs[36]. Indeed, internalized PKCα antibodies were prominently visible in the dendrites and cell bodies of RBCs (**Figure 4-1A**), revealing that antibody uptake is not unique to TRPM1 antibodies. Dead cells with compromised membranes were identified using a fixable viability dye (Zombie; blue). Cells that internalized TRPM1 antibodies but were negative for PKCα labeling were presumed cone ON-BCs. Next, we examined antibody uptake in the split retina model using antibodies against PKCα and an intracellular epitope of GPR179, a G protein coupled receptor localized to the dendritic tips of ON-BCs. Both antibodies were internalized by ON-BCs and were localized according to the expected distribution of the target proteins (**Figure 4-1B**). Furthermore, ON-BCs internalized antibodies targeting the transgenic fluorescent marker protein, Td tomato, revealing their capacity to internalize antibodies against non-endogenous proteins (**Figure 4-1B**). Due to their easily detectable uptake signal and the fact that their protein target is entirely cytosolic, we elected to use antibodies against PKCα to further characterize antibody internalization in the split retina model.

Figure[4-1]

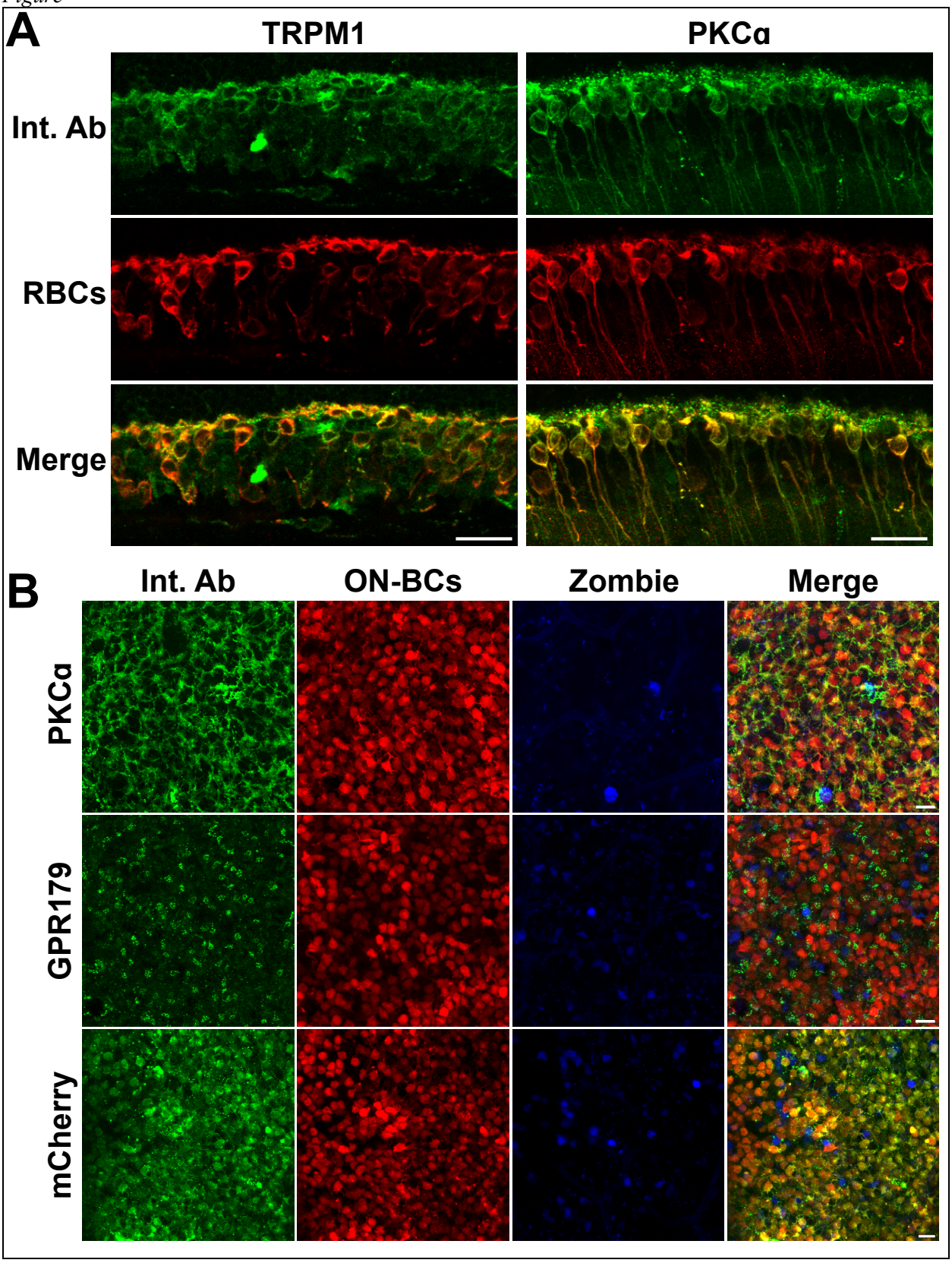
A
TRPM1
PKCα
Int. Ab
RBCs
Merge
B
Int. Ab
ON-BCs
Zombie
Merge
PKCα
GPR179
mCherry

4-1 Antibodies targeting intracellular epitopes are internalized by ON-BCs in transverse slices and split retinas. (**A**) Maximum projections from confocal micrographs of a 250 µm-thick mouse retina slice after a 1-hour incubation with a monoclonal anti-TRPM1 antibody diluted 1:500 in Ames medium. After fixing and permeabilizing the tissue, internalized anti-TRPM1 antibodies were visualized with an anti-mouse, Alexa Fluor 488-labeled secondary antibody (green). A polyclonal rabbit PKCα antibody was used to label RBCs, which were visualized with an Alexa Fluor 594-labeled secondary antibody (red). Internalized anti-TRPM1 antibodies were visible in the dendrites, and cell bodies of ON-BCs. The same uptake procedure was repeated with a monoclonal PKCα antibody. Internalized anti-PKCα antibodies were visible in the dendrites and cell bodies of RBCs. Scale bars = 20 µm. (**B**) Images of split retinas incubated with PKCα, GPR179, and mCherry antibodies diluted into Ames medium (1:500, 1:150, 1:500, and 1:100, respectively). A viability dye (Zombie; blue) was used to monitor cell death during the uptake assay. Internalization of all four antibodies (green) was visible within ON-BCs (red). Scale bars = 10 µm.

4.4.2 ON-BCs internalize antibodies using dynamin-dependent endocytosis

As cold temperatures have been shown to inhibit all forms of endocytosis[37], we next sought to confirm that ON-BCs actively internalize antibodies by comparing uptake at 37 ºC and 4ºC. We found that split retinas incubated at 4 ºC internalized 4.17-fold less antibody than those at 37 ºC (**Figures 4-2A**, **4-2B**; 37 ºC average = 102500.68 ± 53318.56; 4 ºC average = 24597.95 ± 14654.07), consistent with our hypothesis that antibody internalization is an active endocytic process. We next aimed to broadly define the conditions required for antibody endocytosis by interrogating the involvement of dynamin, a GTPase necessary for several forms of endocytosis which mediates the scission of budding vesicles at the plasma membrane[38]. To do so, we employed a noncompetitive dynamin antagonist, dyngo-4a, which abolished the dynamin- and clathrin-dependent uptake of labeled transferrin in HEK293T cells (**Supplemental Figure 4-S4**)[39]. Dyngo-4a treatment (30 µM) in the split retina significantly reduced antibody uptake compared to the DMSO treated control, demonstrating antibody uptake utilizes a dynamin-dependent endocytosis mechanism (**Figure 4-2C, 4-2D**, DMSO = 39282.56 ± 18953.90; Dyngo-4a = 16678.99 ± 7119.61).

Figure[4-2]

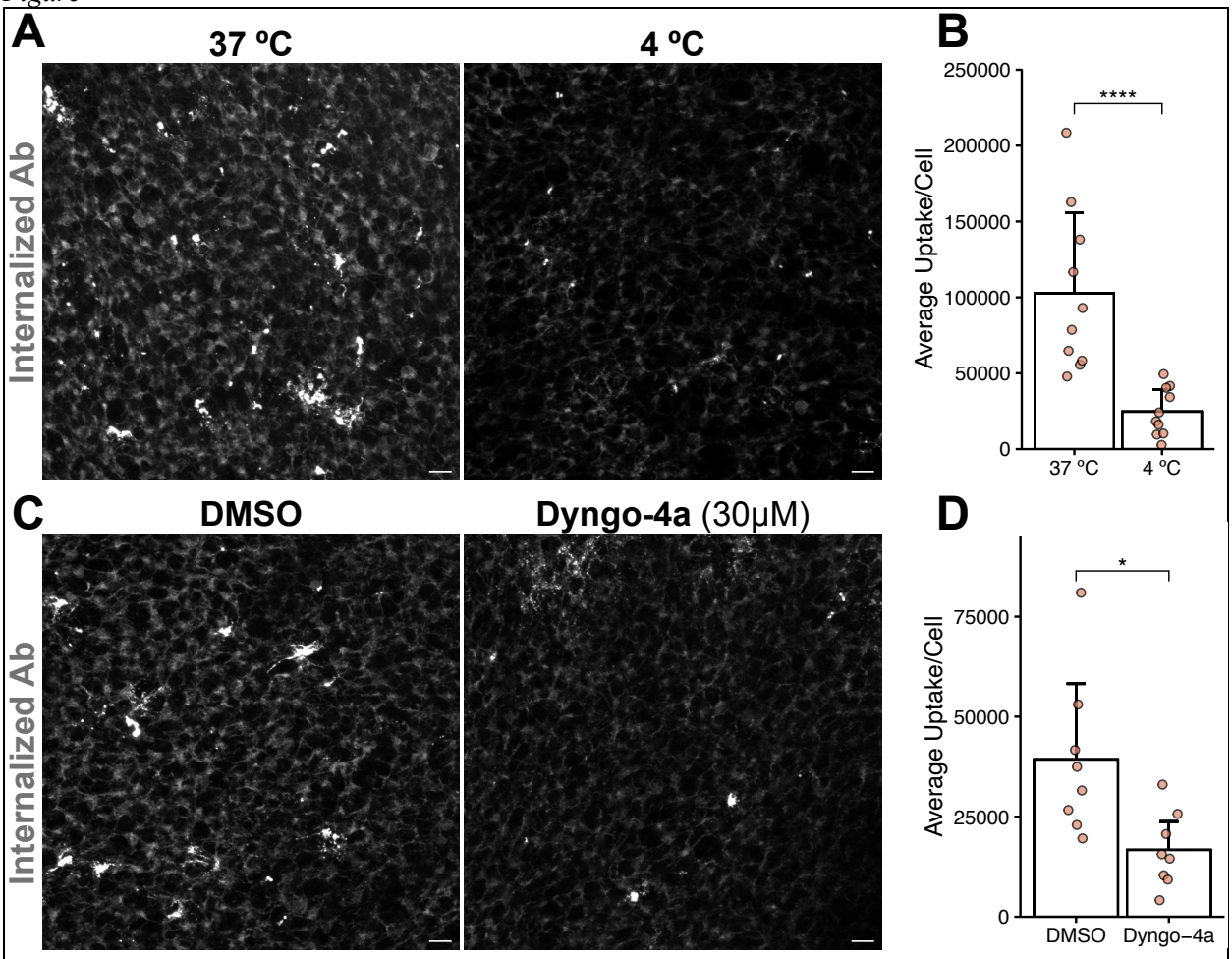

[4-2] ON-BCs internalize antibodies using dynamin-dependent endocytosis. (**A**) Sum projections from single-channel confocal micrographs of split retinas equilibrated to 37 ºC or 4 ºC prior to live incubation with PKCα antibodies. Super bright signal in some image regions results from passive diffusion of antibodies into dead cells. This signal is ignored by the machine learning segmentation model used for quantification in **B**. Compared to those incubated at 37 ºC, a significant reduction in uptake was observed in retinas incubated at 4 ºC (non-parametric Wilcoxon test; p = 2.17e-05). (**C**) To determine the involvement of dynamin activity in antibody internalization, split retinas were treated with 30µM dyngo-4a, an inhibitor of dynamin's GTPase activity, during incubation with PKCα antibodies. Split retinas were incubated with dyngo-4a or DMSO for 15 minutes prior to the addition of antibody, then again throughout the 1-hour antibody incubation. (**D**) Compared to DMSO, dyngo-4a treatment produced a significant reduction in observed antibody uptake (parametric Welch's two-tailed t-test; p = 0.0157. Points in **B** and **D** represent averages from individual pieces of split retina in which the average uptake per cell was calculated across multiple images. Scale bars = 10µm.

4.4.3 Clathrin-mediated endocytosis does not contribute to antibody uptake in ON-BCs

Having established dynamin's involvement in antibody internalization, we next sought to identify the specific dynamin-dependent endocytic pathway responsible for uptake. Clathrin-mediated endocytosis is a well-characterized route for the internalization of transferrin and other cargoes, including antibodies according to several studies using brain neurons[5,40]. To establish whether clathrin-mediated endocytosis contributes to antibody uptake in retinal ON-BCs, we treated split retinas with pitstop 2, a compound that inhibits the assembly of clathrin-coated pits by interfering with adaptor protein binding at the clathrin N-terminal domain[41,42]. While pitstop 2 treatment significantly impaired the uptake of transferrin in HEK293T cells (**Supplemental Figure 4-S5**), no effect was observed on the internalization of PKCα antibodies in ON-BCs (**Figure 4-3**; DMSO = 104188.3 ± 42537.26; pitstop 2 = 130112.2 ± 58383.65), indicating that antibody internalization by ON-BCs is clathrin-independent.

Figure[4-3]

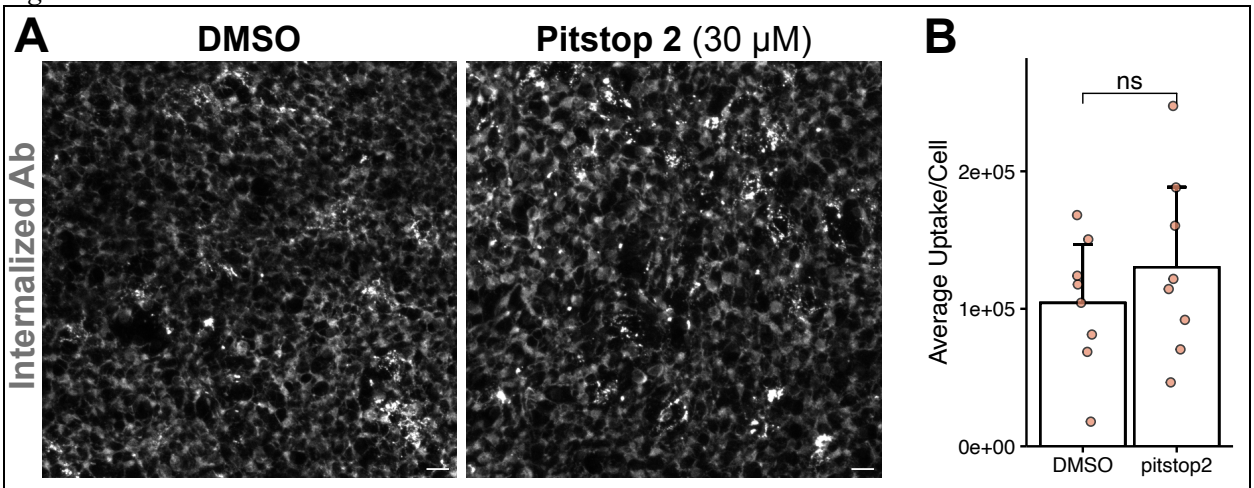

[4-3] Clathrin-mediated endocytosis does not contribute to antibody uptake in ON-BCs. (**A**) Sum projections from single-channel confocal images of split retinas treated with DMSO or 30 μM pitstop 2 during live incubation with PKCα antibodies. Super bright signal in some image regions results from passive diffusion of antibodies into dead cells or antibody accumulation in the tissue. This signal is ignored by the machine learning segmentation model used for quantification in **B**. Treatment with 30 μM pitstop 2 did not significantly impact the amount of internalized antibody compared to DMSO (parametric Welch's two-tailed t-test; p = 0.39). Points in **B** represent averages from individual pieces of split retina in which the average uptake per cell was calculated across multiple images. Scale bars = 10μm.

4.4.4 Antibody internalization does not require the Fcγ receptor

Several studies have reported the involvement of Fc receptors in antibody internalization for multiple cell types, including hippocampal neurons[5], motor neurons[43], and retinal pigment epithelium[44]. Within the context of immune effector cells, these receptors engage an antibody's constant region (Fc) and subsequently induce endocytosis of the complex using a clathrin- and dynamin-dependent mechanism[45]. In mice, there are ten Fc receptor variants that differ in their specificity for immunoglobulin (Ig) classes and subclasses[46]. To determine whether any member of the Fc receptor family contributes to antibody internalization in ON-BCs, we generated Fab fragments from the polyclonal anti-PKCα antibody (**Supplemental Figure 4-S6A**), which are unable to engage any Fc receptor variant but still bind their target antigen (**Supplemental Figure 4-S6B**). Thus, if Fc receptors are required for antibody uptake by ON-BCs, the anti-PKCα Fab fragments should not be internalized. When incubating PKCα Fab fragments with split retinas, Fabs efficiently accumulated within ON-BCs, indicating that Fc receptors do not play a major role in antibody uptake within ON-BCs (**Figure 4-4**).

Figure[4-4]

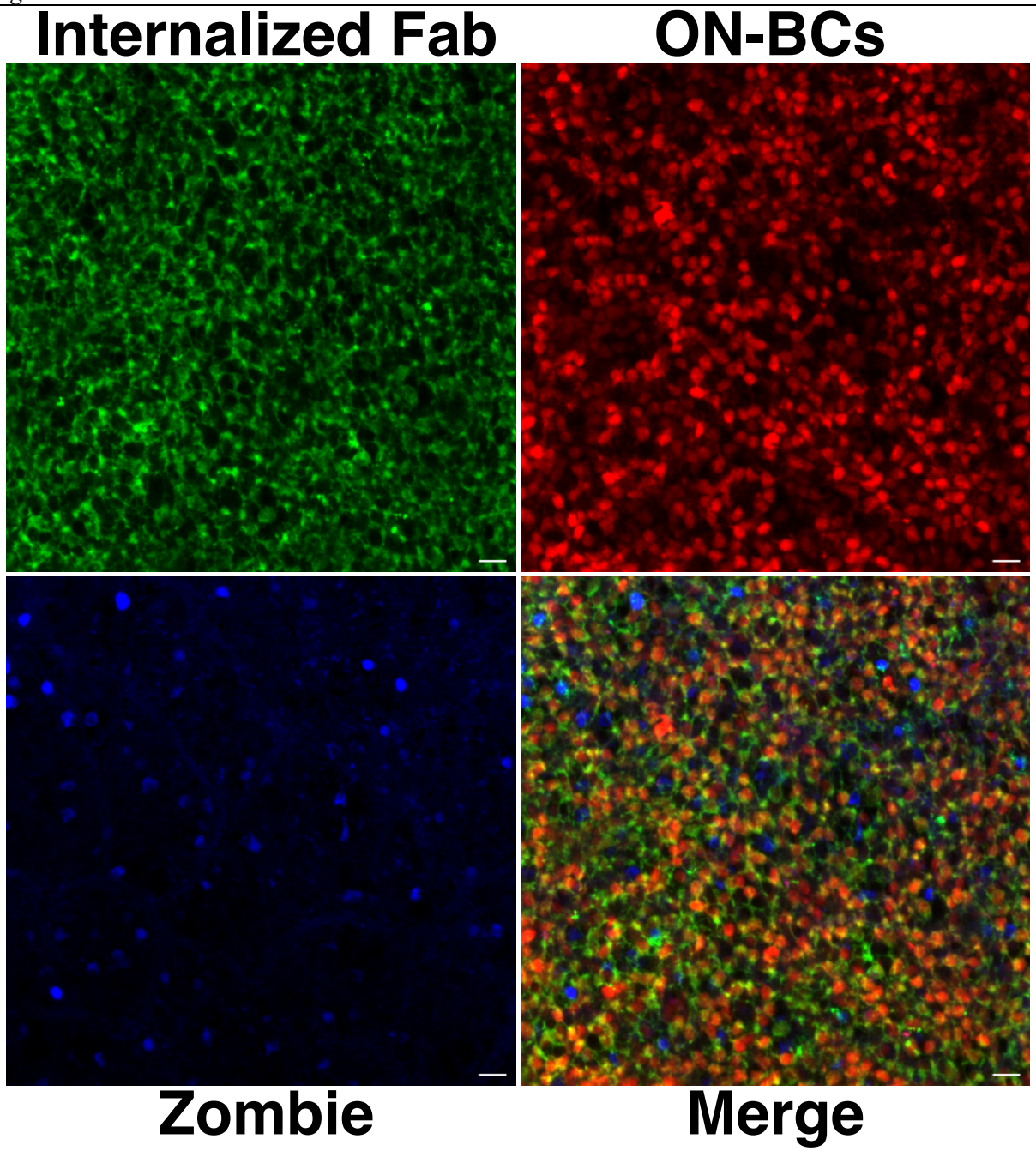

[4-4] **Antibody internalization does not require the Fcγ receptor**. Sum projections made from a 3-channel confocal micrograph of the outer plexiform and inner nuclear layers in a split retina incubated live with PKCα Fab fragments. In this transgenic mouse, Td tomato (red) is expressed under the mGluR6 promoter and labels ON-BCs. Internalized antibody Fab fragments (green) are visible in ON-BC (red) cell bodies and dendrites, indicating that Fc receptors do not play a major role in antibody uptake within retinal ON-BCs. Dead cells are indicated with the Zombie viability dye (blue). Scale bars = 10 µm.

4.4.5 Recognition of the target antigen is not required for antibody uptake

While autoantibodies against extracellular antigens can bind their target on the plasma membrane to induce internalization[27–29], intracellular antigens cannot be recognized from outside the cell. Having excluded the involvement of Fc receptors, which nonspecifically recognize antibodies independent of their target antigen, we next hypothesized a role for target-specific recognition mediated by major histocompatibility complex 1 (MHC I). Classically, MHC I presents 8-11 residue fragments of intracellular proteins on the cell surface for recognition by T cells. However, antibodies could theoretically recognize these MHC-presented antigens, potentially leading to internalization of the entire complex. To investigate the contribution of MHC I in antibody internalization, we compared antibody uptake in split retinas from WT and Beta-2 microglobulin knockout animals (B2M-KO), which lack MHC I[47]. Compared to split retinas from the WT mouse, antibody internalization was not reduced in the B2M-KO animal, indicating that antibody binding to MHC I-presented antigens is not responsible for the observed antibody internalization (**Figure 4-5**; WT = 195082.5 ± 60677.61; B2M-KO = 288029.5 ± 73231.61).

Figure[4-5]

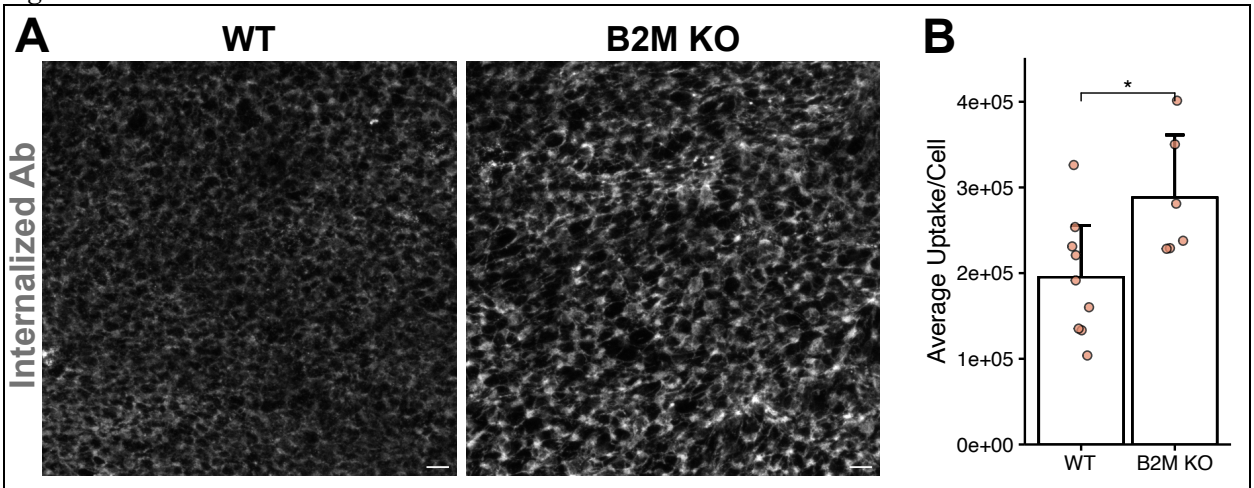

[4-5] **Recognition of the target antigen is not required for antibody uptake**. (**A**) Sum projections from single-channel confocal images of split retinas from either WT or B2M KO mice that were incubated live with PKCα antibodies. Antibody internalization was not reduced in the B2M KO mouse compared to the WT, indicating that MHC I does not mediate antibody internalization in retinal ON-BCs. Super bright signal in some image regions results from passive diffusion of antibodies into dead cells. This signal is ignored by the machine learning segmentation model used for quantification in **B.** Points in **B** represent averages from individual pieces of split retina in which the average uptake per cell was calculated across multiple images. Scale bars = 10µm.

4.4.6 Antibody internalization is only observed in cells expressing the intracellular target antigen

Having shown that recognition of the target antigen on the cell surface is not required for uptake, we next employed two different strategies to determine if intracellular antibody accumulation depends on the presence of the target antigen within the cell. First, split retinas from a PKCα knockout mouse were incubated with anti-PKCα antibodies. Unlike split retinas from the WT mouse, uptake was undetectable in ON-BCs from the PKCα KO mouse (**Figure 4-6A**). We next incubated split retinas with an antibody targeting calbindin-D, an intracellular protein expressed by retinal horizontal cells but not ON-BCs (**Supplemental Figure 4-S7**). We detected no internalized calbindin-D antibodies within ON-BCs (**Figure 4-6B**). However, calbindin-D antibodies were internalized by horizontal cells (**Figure 4-6C**), indicating the capacity for antibody uptake is not unique to ON-BCs in the retina.

Figure[4-6]

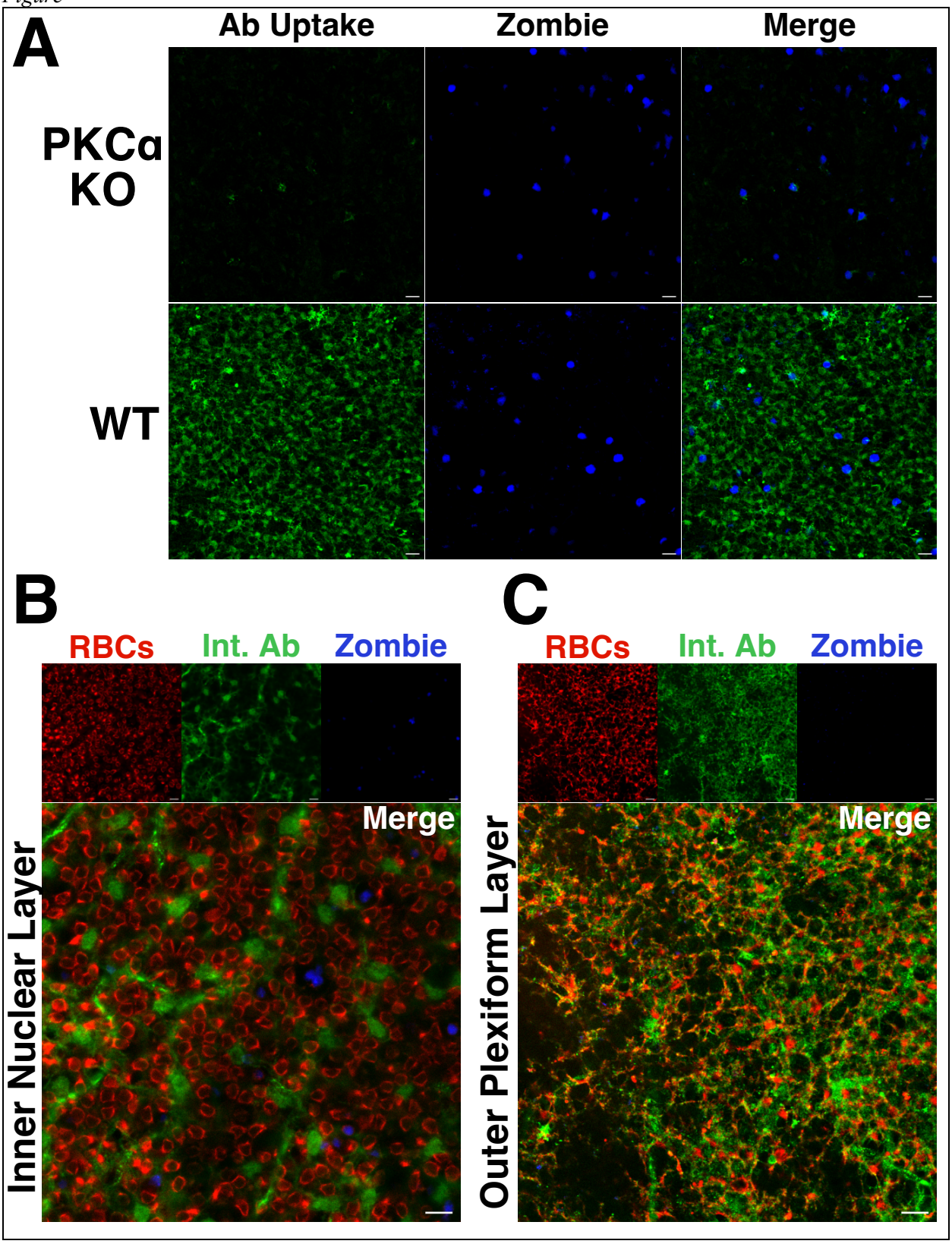
A
Ab Uptake
Zombie
Merge
PKCα KO
WT
B
RBCs
Int. Ab
Zombie
Merge
Inner Nuclear Layer
C
RBCs
Int. Ab
Zombie
Merge
Outer Plexiform Layer

4-6 Antibody internalization is not observed in the absence of the intracellular target antigen. (**A**) Confocal micrographs of split retinas from PKCα KO (top) and WT (bottom) mice incubated live with PKCα antibodies. Incubation with a fixable Zombie viability dye was performed after antibody incubation to label dead cells (blue). Internalization of PKCα antibodies is only seen in split retinas from the WT animal. (**B** and **C**) Confocal images from the split retina of a WT mouse incubated live with calbindin-D antibodies. Internalized calbindin-D antibodies are visible within horizontal cells, both in their cell bodies in the inner nuclear layer (**B**) and their dendrites in the outer plexiform layer (**C**). Internalized calbindin-D antibodies are not detectable within RBCs (red). Scale bars = 10 μm.

4.5: Discussion

This work represents the first mechanistic evaluation of the cellular processes driving pathogenic antibody internalization in retinal neurons. In MAR and other paraneoplastic syndromes in which pathogenic antibodies target intracellular epitopes, antibody internalization is a precursor to disease presentation. Therefore, this process marks a point of potential therapeutic intervention and an important clinical target for the prevention of debilitating disease.

Using the split retina to model the behavior of ON-BCs within their endogenous context in the retina, we introduce an assay for the visualization and evaluation of antibody internalization in retinal neurons. With this tool, we demonstrate ON-BCs are capable of internalizing antibodies outside the context of disease. While MAR involves the internalization of channel-inhibiting TRPM1 autoantibodies, we establish that antibodies against an unrelated cytosolic kinase, PKCα, are also internalized by ON-BCs (**Figure 4-1**). In this model, ON-BC dendrites appear to be a major site of antibody uptake, as the signal from internalized antibodies is brightest at the outer plexiform layer and becomes gradually dimmer traveling through to the deeper segments of the cell. Since PKCα is distributed throughout all regions of the ON-BC[36], the observed intensity gradient may indicate the dendrites as a point of entry into the cell. Alternatively, it may reflect the fact that other sites on the cell are less accessible to the antibodies in solution, as they are buried deeper within the tissue. Support for antibody uptake at other subcellular sites comes from the uniform internalization of TRPM1 autoantibodies observed in ON-BCs in a dissociated retinal neuron culture model[13].

In dissecting the specific cellular processes involved in antibody internalization, we find that uptake depends on the activity of dynamin, a GTPase required for endosomal fission from the membrane in some endocytic pathways (**Figure 4-2**). In contrast to reports of antibody uptake by brain neurons, pharmacological inhibition of clathrin-mediated (dynamin-dependent) endocytosis did not impact antibody uptake (**Figure 4-3**), suggesting uptake proceeds by different pathways in different neural cell types. Engagement with Fcγ receptors has also been shown to play a role in antibody endocytosis within brain neurons[5,40,48]. However, retinal ON-BCs readily internalize PKCα Fab fragments which are unable to interact with Fc receptors (**Figure 4-4**). These findings demonstrate that Fc receptors are not required for uptake in ON-BCs and that the mechanisms of antibody uptake in ON-BCs diverge from those identified in brain neurons.

Direct antibody engagement with membrane proteins can induce internalization of the antibody-target complex, providing a pathway for the delivery of antibodies to the cytosol[27–29]. However, this mechanism is only applicable to proteins on the cell surface. While cytosolic proteins are typically inaccessible to extracellular antibodies, peptide fragments of self-proteins are constantly displayed on the cell surface by MHC I, theoretically presenting an opportunity for antibodies to engage these targets and induce internalization of the MHC-peptide-antibody complex[49]. To explore whether antibody internalization in ON-BCs is mediated by recognition of peptides displayed by MHC I, we examined antibody uptake in split retinas from B2M-KO mice that lack MHC I. Internalization of PKCα antibodies was still observed in B2M-KO mice (**Figure 4-5**), demonstrating recognition of the target antigen is not required for antibody uptake.

Having shown that target engagement at the cell surface is not required for antibody uptake, we speculate that antibodies are internalized in a target-independent manner, but that antibody accumulation in the cell depends on expression of the target antigen and binding of the antibody. We detected no internalized PKCα antibodies in split retinas from PKCα KO mice (**Figure 4-6**). Although antibody uptake was only observed in cells expressing the target antigen, a previous study examining antibody uptake in CHO cells that overexpressed TRPM1 demonstrated that expression of the target antigen is not *sufficient* for uptake[13]. These results could imply that expression of the target antigen is *necessary* for uptake and that cells selectively internalize antibodies that recognize target antigens within the cell, even if that target is not represented on

the membrane. Perhaps more plausibly, antibodies are non-specifically endocytosed then subjected to lysosomal or proteasomal degradation unless they encounter their target antigen. This would explain our inability to detect internalized calbindin-D antibodies within ON-BCs, or internalized PKCα antibodies within horizontal cells, despite evidence that both cell types are capable of internalizing antibodies to intracellular proteins. These findings also provide evidence for endosomal escape of cargo, as internalized antibodies that have engaged their cytosolic target must have breached endosomes to avoid lysosomal degradation.

These data comprise an important early characterization of the cellular requirements for the uptake of pathogenic autoantibodies by retinal ON-BCs, as occurs in MAR. Using antibodies against TRPM1, PKCα, GPR179, and mCherry, we demonstrate that antibodies against intracellular antigens are internalized by ON-BCs in a manner that does not require extracellular target engagement for cell entry. Horizontal cells were also capable of antibody uptake, and photoreceptors internalize antibodies against intracellular antigens in cancer-associated retinopathy[50], indicating this behavior is not unique to ON-BCs in the retina. The evidence points to a dynamin-dependent, clathrin-independent, and FcR-independent mechanism driving the internalization of antibodies by ON-BCs. Qualifying endocytic pathways include FEME and caveolae-mediated endocytosis, although the dynamin-dependence of the latter is the subject of current debate[51]. The verification of a specific endocytic pathway will be greatly expedited by employing more precise genetic tools, such as knockouts or mutants of pathway specific genes, to eliminate the challenges associated with pharmacological tools. While expression of the target antigen is required to *observe* antibody accumulation, future studies are needed to confirm if the absence of the target antigen results in antibody exclusion from the cell, internalization followed by efflux, or most plausibly, rapid degradation of the antibody following non-specific uptake. These data also implicitly support the notion of antibody escape from endosomes; resolving the mechanism of their escape may have broader implications for improving the delivery of drug-antibody conjugates to neurons in the treatment of other diseases.

4.6: Acknowledgements

We thank Tammie Haley and Gaoying Ren for their expert preparation of mouse retinal cryosections and animal husbandry. We would also thank Felice Kelley at the OHSU Advanced Light Microscopy core for assistance in designing the machine learning segmentation pipeline. Thank you as well to the Phillip Streeter Lab at OHSU for assistance in developing the TRPM1 monoclonal antibodies.

4.7: Supplemental Information

Figure[4-S1]

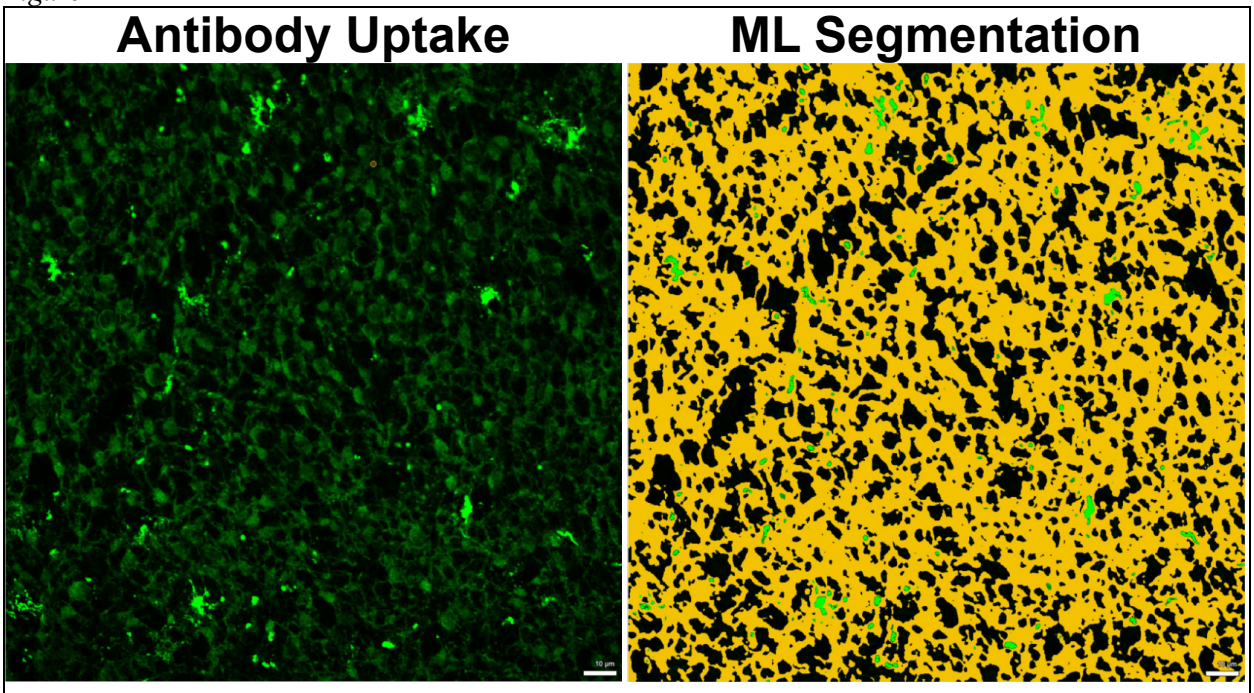

[4-S1] **Machine learning model for segmentation of antibody uptake signal**. Image analysis software was used to train a machine learning model on images from split retinas taken after the live antibody uptake assay. An example image shows internalized PKCα antibody within ON-BCs (left). Patches of hyper-bright signal resulted from antibodies passively diffusing into dead cells. The right image shows an overlay (yellow) produced by the segmentation model, which was trained to detect true antibody uptake signal while excluding the bright artifacts. Note the absence of yellow overlay in the regions of bright signal. ML = machine learning. Scale bars = 10 µm.

Figure[4-S2]

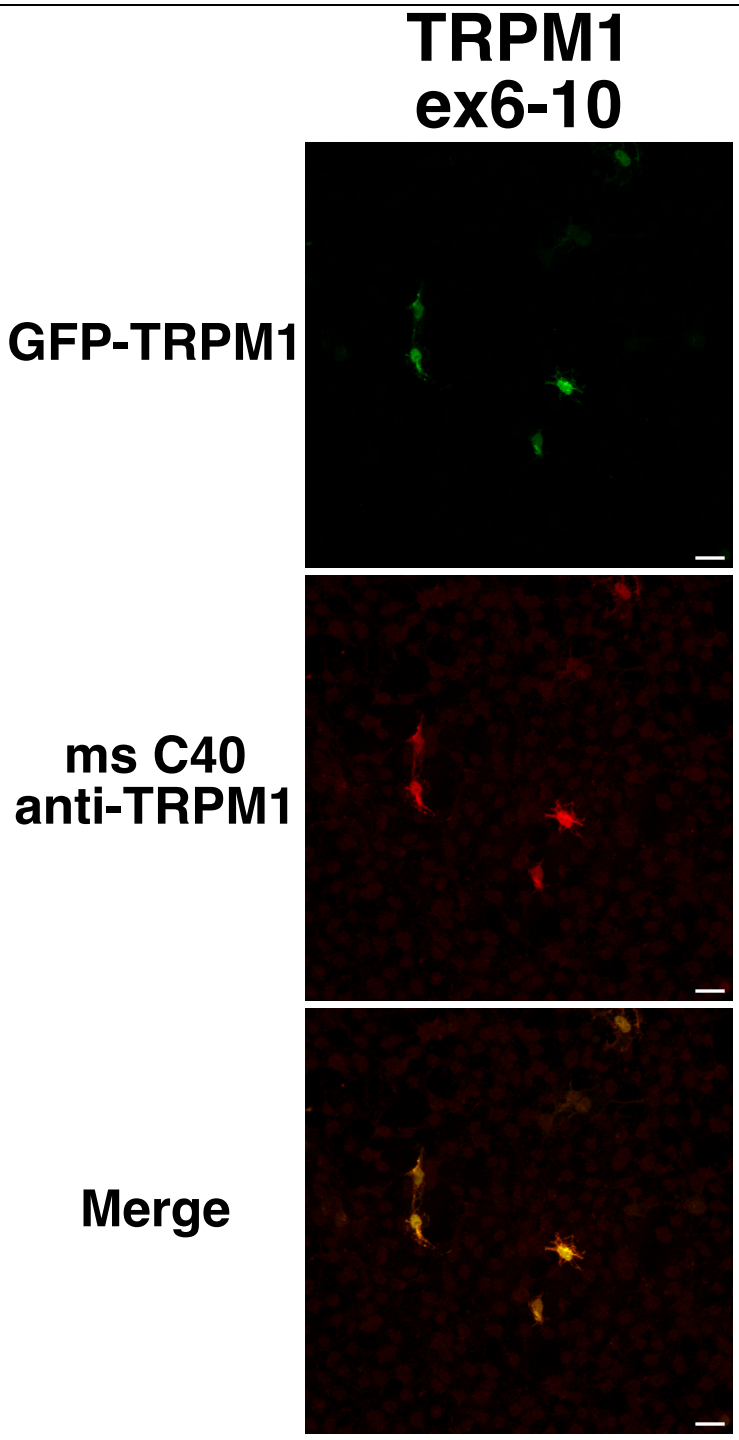

[4-S2] A custom made mouse anti-TRPM1 antibody targets an intracellular region of TRPM1. HEK293T cells were transfected with a plasmid encoding an EGFP-tagged TRPM1 polypeptide (green) derived from an intracellular region of the TRPM1 N-terminus: exons 6-10 (ex6-10). The C40 mouse monoclonal TRPM1 antibody (red) reacts only with cells expressing the TRPM1 construct. The brightness of the red channel was increased to reveal negative cells in the background. Scale bars = 20 μm.

Figure[4-S3]

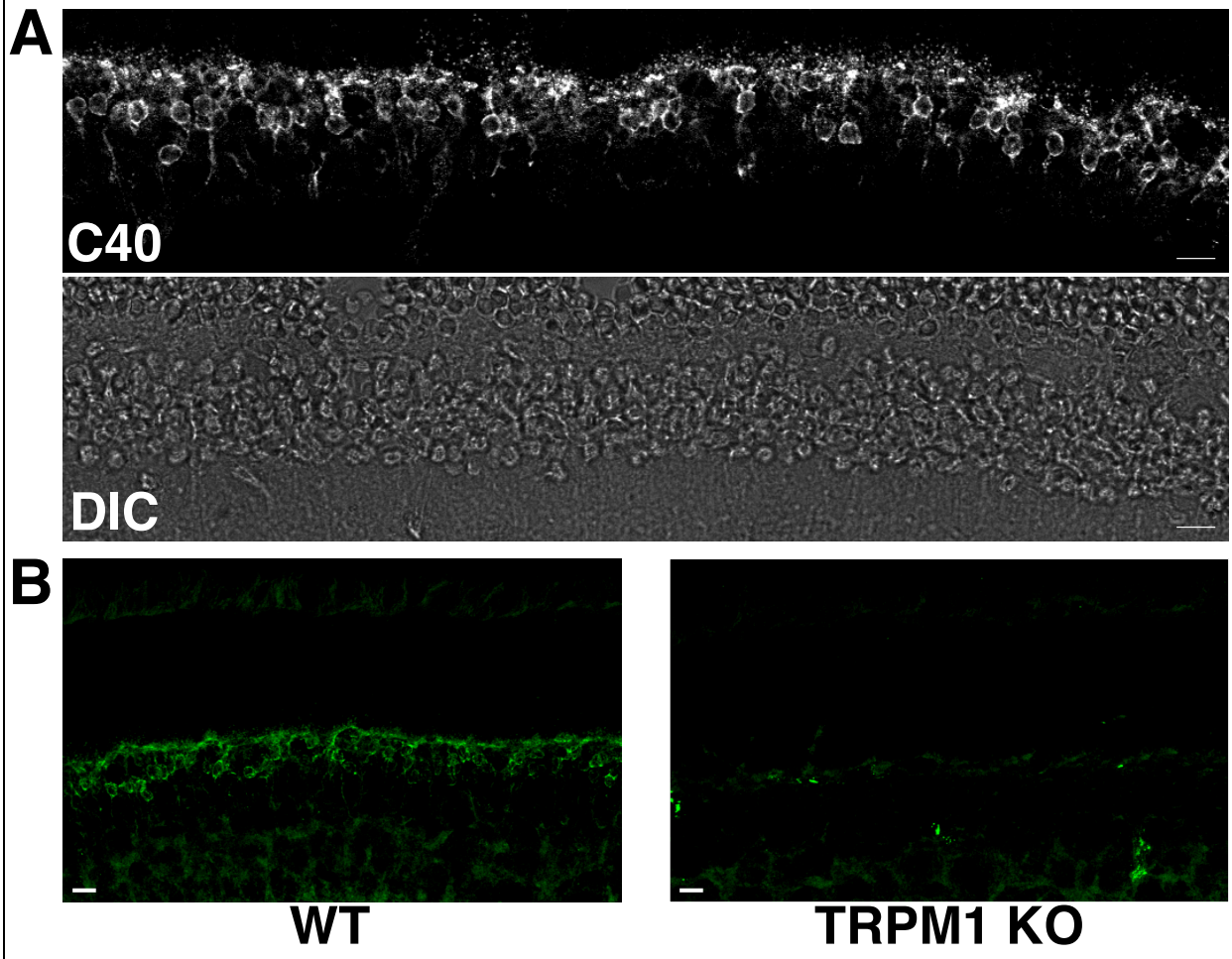

[4-S3] The TRPM1 C40 monoclonal antibody selectively binds TRPM1 in the mouse retina. (**A**) Incubating the TRPM1 C40 antibody (diluted 1:5000 in AIS) with cryosections of mouse retina labeled the cell bodies and dendrites of ON-BCs, the only cells in the retina that express TRPM1. (**B**) In retina sections from TRPM1 knockout mice, ON-BC labeling is absent, and only blood vessels and background staining are visible. Scale bars = 10 µm.

Figure[4-S4]

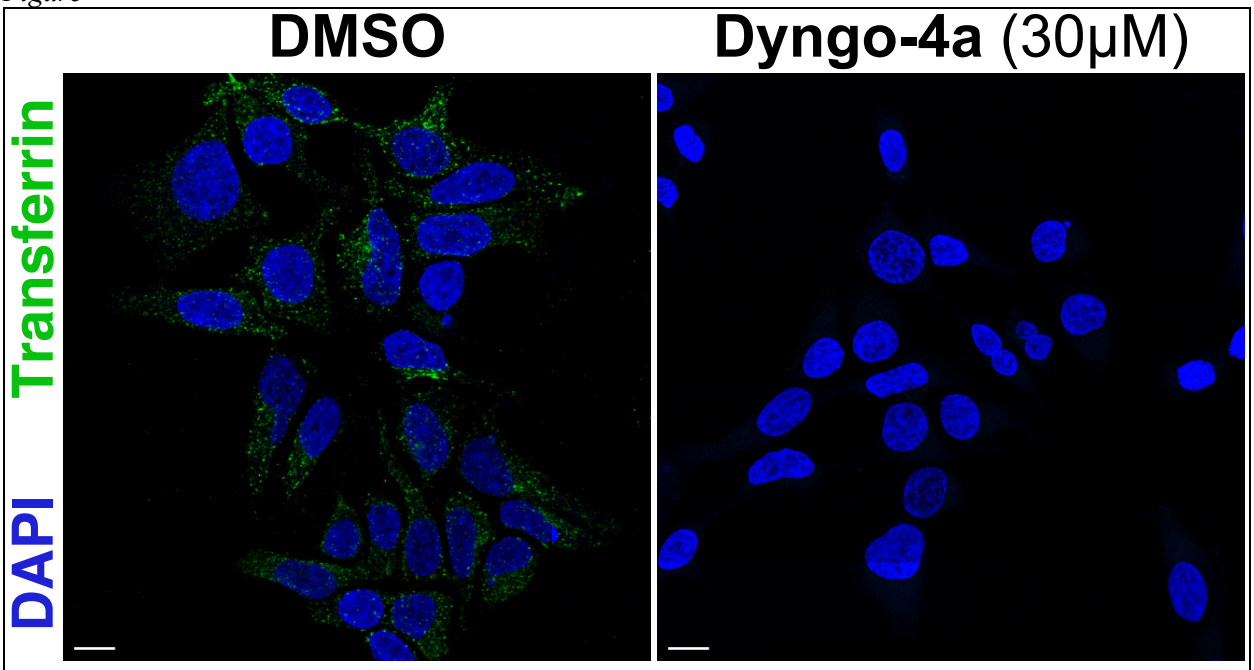

[4-S4] **Dyngo-4a inhibits dynamin-dependent endocytosis in HEK293T cells.** HEK293T cells were treated with DMSO or 30 μM Dyngo-4a, a dynamin inhibitor, for 15 minutes prior to the addition of Alexa Fluor 488-labeled transferrin for an additional 15 minutes. Surface-bound transferrin was removed through an acid wash, and internalized transferrin (green) was visualized by confocal microscopy. Treatment with 30 μm Dyngo-4a almost completely abolished transferrin uptake compared to the DMSO control. Nuclei were stained with DAPI (blue). Scale bars = 10 μm.

Figure[4-S5]

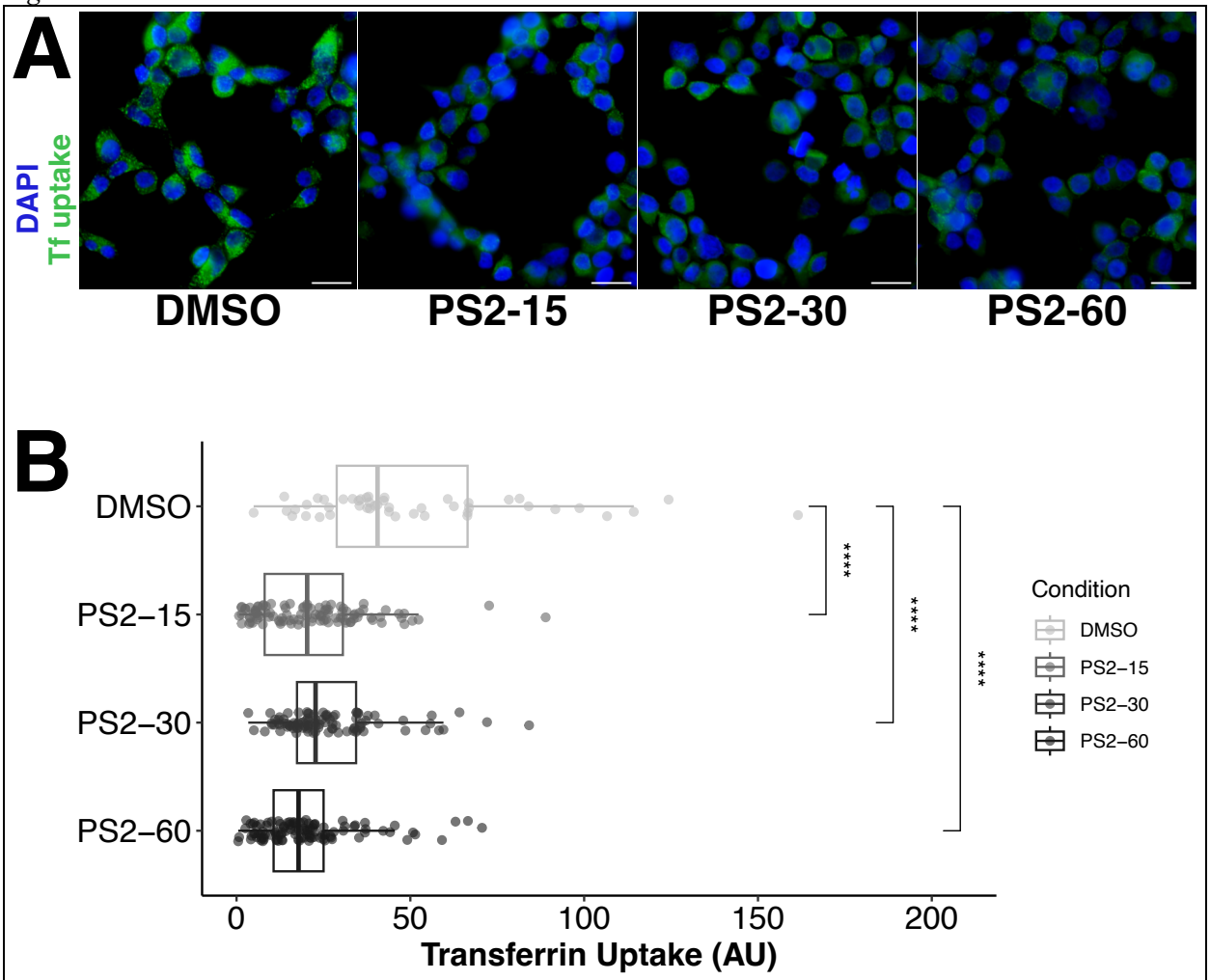

[4-S5] Pitstop2 inhibits clathrin-mediated endocytosis in in HEK293T cells. HEK293T cells were treated with DMSO or 30 µM piststop2, a clarthrin-inhibitor, for 15, 30, or 60 minutes prior to the addition of Alexa Fluor 488-labeled transferrin for an additional 15 minutes. Surface-bound transferrin was removed in an acid wash, and images of internalized transferrin was acquired with an epifluorescent microscope (**A**). Image quantification revealed that treatment with pitstop2 significantly reduced transferrin uptake compared to the DMSO control (**B**). Longer pre-treatment times did not increase the efficacy of the inhibitor. Comparison of means was performed using a Mann-Whitney U test followed by a post-hoc pairwise Wilcox test. Scale bars in **A** are 20 µm.

Figure[4-S6]

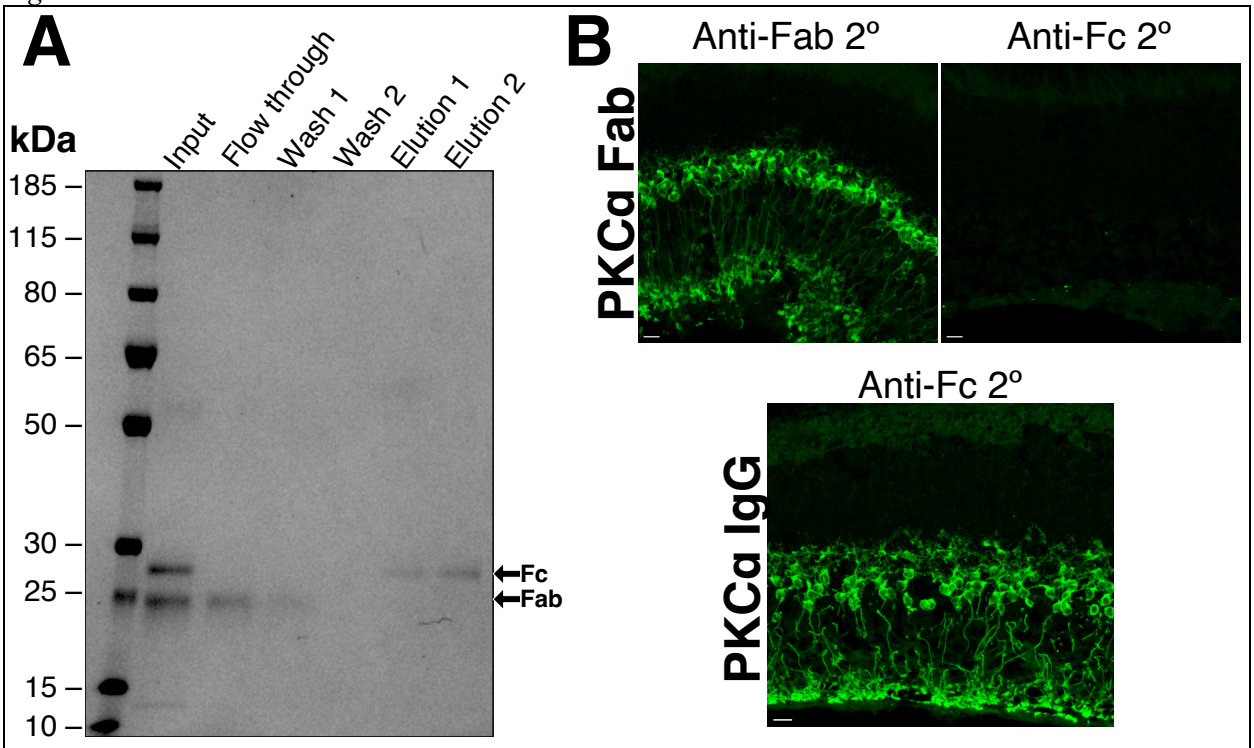

[4-S6] **Production and validation of PKCα Fab fragments.** Antibody Fab fragments were prepared from a polyclonal anti-PKCα antibody by digestion with papain followed by purification over a protein A column. The purity of the Fabs was confirmed by reducing SDS-PAGE and Coomassie staining (**A**). The input contained the product of the papain digestion, composed of Fab fragments (~25 kDa) and Fc fragments (~28 kDa). Fab fragments are unable to bind protein A and are therefore detectable in the flow through the wash. Fc fragments remain bound to protein A and can be eluted with an acid buffer. Purified Fabs maintained their capacity to bind PKCα, as they specifically labeled RBCs in the mouse retina (**B**). Fabs were undetectable using an anti-Fc specific secondary antibody, confirming that no undigested IgG contaminants remained. The efficacy of the anti-Fc specific secondary antibody was validated on retina sections incubated with the original PKCα IgG antibody (**C**). Scale bars = 10 µm.

Figure[4-S7]

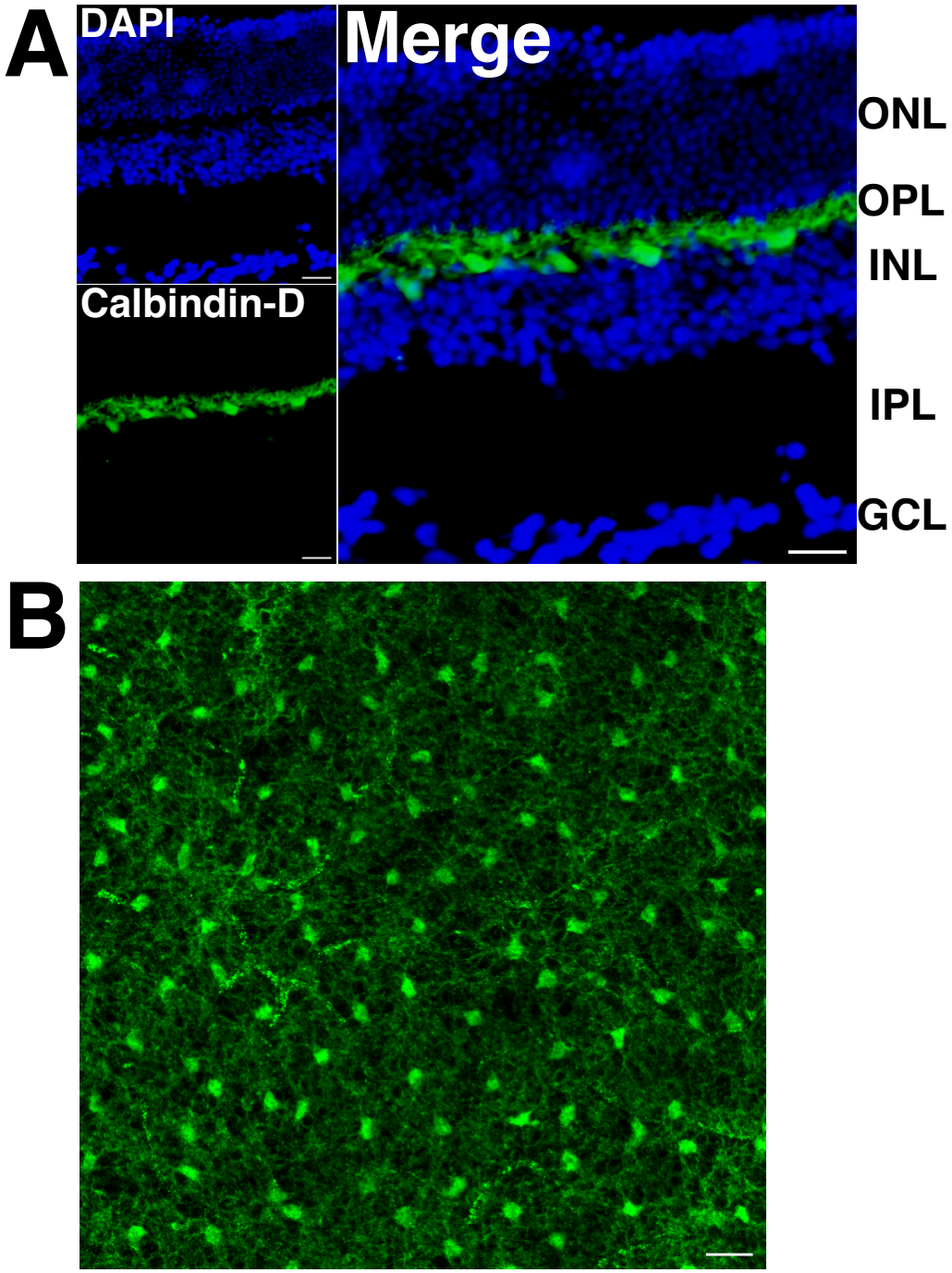

[4-S7] **A Calbindin-D antibody labels horizontal cells in fixed retinas.** Fixed retinal cryosections (**A**) and split retinas (**B**) were incubated with a monoclonal antibody targeting calbindin-D, a marker for retinal horizontal cells. In these fixed and permeabilized preparations, the antibody clearly labeled horizontal cell bodies and processes in the inner nuclear layer and outer plexiform layers, respectively. In live split retinas, internalized calbindin-D antibodies were visible within horizontal cells but not ON-BCs, (**Figure 4-6B)**, indicating that antibody internalization is only observed in cells expressing the target antigen. Scale bars = 20 µm.

Supplemental Table 4-S1 – DNA and protein sequences

Name	Description	Sequence
TRPM1 ex6-10	Human polypeptide immunogen used to immunize mice for development of TRPM1 monoclonal antibody	MGSSHHHHHHSSGLVPRGSHMARNVTRVYQTMSNPLSKL SVLNNSHTHFILADNGTLGKYGAEVKLRRLLEKHISLQKI NTRLGQGVPLVGLVVEGGPNVVSIVLEYLQEEPPIPVVICD GSGRASDILSFAHKYCEEGGIINESLREQLLVTIQKTFNYNK AQSHQLFAIIMECMKKKELVTVFRMGSEGQQDIEMAILTA LLKGTNVSAPDQLSLALAWNRVDIARSQIFVFGPH
TRPM1 ex2-7	Human polypeptide immunogen used to immunize mice for development of TRPM1 monoclonal antibody	MGSSHHHHHHSSGLVPRGSHMARNMKDSNRCCCGQFTN QHIPPLPSATPSKNEEESKQVETQPEKWSVAKHTQSYPTDS YGVLEFQGGGYSNKAMYIRVSYDTKPDSLLHLMVKDWQ LELPKLLISVHGGLQNFEMQPKLKQVFGKGLIKAAMTTGA WIFTGGVSTGVISHVGDALKDHSSKSRGRVCAIGIAPWGIV ENKEDLVGKDVTRVYQTMSNPLSKLSVLNNSHTHFILADN GTLGKYGAEVKLRRLLEKHISLQKINTRLGQGVPLVGLVV EGGPNVVSIVLEYLQEEPPIPVVICDGSGRASDILSFAHKYC EEGG

Supplemental Table 4-S2 – Antibodies

Target	Host Species	Conjugate	Usage in Manuscript	Manufacture	Catalog Number
TRPM1	mouse	NA	Fig. 1A, S2, S3	Custom made. See Methods in main text	NA
PKCα	mouse	NA	Fig. 1A	Santa Cruz Biotechnology; Dallas, TX	sc-80
PKCα	rabbit	NA	Figs. 1A (fixed labeling), 1B (uptake), 2, 3, 4, 5, 6A, S1, S6	Sigma-Aldrich; Burlington, MA	P4334
PKCα	mouse	Alexa Fluor 594	Figs. 6B, 6C	Santa Cruz Biotechnology; Dallas, TX	sc8393-AF594
Calbindin-D28K (AF2E5)	mouse	NA	Figs. 6B, 6C, S7	Santa Cruz Biotechnology; Dallas, TX	sc135666
Anti-rabbit [$F(ab)_2$ specific]	goat	Alexa Fluor 488	Figs. 4, S6B	Jackson ImmunoResearch; West Grove, PA	111-545-006 (RRID: AB_2338047)
Anti-rabbit [Fc specific]	goat	Alexa Fluor 488	Fig. 6B	Jackson ImmunoResearch; West Grove, PA	111-545-008 (RRID: AB_2338048)
Anti-rabbit	goat	Alexa Fluor 488	Figs. 1, 2, 3, 5, 6A	Invitrogen; Waltham, MA	A32731
Anti-mouse	donkey	Alexa Fluor 488	Figs. 1, S3	Invitrogen; Waltham, MA	A21202

Chapter 4 Bibliography

1. Burbelo, P. D., Iadarola, M. J., Keller, J. M. & Warner, B. M. Autoantibodies Targeting Intracellular and Extracellular Proteins in Autoimmunity. *Front Immunol* **12**, 548469 (2021).

2. Zekeridou, A. Paraneoplastic Neurologic Disorders. *Autoimmune Neurology* **30**, 1021–1051 (2024).

3. Duvoisin, R. M., Ren, G., Haley, T. L., Taylor, M. H. & Morgans, C. W. TRPM1 Autoantibodies in Melanoma Patients Without Self-Reported Visual Symptoms. *Invest. Ophthalmol. Vis. Sci.* **60**, 2330 (2019).

4. Sculier, C. *et al.* Autoimmune paraneoplastic syndromes associated to lung cancer: A systematic review of the literature: Part 5: Neurological auto-antibodies, discussion, flow chart, conclusions. *Lung Cancer* **111**, 164–175 (2017).

5. Rocchi, A. *et al.* Autoantibodies to synapsin I sequestrate synapsin I and alter synaptic function. *Cell Death Dis* **10**, 1–16 (2019).

6. Greenlee, J. E. *et al.* Anti-Yo Antibody Uptake and Interaction with Its Intracellular Target Antigen Causes Purkinje Cell Death in Rat Cerebellar Slice Cultures: A Possible Mechanism for Paraneoplastic Cerebellar Degeneration in Humans with Gynecological or Breast Cancers. *PLoS ONE* **10**, e0123446 (2015).

7. Elsheikh, S., Gurney, S. P. & Burdon, M. A. Melanoma-associated retinopathy. *Clin Exp Dermatol* **45**, 147–152 (2020).

8. Berson, E. L. & Lessell, S. Paraneoplastic night blindness with malignant melanoma. *Am J Ophthalmol* **106**, 307–311 (1988).

9. Weinstein, J. M., Kelman, S. E., Bresnick, G. H. & Kornguth, S. E. Paraneoplastic Retinopathy Associated with Andretinal Bipolar Cell Antibodies in Cutaneous Malignant Melanoma. *Ophthalmology* **101**, 1236–1243 (1994).

10. Dhingra, A. *et al.* Autoantibodies in Melanoma-Associated Retinopathy Target TRPM1 Cation Channels of Retinal ON Bipolar Cells. *J Neurosci* **31**, 3962–3967 (2011).

11. Koike, C. *et al.* TRPM1 is a component of the retinal ON bipolar cell transduction channel in the mGluR6 cascade. *Proc Natl Acad Sci U S A* **107**, 332–337 (2010).

12. Morgans, C. W. *et al.* TRPM1 is required for the depolarizing light response in retinal ON-bipolar cells. *PNAS* **106**, 19174–19178 (2009).

13. Xiong, W.-H. *et al.* Serum TRPM1 Autoantibodies from Melanoma Associated Retinopathy Patients Enter Retinal ON-Bipolar Cells and Attenuate the Electroretinogram in Mice. *PLoS ONE* **8**, e69506 (2013).

14. Lei, B., Bush, R. A., Milam, A. H. & Sieving, P. A. Human Melanoma-Associated Retinopathy (MAR) Antibodies Alter the Retinal ON-Response of the Monkey ERG In Vivo. *Invest Ophthalmol Vis Sci* **41**, 262–266 (2000).

15. Guo, H., Carlson, J. A. & Slominski, A. Role of TRPM in melanocytes and melanoma. *Exp Dermatol* **21**, 650–654 (2012).

16. Duncan, L. M. *et al.* Down-Regulation of the Novel Gene Melastatin Correlates with Potential for Melanoma Metastasis. *Cancer Res* **58**, 1515–1520 (1998).

17. Gilbert, A. E. *et al.* Monitoring the Systemic Human Memory B Cell Compartment of Melanoma Patients for Anti-Tumor IgG Antibodies. *PLOS ONE* **6**, e19330 (2011).

18. Chiaruttini, G. *et al.* B cells and the humoral response in melanoma: The overlooked players of the tumor microenvironment. *Oncoimmunology* **6**, e1294296 (2017).

19. Mose, L. E. *et al.* Assembly-based inference of B-cell receptor repertoires from short read RNA sequencing data with V'DJer. *Bioinformatics* **32**, 3729–3734 (2016).

20. Bolotin, D. A. *et al.* Antigen receptor repertoire profiling from RNA-seq data. *Nat Biotechnol* **35**, 908–911 (2017).

21. Crescioli, S. *et al.* B cell profiles, antibody repertoire and reactivity reveal dysregulated responses with autoimmune features in melanoma. *Nat Commun* **14**, 3378 (2023).

22. Milam, A. H. *et al.* Autoantibodies against retinal bipolar cells in cutaneous melanoma-associated retinopathy. *Invest. Ophthalmol. Vis. Sci.* **34**, 91–100 (1993).

23. Maverakis, E., Goodarzi, H., Wehrli, L. N., Ono, Y. & Garcia, M. S. The Etiology of Paraneoplastic Autoimmunity. *Clinic Rev Allerg Immunol* **42**, 135–144 (2012).

24. Duvoisin, R. M. *et al.* Autoantibodies in Melanoma-Associated Retinopathy Recognize an Epitope Conserved Between TRPM1 and TRPM3. *Invest. Ophthalmol. Vis. Sci.* **58**, 2732 (2017).

25. Gyoten, D. *et al.* Broad locations of antigenic regions for anti-TRPM1 autoantibodies in paraneoplastic retinopathy with retinal ON bipolar cell dysfunction. *Exp Eye Res* **212**, 108770 (2021).

26. Mosavi-Hecht, R. M. *et al.* Case report: Longitudinal evaluation and treatment of a melanoma-associated retinopathy patient. *Front. Med.* **11**, (2024).

27. Hammood, M., Craig, A. W. & Leyton, J. V. Impact of Endocytosis Mechanisms for the Receptors Targeted by the Currently Approved Antibody-Drug Conjugates (ADCs)—A Necessity for Future ADC Research and Development. *Pharmaceuticals (Basel)* **14**, 674 (2021).

28. Sung, M. *et al.* Caveolae-Mediated Endocytosis as a Novel Mechanism of Resistance to Trastuzumab Emtansine (T-DM1). *Mol Cancer Ther* **17**, 243–253 (2018).

29. Opaliński, Ł. *et al.* High Affinity Promotes Internalization of Engineered Antibodies Targeting FGFR1. *Int J Mol Sci* **19**, 1435 (2018).

30. Hecht, R. M., Shi, Q., Garrett, T. R., Sivyer, B. & Morgans, C. Split Retina as an Improved Flatmount Preparation for Studying Inner Nuclear Layer Neurons in Vertebrate Retina. *J Vis Exp* e65757 (2024) doi:10.3791/65757.

31. Kerschensteiner, D., Morgan, J. L., Parker, E. D., Lewis, R. M. & Wong, R. O. L. Neurotransmission selectively regulates synapse formation in parallel circuits in vivo. *Nature* **460**, 1016–1020 (2009).

32. Braz, J. C. *et al.* PKC-α regulates cardiac contractility and propensity toward heart failure. *Nat Med* **10**, 248–254 (2004).

33. Quan, A. *et al.* Myristyl Trimethyl Ammonium Bromide and Octadecyl Trimethyl Ammonium Bromide Are Surface-Active Small Molecule Dynamin Inhibitors that Block Endocytosis Mediated by Dynamin I or Dynamin II. *Mol Pharmacol* **72**, 1425–1439 (2007).

34. Stringer, C., Wang, T., Michaelos, M. & Pachitariu, M. Cellpose: a generalist algorithm for cellular segmentation. *Nat Methods* **18**, 100–106 (2021).

35. Pachitariu, M. & Stringer, C. Cellpose 2.0: how to train your own model. *Nat Methods* **19**, 1634–1641 (2022).

36. Greferath, U., Grünert, U. & Wässle, H. Rod bipolar cells in the mammalian retina show protein kinase C-like immunoreactivity. *J Comp Neurol* **301**, 433–442 (1990).

37. Szewczyk-Roszczenko, O. K. *et al.* The Chemical Inhibitors of Endocytosis: From Mechanisms to Potential Clinical Applications. *Cells* **12**, 2312 (2023).

38. Marks, B. *et al.* GTPase activity of dynamin and resulting conformation change are essential for endocytosis. *Nature* **410**, 231–235 (2001).

39. McCluskey, A. *et al.* Building a Better Dynasore: The Dyngo Compounds Potently Inhibit Dynamin and Endocytosis. *Traffic* **14**, 1272–1289 (2013).

40. Congdon, E. E., Gu, J., Sait, H. B. R. & Sigurdsson, E. M. Antibody Uptake into Neurons Occurs Primarily via Clathrin-dependent Fcγ Receptor Endocytosis and Is a Prerequisite for Acute Tau Protein Clearance. *J. Biol. Chem.* **288**, 35452–35465 (2013).

41. von Kleist, L. *et al.* Role of the Clathrin Terminal Domain in Regulating Coated Pit Dynamics Revealed by Small Molecule Inhibition. *Cell* **146**, 471–484 (2011).

42. Dutta, D., Williamson, C. D., Cole, N. B. & Donaldson, J. G. Pitstop 2 Is a Potent Inhibitor of Clathrin-Independent Endocytosis. *PLoS ONE* **7**, e45799 (2012).

43. Mohamed, H. A. *et al.* Immunoglobulin Fcγ receptor promotes immunoglobulin uptake, immunoglobulin-mediated calcium increase, and neurotransmitter release in motor neurons. *J Neurosci Res* **69**, 110–116 (2002).

44. Dithmer, M. *et al.* The role of Fc-receptors in the uptake and transport of therapeutic antibodies in the retinal pigment epithelium. *Exp Eye Res* **145**, 187–205 (2016).

45. Junker, F., Gordon, J. & Qureshi, O. Fc Gamma Receptors and Their Role in Antigen Uptake, Presentation, and T Cell Activation. *Front Immunol* **11**, (2020).

46. Bruhns, P. & Jönsson, F. Mouse and human FcR effector functions. *Immunol Rev* **268**, 25–51 (2015).

47. Koller, B. H., Marrack, P., Kappler, J. W. & Smithies, O. Normal Development of Mice Deficient in β2M, MHC Class I Proteins, and CD8+ T Cells. *Science* **248**, 1227–1230 (1990).

48. Deissler, H. L., Lang, G. K. & Lang, G. E. Internalization of bevacizumab by retinal endothelial cells and its intracellular fate: Evidence for an involvement of the neonatal Fc receptor. *Exp Eye Res* **143**, 49–59 (2016).

49. Mahmutefendić, H., Blagojević, G., Kučić, N. & Lučin, P. Constitutive internalization of murine MHC class I molecules. *J Cell Physiol* **210**, 445–455 (2007).

50. Adamus, G. & Seigel, G. Apoptotic Retinal Cell Death Induced by Antirecoverin Autoandbodies of Cancer-Associated Retinopathy. 9 (1997).

51. Parton, R. G., Taraska, J. W. & Lundmark, R. Is endocytosis by caveolae dependent on dynamin? *Nat Rev Mol Cell Biol* 1–2 (2024) doi:10.1038/s41580-024-00735-x.

Chapter 5

Summary and Conclusions

5.1: Highlights

5.1.1 Chapter 2: A longitudinal case report on a MAR patient

1. **Vascular leakage and heightened inflammation are discovered in a MAR patient eye**
    a. Leakage may represent an avenue for autoantibodies to access the retina.
2. **Intraocular corticosteroids restore visual function and alleviate MAR visual symptoms**
    a. Dexamethasone treatment restores the ERG b-wave, indicating a return to normal ON-BC function despite the presence of TRPM1 autoantibodies.
3. **TRPM1 autoantibodies persist in patient serum throughout immunotherapy and vision treatment**
    a. The discovery that TRPM1 autoantibody titer doesn't correlate directly with vision impairment implies a secondary factor in pathogenesis… possibly related to antibody access to the retina.
4. **Patient autoantibodies target a region of TRPM1 encoded by exons 8-10**
    a. This region maps to TRPM1's intracellular N-terminus, meaning that autoantibodies must penetrate the ON-BC cytosol to cause MAR…

5.1.2 Chapter 3: Development of the split retina for visualizing antibody uptake

1. **The split retina preparation is fast, simple, and requires no specialized equipment**
    a. Quarters of dissected mouse retina are sandwiched between two pieces of nitrocellulose which are then pulled apart, splitting the retina through the photoreceptor axons.
2. **In the split retina, photoreceptor cell bodies are removed but their terminals remain**
    a. This means that the retina's outer plexiform layer (OPL), which houses the synapses between photoreceptors and bipolar cells, remains intact.
    b. An intact OPL means intact ON-BC dendrites; this is important in an antibody uptake model since these structures could be critical sites of internalization.
3. **Outer plexiform layer synapses remain intact in the split retina**
    a. A more nuanced demonstration that the contact sites between photoreceptors and bipolar cells appear as one would expect in other retina preparations.
4. **ON-BCs remain viable in the split retina**
    a. Incubation with a viability dye after splitting demonstrates that ON-BCs survive the preparation. Living, healthy ON-BCs are a pre-requisite for antibody internalization assays.
5. **The split retina preparation is amenable to dual IHC and ISH**
    a. A demonstration of simultaneous mRNA and protein labeling within inner retinal neurons in the split retina.
    b. While not relevant to its suitability as an antibody uptake model, this feature of the split retina preparation may be of interest to the broader research community.
6. **The split retina enables patch clamp recording of ON-BCs and horizontal cells**
    a. Patch clamp recording from ON-BCs serves as another testament to the health and viability of these neurons, further establishing the suitability of the preparation for antibody uptake assays.
7. **The split retina enables rapid protein immunolabeling in inner retinal neurons**
    a. While traditional wholemount retina preparations necessitate 48–96-hour antibody incubations to label inner retinal neurons, the task can be achieved in just 1 hour in the split retina.

5.1.3 Chapter 4: Probing the mechanism of antibody uptake in ON-BCs

1. **ON-BCs internalize antibodies targeting multiple intracellular epitopes**
    a. The first demonstration of antibody uptake in the split retina.
    b. Antibody uptake is not unique to TRPM1. Antibodies against PKCα, GPR179, and mCherry are also internalized.
2. **ON-BCs internalize antibodies using dynamin-dependent endocytosis**
    a. Treatment with dyngo-4a, a dynamin antagonist, significantly impairs uptake of anti-PKCα antibodies
3. **Clathrin-mediated endocytosis (CME) does not contribute to antibody uptake in ON-BCs**
    a. Treatment with pitstop 2, a CME inhibitor, does not significantly inhibit antibody uptake in ON-BCs.
    b. Pitstop 2 *does* inhibit uptake of transferrin (a CME-dependent process) in HEK293T cells.
4. **Antibody internalization does not require the Fcγ receptor**
    a. Fab fragments made from anti-PKCα antibodies, which cannot engage FcγR, are internalized by ON-BCs
5. **Recognition of the target antigen is not required for antibody uptake**
    a. Antibodies used in this study target intracellular antigens and cannot recognize surface epitopes.
    b. Uptake is still observed in MHC I knockout mice, precluding the possibility that antibodies recognize target epitopes displayed by MHC I on the cell surface.
6. **Antibody uptake is only observed in cells expressing the target antigen**
    a. Uptake of anti-PKCα antibodies is not observed in retinas from PKCα KO mice
    b. ON-BCs do not internalize antibodies targeting calbindin-D, a protein expressed by horizontal cells but not ON-BCs.
    c. Antibodies are likely internalized non-specifically and only persist in the cell if they engage their target epitope.

5.2: Summary

This dissertation contributes several significant findings and one novel tool that advance our understanding of MAR's molecular mechanisms. First, the long-term MAR case study in **Chapter 2** demonstrates a strategy for successful treatment of visual symptoms, highlights the potential influences of cancer treatment/progression on MAR pathology, and proposes a mechanism by which autoantibodies may cross from the blood stream into the retina. Like previously characterized individuals, the patient produced autoantibodies targeting intracellular epitopes on TRPM1, posing the question as to how such antibodies could access the cytoplasm of ON-BCs. In preparation for evaluating this question, **Chapter 3** presents a model system for studying antibody internalization in retinal ON-BCs. Through a rigorous set of experiments, ON-BCs are shown to be structurally intact, viable, and healthy in the split retina preparation. After establishing the

suitability of this new model, **Chapter 4** brandishes this tool as the cornerstone for experiments probing the behavior of ON-BCs during antibody internalization. The results reveal a distinct, dynamin-dependent, but clathrin- and FcγR-independent endocytosis pathway not yet observed in other neurons. These developments establish a clear framework on which to launch additional studies focused on refining the specific endocytic pathway used by ON-BCs to internalize antibodies.

5.3: Future Directions

While exciting and informative in their own right, the results of **Chapters 2 and 4** engender new ideas that should be explored in greater depth in future studies. The matter of antibody access to the retina has perhaps the most pertinent clinical relevance, as preventing this breach would eliminate MAR symptoms entirely. However, insubstantial evidence on the nature of this intrusion currently precludes the development of therapies that might exclude antibodies from the retina. Although the BRB is almost certainly the structure regulating antibody access to the retina, is it B cells that extravasate across this barrier, or the antibodies themselves? Are antibodies trafficked across by endothelial cells, or do they passively flow through damaged regions of the barrier. The answers to these questions will be massively impactful on the future of MAR research and treatment.

With new non-invasive microscopy techniques capable of imaging individual immune cells in the living retina, we can begin to search for evidence of B cell infiltration into the retina that would support the hypothesis of local antibody secretion from within the eye[1]. While this approach is currently only available in mice, the same could be achieved using traditional confocal microscopy with immunofluorescent B-cell markers on post-mortem MAR retinal tissue. To assess factors that could potentially mediate BRB damage in MAR, *in cellulo* trans-well models of the BRB may be a practical choice[2,3]. One application would be assessing trans-well permeability to labeled antibodies following treatment with the inflammatory cytokines identified in the MAR patient eye. An increase in permeability would suggest that these cytokines are responsible for BRB damage in MAR. Our study revealed dexamethasone treatment to be successful in restoring normal vision, despite the continued presence of anti-TRPM1 autoantibodies in the blood stream. It is possible that the immunosuppressive effects of dexamethasone allow the BRB to recover from putative

inflammatory damage to exclude antibodies from the retina. This hypothesis could be explored in animal and cellular BRB models. Previously, our lab has attempted to reproduce MAR in mice by immunization with TRPM1 to induce autoantibody production, although all efforts have failed (unpublished; data not shown). If BRB integrity is a secondary factor regulating the onset of MAR, then perhaps MAR symptoms would manifest in a BRB-ablated mouse following TRPM1 immunization[2]. Although substantial effort would be required to optimize such a model, its success would dramatically expand experimental options for studying MAR etiology.

Regarding the mechanism of antibody uptake by ON-BCs, there is much opportunity to expand upon the experiments detailed in **Chapter 4**. As new compounds become available for the selective inhibition of endocytic pathways, the same split retina strategy can be employed to observe the effects on antibody uptake. Although none currently exist, inhibitors of fast endophilin mediated endocytosis would be a logical choice, as our evidence implicates this pathway given its dependence on dynamin but lack of dependence on clathrin. Amongst currently available compounds, dexamethasone would be another curious candidate; the mechanism of dexamethasone's therapeutic benefit is not known. One possibility is that it ameliorates BRB damage following inflammation. It is also conceivable that dexamethasone acts directly on ON-BCs to inhibit antibody uptake, thereby protecting them. Soluble dexamethasone could be easily implemented in the split retina assay to test this hypothesis.

Beyond chemical approaches to pathway inhibition, future implementation of genetic tools could provide addition results validation, and may offer enhanced target specificity. More precisely, knockdowns to genes involved in specific endocytosis pathways (i.e., clathrin heavy chain, caveolin-1, etc.) using siRNA, an approach that has already been implemented in the retina[4]. Not only would this approach fortify the results of the study, it could expand the number of eligible pathways to target as it no longer relies on the laborious development of chemical inhibitors.

In the approach described in **Chapter 4**, antibody uptake was quantified from images collected on a confocal microscope using a custom image analysis pipeline. While micrographs contain valuable qualitative and quantitative data, collection of these data is tedious and low throughput. To complement microscopy in future studies, flow cytometry may offer a means to expedite data

collection and expand the number of experimental conditions possible for a given study. This strategy would entail the preparation of dissociated retinal neuron cultures prior to antibody uptake. After antibody incubation, the cultured cells could be resuspended and processed on a flow cytometer where uptake signal within Td-tomato positive (ON-BCs) and viability dye negative (living cells) cells could be quantified. Although this approach lacks the physiological power of the split retina, it may have considerable merit when used in conjunction with microscopy.

5.4: Acknowledgements

I'd like to thank my advisors Catherine and Robert for five years of exceptional mentorship. Under your guidance, I was never limited in my opportunities to think creatively, try new ideas, or fail. By providing me with a nourishing, stimulating, and comfortable environment to explore, you strengthened my confidence and independence as a young scientist.

Chapter 5 Bibliography

1. Joseph, A., Chu, C. J., Feng, G., Dholakia, K. & Schallek, J. Label-free imaging of immune cell dynamics in the living retina using adaptive optics. *eLife* **9**, e60547 (2020).

2. Bora, K. *et al.* Assessment of Inner Blood-Retinal Barrier: Animal Models and Methods. *Cells* **12**, 2443 (2023).

3. Byrne, E. M. *et al.* IL-17A Damages the Blood–Retinal Barrier through Activating the Janus Kinase 1 Pathway. *Biomedicines* **9**, 831 (2021).

4. Taniguchi, T. *et al.* Novel use of a chemically modified siRNA for robust and sustainable in vivo gene silencing in the retina. *Sci Rep* **10**, 22343 (2020).

Appendix 1

The Role of TRPM1 Alternative Splicing in Melanoma Progression and Paraneoplastic Autoimmunity

DOI: *unpublished work, preliminary data*

A1.1: Abstract

The etiology of paraneoplastic autoimmunity is complex, diverse, and elusive. Which elements of oncogenesis trigger an immune response against self-proteins? What determines a tissue's susceptibility to autoimmune attack? These questions and others motivate current research on the cause for adverse side-effects during anti-cancer immune responses. Melanoma-associated retinopathy (MAR) is an example of a neurological paraneoplastic syndrome with unknown etiology; autoantibodies directed against an ion channel called TRPM1 impair vision by blocking the depolarization of retinal ON bipolar cells, but the trigger for TRPM1 autoantibody production is not understood. Neoepitope formation due to translation of alternatively spliced mRNA is a documented primer for autoimmunity, and several studies have identified an upregulation of TRPM1 alternative splicing in melanoma. Melanoma cells also downregulate expression of a tumor suppressor microRNA, miR-211, which may also be a consequence of TRPM1 alternative splicing since miR-211 is encoded by TRPM1's sixth intron. In this preliminary study, we explored the possibility that alternative splicing of TRPM1 mRNA is simultaneously responsible for triggering TRPM1 autoantibody production and depleting miR-211 expression. After quantifying miR-211 and three TRPM1 isoforms in melanoma cell lines and tumors, we searched for correlations in expression that may suggest a particular splicing pattern is associated with reduced miR-211. However, all three TRPM1 isoforms were weakly but positively correlated with miR-211. Quantifying additional known and unknown TRPM1 isoforms may still reveal a link between splicing and TRPM1 autoantibody generation that elucidates MAR etiology.

A1.2: Introduction

A1.2.1 Background

Cutaneous melanoma (CM) is an aggressive form of skin cancer that originates in the pigment-producing cells of the epidermis known as melanocytes[1]. These melanocytes utilize the amino acid tyrosine to synthesize melanin, a pigment that protects the skin from the harmful UV-B radiation in sunlight[2]. During their malignant transformation, melanocytes progressively lose their pigmentation, a phenomenon believed to result from diminishing expression of a gene called transient receptor potential melastatin 1 (TRPM1)[3–5]. The TRPM1 gene encodes an ion channel required for melanin production and intracellular calcium regulation in melanocytes[6]. Therefore,

as melanoma cells become more malignant and produce less TRPM1, they also produce less melanin and lose their pigmentation. Another consequence of reduced TRPM1 expression is the loss of the tumor suppressor microRNA, miR-211, encoded by the sixth intron of TRPM1[7,8]. Micro RNA (miRNA) regulate gene expression through complementary base pair binding to the 3' or 5' UTR of their mRNA target[9]. While miR-211 has diverse regulatory roles in different cancers, it is generally accepted that miR-211 represses cancer progression in melanoma by inhibiting genes involved in migration, cell proliferation, invasiveness/metastasis, and metabolism[7,8,10,11]. It has been shown that TRPM1 mRNA and miR-211 are cotranscribed[12]. Thus, reduced TRPM1 expression in melanoma means the simultaneous loss of miR-211, enabling unchecked expression of the growth pathway genes typically suppressed by miR-211.

Some patients with CM develop a paraneoplastic syndrome called melanoma-associated retinopathy (MAR) in which autoantibodies directed against TRPM1 cause visual impairment. While autoantibodies in paraneoplastic syndromes are often correlated with improved survival rates[13–15], they can exert pathogenic effects in healthy tissues. In the case of MAR, TRPM1 autoantibodies interfere with neurotransmission from retinal neurons called ON-bipolar cells (ON-BCs), as ON-BCs rely on TRPM1 conductivity for depolarization. The production of autoantibodies against TRPM1 implies a breach of immune tolerance to this self-protein, yet the precise trigger for autoantibody generation of is unknown. Understanding the mechanism of TRPM1 autoantibody production may lead to intervention strategies or therapies for the prevention of MAR and other paraneoplastic syndromes.

A1.2.2 Rationale

One mechanism by which self-proteins in cancerous cells can become immunogenic is through the formation of neoepitopes encoded by alternatively spliced transcripts[16]. As protein folding patterns for alternatively spliced transcripts are likely to differ from those of classical isoforms, the immune system may perceive these unique protein epitopes as foreign, eliciting a cellular and humoral response. Several groups have identified an increase in alternatively spliced TRPM1 mRNA isoforms in melanoma cells compared to healthy melanocytes[4,17]. It is possible these mRNA isoforms encode some of the TRPM1 protein isoforms expressed in melanoma that are not found in healthy melanocytes[18]. Furthermore, several of these alternatively spliced transcripts feature

stop codons that terminate near the miR-211 intron (**Supplemental Figure A1-S1**), which could lead to aberrant or reduced miR-211 expression and subsequent dysregulation of cell growth pathways. Therefore, TRPM1 alternative splicing could be dually responsible for the loss of miR-211 expression observed during malignant transformation, and the production of immunogenic polypeptides that elicit an autoantibody response. Under this hypothesis, the alternative splicing pattern giving rise to a truncated, immunogenic TRPM1 protein isoform would also repress miR-211 transcription, leading to a negative correlation between the expression of miR-211 and the aberrant TRPM1 isoform. If expression of these putative isoform(s) is a consequence of the transition to a cancerous state, one would expect the isoforms and their corresponding proteins, to be more abundant in melanoma cells than healthy melanocytes. An inverse correlation between an alternatively spliced TRPM1 isoform and the expression of miR-211, in addition to the expression of this isoform in cancerous, but not healthy melanocytes, would indirectly support the hypothesis that expression of an alternative TRPM1 isoform is associated with an anti-TRPM1 immune response.

A1.2.3 Study description

In this work, the expression of miR-211 and three TRPM1 isoforms was quantified in primary melanocytes, melanoma cell lines, and melanoma tumor samples to identify trends in expression that could explain the loss of miR-211 and the anti-TRPM1 autoantibody response in MAR. One full-length isoform (TRPM1-201) and two truncated, alternatively spliced isoforms (TRPM1-210, TRPM1-211) that do not encode functional ion channels were chosen for comparison. While expression of miR-211 was shown to vary widely across melanoma tumors and cell lines, melanoma samples generally expressed less miR-211 than primary melanocytes. For the two truncated TRPM1 mRNA isoforms examined (TRPM1-210 and TRPM1-211), expression was observed in both primary melanocytes and melanoma samples, demonstrating even healthy melanocytes express TRPM1 isoforms that do not encode functional channel proteins. Furthermore, expression of TRPM1-201 was observed in both primary melanocytes and melanomas, establishing that expression of a full length TRPM1 isoform is maintained in some melanomas. Combined analysis of TRPM1 and miR-211 revealed their expression to be correlated, regardless of which TRPM1 isoform was expressed. Therefore, splicing of these two truncated TRPM1 isoforms is likely not responsible for the loss of miR-211, and their expression is unlikely

to trigger the anti-TRPM1 autoantibody response in MAR since they are also expressed at similar levels in primary melanocytes.

A1.3: Results

A1.3.1 Validation of endogenous control genes for qPCR quantification of miRNA and TRPM1 mRNA

Before quantifying the miR-211 and TRPM1 mRNA transcripts, stably expressed endogenous control genes were established using two melanoma cell lines and two primary melanocyte cell lines. A small non-coding nuclear RNA, RNU6B, was found to be stable across all five cell lines and was selected as an endogenous control for miR-211 quantification (**Figure A1-1A**). For quantification of TRPM1 transcripts, RPS2, which encodes a component of the 40S ribosome, was shown to be stably expressed across the same cell lines (**Figure A1-1B**).

Figure[A1-1]

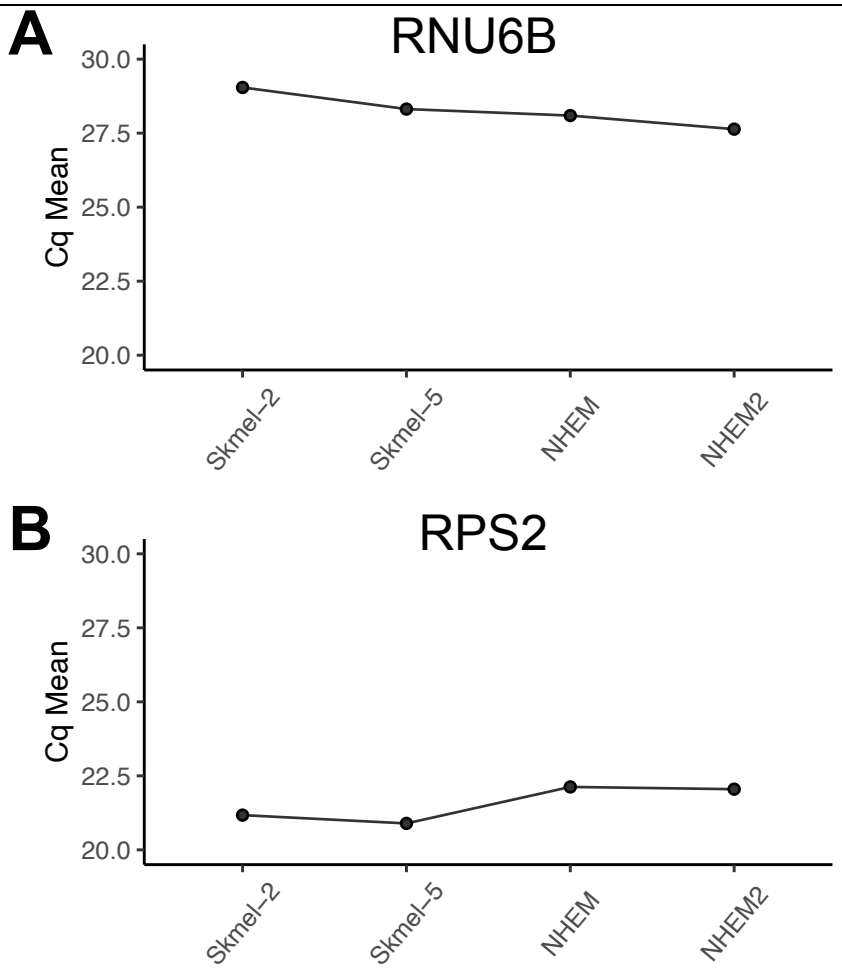

[A1-1] Validation of endogenous control genes for qPCR quantification of miRNA and TRPM1 mRNA. Mean Cq values of amplification for RNU6B (**A**) and RPS2 (**B**) in two melanoma cell lines (Skmel-2, Skmel-5) and two primary melanocyte cell lines (NHEM, NHEM2). Expression of RNU6B and RPS2 are stable across all four cell lines and were selected to serve as endogenous control genes for the quantification of miR-211 and TRPM1 respectively.

A1.3.2 Expression of miR-211 varies widely in melanoma cells and tumors

Consistent with previous reports[7,8], miR-211 expression was reduced in almost all melanoma samples compared to normal human epidermal melanocytes (NHEM) (**Figure A1-2**). However, expression of miR-211 within melanoma samples varied enormously. For melanoma cell lines, values ranged from about five times less to five-thousand times less than the level observed in NHEM. For melanoma tumors, values ranged from about ten times more to five-thousand times less miR-211 than NHEM, demonstrating metastatic melanomas express very different levels of

miR-211. One melanoma tumor sample expressed about ten times more miR-211 than NHEM, revealing that malignancy is not directly correlated to the loss of miR-211 in melanoma.

Figure[A1-2]

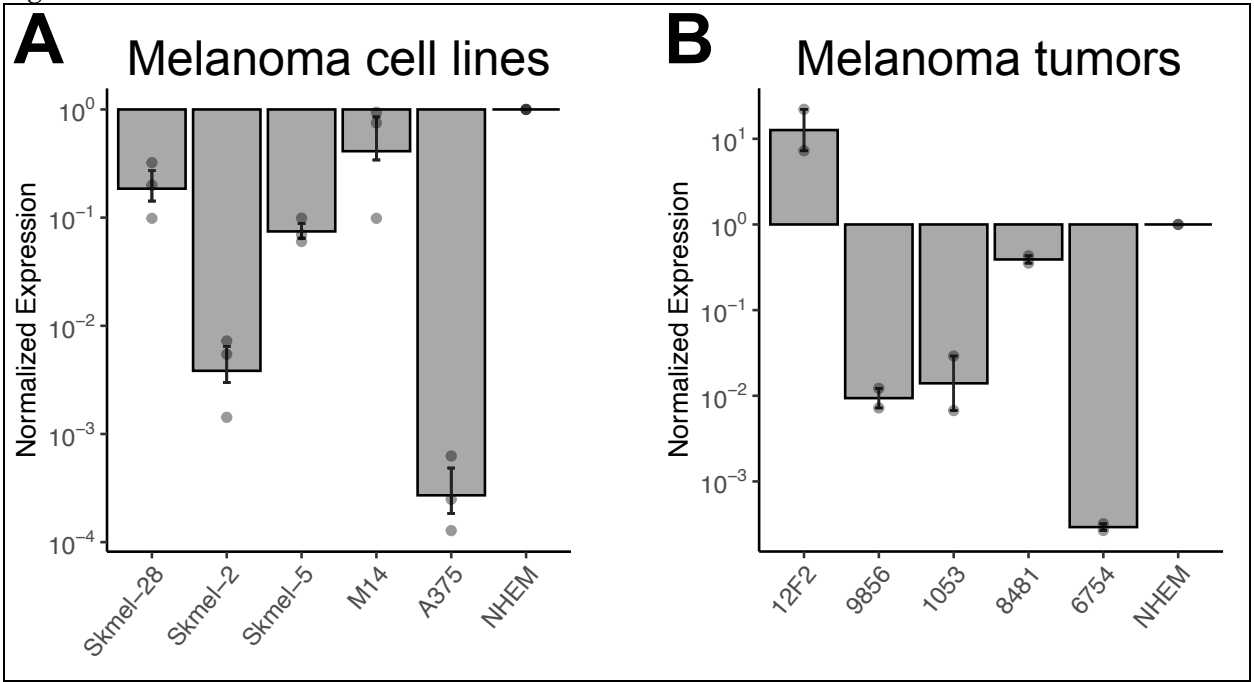

[A1-2] **Expression of miR-211 varies widely in melanoma cells and tumors.** Expression of miR-211 in melanoma cell lines (**A**) and melanoma tumor samples (**B**) normalized to the expression in normal human epidermal melanocytes (NHEM). Error bars represent SEM.

A1.3.3 Healthy and cancerous melanocytes both express full length and truncated TRPM1 mRNA isoforms

As previous studies identified an upregulation of short, alternatively spliced TRPM1 isoforms in melanoma, we expected to find higher expression of the two truncated TRPM1 mRNA isoforms (TRPM1-210 and TRPM1-211) in melanoma cells compared to primary melanocytes. Compared to melanoma cell lines, however, primary melanocytes were the second highest expresser of the two short TRPM1 isoforms, with only M14 melanoma cells expressing more of these variants (**Figure A1-3A**). A similar trend was observed in melanoma tumors (**Figure A1-3B**). We also expected full-length isoform expression to be higher in primary melanocytes than melanomas. Instead, expression was highly variable across the melanomas, and in some cases (Skmel-28, M14, 12F2), levels of TRPM1-201 were higher than in primary melanocytes (**Figure A1-3**). Two melanoma cell lines (Skmel-2 and A375) and two melanoma tumors (1053 and 6754) expressed

very little TRPM1 across all three isoforms, mirroring their low expression of miR-211 (**Figure A1-2**). In the M14 and 9856 samples, expression of all three isoforms was highly inconsistent, perhaps indicating that TRPM1 transcription fluctuates in some melanomas.

Figure[A1-3]

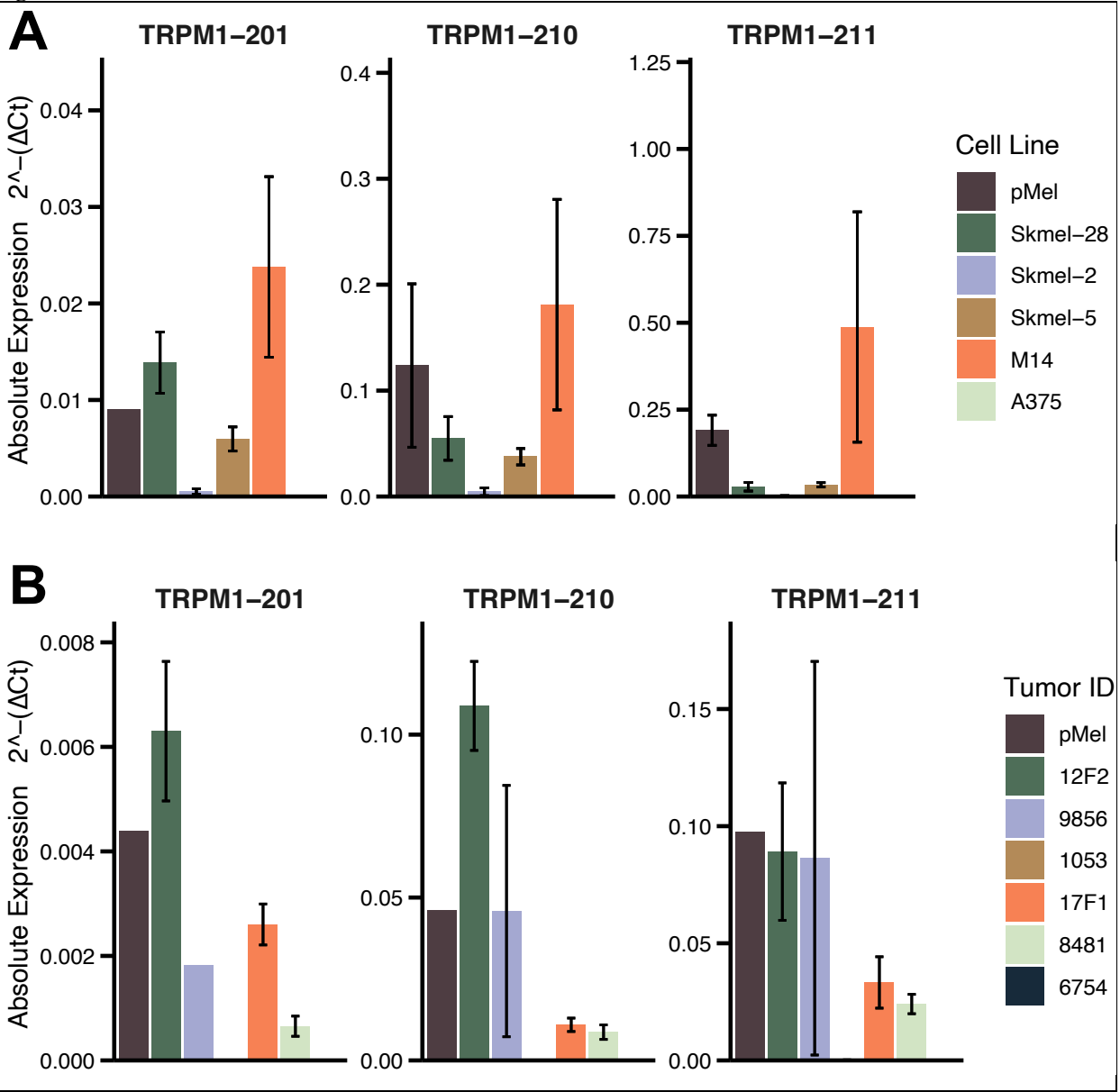

[A1-3] **Healthy and cancerous melanocytes both express full length and truncated TRPM1 mRNA isoforms**. One full length (TRPM1-201) and two truncated (TRPM1-210, TRPM1-211) isoforms were quantified in melanoma cell lines (**A**), melanoma tumors (**B**) and primary melanocytes (pMel) using qPCR. For each sample, TRPM1 expression is normalized to RPS2. Error bars represent SEM. Bars lacking SEM have only a single measurement.

A1.3.4 miR-211 and TRPM1 expression are correlated regardless of isoform

To identify trends in expression between individual TRPM1 isoforms and miR-211, tumor and cell line samples were plotted according to their expression of miR-211 and each TRPM1 variant. Contrary to our hypothesis, expression of truncated and full-length isoforms both correlated positively with miR-211. Although, since Spearman correlation values were low and mostly insignificant, TRPM1 appears to be a poor predictor of miR-211 expression, at least for the isoforms examined in this study.

Figure[A1-4]

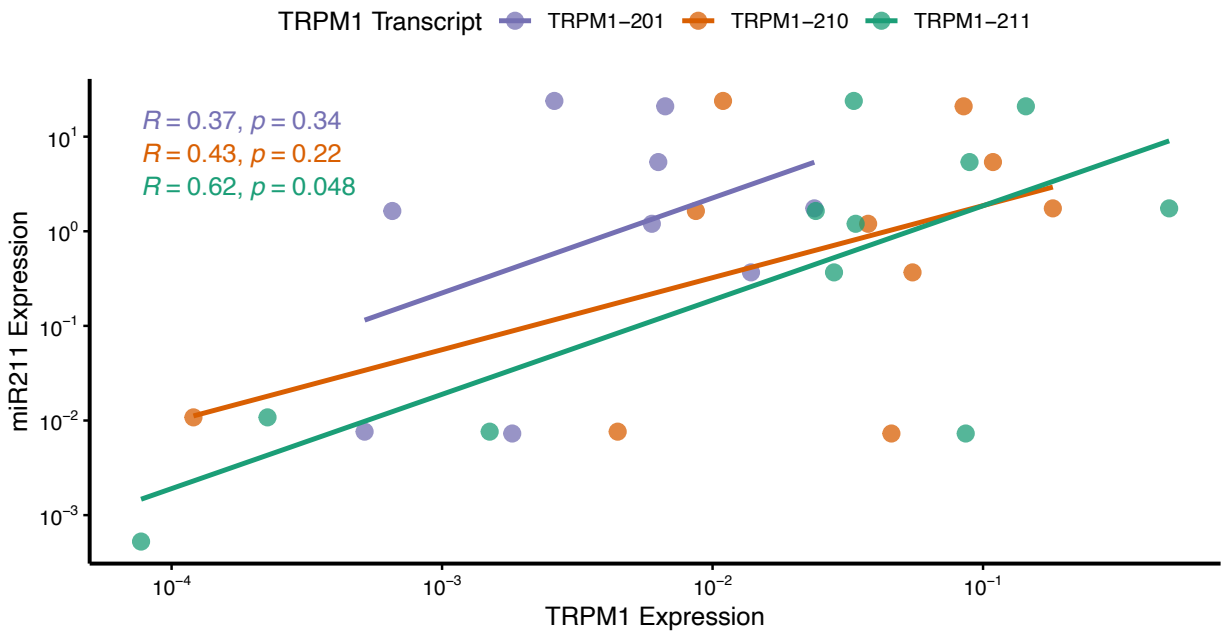

[A1-4] **miR-211 and TRPM1 expression are correlated regardless of isoform**. All melanoma cell line and tumor samples were plotted according to their absolute expression of miR-211 (y-axis) each TRPM1 isoform (x-axis). For each isoform, a Spearman coefficient was used to identify correlations with miR-211 expression and to generate trend lines. Truncated and full length TRPM1 isoforms both correlate weakly, but positively with miR-211 expression.

A1.4: Discussion

In the paraneoplastic syndrome, MAR, autoantibodies are generated against a channel protein called TRPM1 expressed by cutaneous melanocytes and ON-BCs of the retina. While the trigger for the autoantibody response is unknown, observations of dysregulated TRPM1 mRNA

production in melanoma may hint at a role for alternative splicing in MAR etiology. Several studies have identified truncated TRPM1 isoforms in melanoma that are absent in healthy melanocytes[4,17,18]; these isoforms produced by aberrant alternative splicing may encode proteins with neoepitopes that trigger an autoimmune response against TRPM1. Perhaps relatedly, other researchers have shown that melanomas downregulate expression of a tumor suppressor micro-RNA, miR-211, encoded by the sixth intron of TRPM1. We hypothesized that aberrant alternative splicing in melanoma truncates TRPM1 mRNA, preventing production of miR-211 and simultaneously generating novel protein isoforms that elicit an immune response.

This preliminary study explores the relationship between miR-211 and TRPM1 expression in melanoma to identify the contribution of TRPM1 alternative splicing to MAR etiology. Toward this goal, we quantified miR-211 in melanoma cell lines and tumors. We next correlated this with expression of truncated and full-length TRPM1 isoforms to discern if expressing specific TRPM1 isoforms was correlated with the loss of miR-211. Like previous studies, we found that miR-211 is generally reduced in melanoma compared to healthy melanocytes (**Figure A1-2**). However, miR-211 levels varied widely between different melanoma tumors and cell lines. Opposite our expectations, we observed higher expression of truncated TRPM1 isoforms in primary melanocytes than most melanomas (**Figure A1-3**). Further, we found unexpected expression of full-length TRPM1 within melanomas. Therefore, expression of truncated TRPM1 isoforms is not a generalizable or unique feature of melanoma cells, and expression of full-length TRPM1 isoforms is not unique to healthy melanocytes. Ultimately, melanoma alone is a poor predictor of miR-211 expression levels or TRPM1 mRNA variants, and expression of these TRPM1 isoforms is only loosely correlated with miR-211 (**Figure A1-4**). Importantly, none of these TRPM1 isoforms were correlated with reduced miR-211 expression. However, at the time of writing, there are at least 12 documented – and perhaps additional unidentified – TRPM1 isoforms whose splicing patterns could interfere with miR-211 production. Due to restrictions in qPCR primer design that ensure unique detection of single variants, only three of these isoforms were examined in this study.

Future studies should employ strategies such as open reading frame capture-seq to identify all existing TRPM1 isoforms across a larger repository of melanoma samples before correlating each

with miR-211 expression. Additionally, monoclonal antibodies targeting the TRPM1 N-terminus will be useful for identifying the protein isoforms encoded by truncated mRNAs (see **Appendix 2**). Using these approaches, causal relationships between aberrant TRPM1 splicing and miR-211 loss may yet be identified. Should malignant splicing patterns be identified in melanoma, manipulation of isoform production through splice site silencing or other means may provide a therapeutic solution for eliminating autoantibody generation against TRPM1 and preventing MAR.

A1.5: Materials & Methods

Melanoma tumor samples

Frozen human melanoma tumor samples were acquired from the Knight Cancer Institute BioLibrary at Oregon Health & Science University. All samples were taken from stage III and stage IV metastatic melanoma tumors. To prepare for RNA extraction, 10-30 mg samples of frozen tissue were ground to a fine powder with a mortar and pestle that were chilled with dry ice and repeated applications of liquid nitrogen. The powder was then transferred to chilled microfuge tubes containing RNA lysis buffer and stored at -80 ºC until RNA extraction.

Cell culture and RNA extraction

Melanoma cell lines (Skmel-28, Skmel-2, Skmel-5, M14, A375) were cultured in DMEM supplemented with 10% FBS, penicillin, and streptomycin. Primary melanocytes (NHEM, NHEM-M2) were purchased as cell pellets from PromoCell (Cat#: C-14040). Additional adult primary epidermal melanocytes (pMel; ATCC; Manassas, VA; Cat# PCS-200-013) were cultured in dermal cell basal medium (ATCC; Manassas, VA; Cat# PCS-200-030) supplemented with adult melanocyte growth factors (ATCC; Manassas, VA; Cat# PCS-200-042). Melanoma cell lines (gifted from the Pam Cassidy lab at OHSU) were grown to 95-100% confluence in 60mm dishes. The cells were trypsinized, centrifuged, and stored at -20 ºC as pellets until RNA extraction. Small and large RNA fractions were isolated in parallel from cell pellets using a miRNA isolation kit (Machery Nagel; Nordrhein-Westfalen, Germany; Nucleospin miRNA mini kit; Cat#: 740971.50).

cDNA synthesis and qPCR

For quantification of miRNA by qPCR, the small RNA fraction was used to synthesize cDNA with miR-211- or RNU6B-specific stem-loop primers (Thermo Fisher; Waltham, MA; Cat#: 4427975;

Assay ID: 000514, 001093) and the TaqMan MicroRNA RT kit (Thermo Fisher; Waltham, MA; Cat#: 4366596). For quantification of mRNA by qPCR, the large RNA fraction was used to synthesize cDNA (Qiagen; Germantown, MD; Quantitech RT Kit; Cat#: 205311). Primer and TaqMan probe sets for TRPM1 transcript amplification were designed and synthesized by IDT (**Additional File 1**). Quantification of miRNA by qPCR was achieved using pre-formulated assays (Thermo Fisher; Waltham, MA; Cat#: 4427975; Assay ID: 000514, 001093). All qPCR assays were performed on an Applied Biosystems QuantStudio 7 Flex (Thermo Fisher; Waltham, MA; Cat#: 4485701). Data analysis was carried out using Design and Analysis 2 software and a custom R package for qPCR analysis[19]. All sample conditions were assayed in triplicate. In groupings with a SD > 0.5 the most deviant measurement was omitted as an outlier.

A1.6: Supplemental Information

Figure[A1-S1]

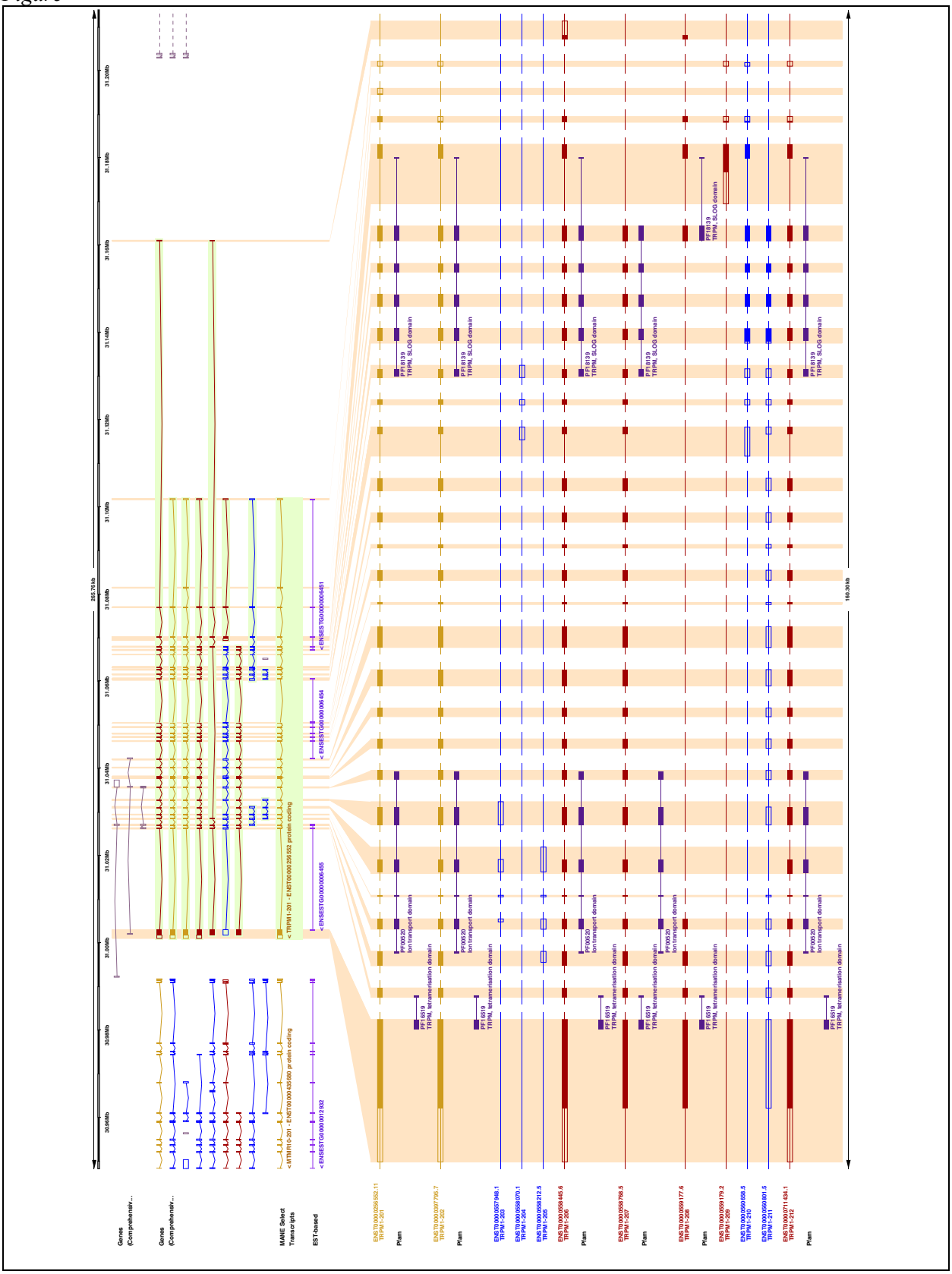
Genes (Comprehensiv...
Genes (Comprehensiv...
MANE Select Transcripts
EST-based
Pfam
TRPM1-201 - ENST00000256552 protein coding
MTMR10-201 - ENST00000435680 protein coding
ENSESTG00000006455
ENSESTG00000006454
ENSESTG00000006451
ENSESTG00000012932
PF06520 Ion transport domain
PF16519 TRPM, tetramerisation domain
PF16139 TRPM, SLOG domain

[A1-S1] **TRPM1 transcript schematic**. A schematic of alternatively spliced TRPM1 isoforms registered in the Ensemble Gene Browser database.

Appendix 1 Bibliography

1. Leonardi, G. C. *et al.* Cutaneous melanoma: From pathogenesis to therapy (Review). *International Journal of Oncology* **52**, 1071–1080 (2018).

2. Moreiras, H., Seabra, M. C. & Barral, D. C. *Melanin Transfer in the Epidermis: The Pursuit of Skin Pigmentation Control Mechanisms*. https://www.preprints.org/manuscript/202104.0441/v1 (2021) doi:10.20944/preprints202104.0441.v1.

3. Duncan, L. M. *et al.* Down-Regulation of the Novel Gene Melastatin Correlates with Potential for Melanoma Metastasis. *Cancer Res* **58**, 1515–1520 (1998).

4. Oancea, E. *et al.* TRPM1 Forms Ion Channels Associated with Melanin Content in Melanocytes. *Science Signaling* **2**, ra21–ra21 (2009).

5. Deeds, J., Cronin, F. & Duncan, L. M. Patterns of melastatin mRNA expression in melanocytic tumors. *Hum Pathol* **31**, 1346–1356 (2000).

6. Guo, H., Carlson, J. A. & Slominski, A. Role of TRPM in melanocytes and melanoma. *Exp Dermatol* **21**, 650–654 (2012).

7. Mazar, J. *et al.* The Regulation of miRNA-211 Expression and Its Role in Melanoma Cell Invasiveness. *PLoS ONE* **5**, e13779 (2010).

8. Levy, C. *et al.* Intronic miR-211 Assumes the Tumor Suppressive Function of Its Host Gene in Melanoma. *Molecular Cell* **40**, 841–849 (2010).

9. Valinezhad Orang, A., Safaralizadeh, R. & Kazemzadeh-Bavili, M. Mechanisms of miRNA-Mediated Gene Regulation from Common Downregulation to mRNA-Specific Upregulation. *Int J Genomics* **2014**, 970607 (2014).

10. Mazar, J. *et al.* MicroRNA 211 Functions as a Metabolic Switch in Human Melanoma Cells. *Mol. Cell. Biol.* **36**, 1090–1108 (2016).

11. Ye, L. *et al.* Role and mechanism of miR-211 in human cancer. *J Cancer* **13**, 2933–2944 (2022).

12. Janas, M. M. *et al.* Feed-Forward Microprocessing and Splicing Activities at a MicroRNA–Containing Intron. *PLOS Genetics* **7**, e1002330 (2011).

13. Jing, K. *et al.* The presence of autoantibodies is associated with improved overall survival in lung cancer patients. *Frontiers in Oncology* **13**, 1234847 (2023).

14. Bachelot, T. *et al.* Autoantibodies to endostatin in patients with breast cancer: correlation to endostatin levels and clinical outcome. *Br J Cancer* **94**, 1066–1070 (2006).

15. Gogas, H. *et al.* Prognostic Significance of Autoimmunity during Treatment of Melanoma with Interferon. *New England Journal of Medicine* **354**, 709–718 (2006).

16. Bernard, A., Boidot, R. & Végran, F. Alternative Splicing in Cancer and Immune Cells. *Cancers* **14**, 1726 (2022).

17. Fang, D. & Setaluri, V. Expression and Up-Regulation of Alternatively Spliced Transcripts of Melastatin, a Melanoma Metastasis-Related Gene, in Human Melanoma Cells. *Biochemical and Biophysical Research Communications* **279**, 53–61 (2000).

18. Zhiqi, S. *et al.* Human melastatin 1 (TRPM1) is regulated by MITF and produces multiple polypeptide isoforms in melanocytes and melanoma: *Melanoma Research* **14**, 509–516 (2004).

19. Ryan, M.-H. rhecht95/qPCR. https://doi.org/10.5281/zenodo.13904564 (2022).

Appendix 2

Contributions to Retinal Physiology

Note: Appendix 2 does not include full methods descriptions or results sections. For more detailed method information, please reference the previous chapters.

A2.1: The Effect of Dark Adaptation on the Bipolar Cell Light Response

The following section describes a contribution to work published in *Frontiers in Ophthalmology*[1]:

Light-dependent changes in the outer plexiform layer of the mouse retina

Tammie L. Haley, **Ryan M. Hecht**, Gaoying Ren, James R. Carroll, Sue A. Aicher, Robert M. Duvoisin and Catherine W. Morgans*

Department of Chemical Physiology & Biochemistry, Oregon Health & Science University, Portland, OR, United States

A2.1.1 Summary of published work

Human vision's operating range spans 10^9 log units of light intensity, a feat largely attributable to the remarkable adaptation mechanisms of retinal neurons. To enable adaptation across this large gamut of light intensity, the retina employs a diverse and complex set of mechanisms at both the network and cellular levels. The sensitivity difference between rod and cone photoreceptors illustrates a network-level mechanism of adaptation, whereby vision in both candlelight and bright daylight are made possible by the transition from rod usage in dim light to cones usage in bright light[2]. On the cellular level, photoreceptors modulate their sensitivity to light through complex changes to the molecular machinery of the phototransduction cascade, which takes place in the photoreceptor outer segments. Like the outer segments, studies indicate the photoreceptor synapses as another site of light adaptation[3,4]. However, little is known about how neurotransmission in the outer plexiform layer (OPL) modulates the retinal circuit's responsiveness to light. The first synapse to processes image-forming input, neuronal activity in the OPL has an enormous impact on vision. Therefore, biochemical and morphological modulation of this synapse would directly affect neurotransmission and could represent an under-studied mechanism of light adaptation. In an effort to identify such mechanisms, this study examined the effects of light and dark adaptation on OPL morphology, and synaptic protein abundance and distribution.

The study found that prolonged dark adaptation (72 hours) caused significant changes to the abundance and localization of several synaptic proteins in the outer plexiform layer. Ribeye, for example–a component of the photoreceptor synaptic ribbon–was almost entirely undetectable by western blot or immunohistochemistry following a 72-hour dark adaptation period, but returned to standard levels after just 30 minutes of light exposure. This dramatic change is too rapid to be accounted for by protein degradation and re-synthesis and may instead signify a post-translational modification to ribeye that masks the antibody epitope. Despite the observed changes to pre-synaptic proteins, no gross morphological differences were apparent by electron microscopy after 72 hours of dark adaptation. As with the pre-synaptic protein, ribeye, several changes to post-synaptic proteins were observed in response to prolonged dark adaptation. After 72 hours of darkness, TRPM1 immunolabeling was dimmer throughout bipolar cells and nearly absent from the dendritic tips. Unlike ribeye, however, western blotting revealed that total TRPM1 abundance did not change in response to dark adaptation, suggesting instead that prolonged darkness induces conformational changes to TRPM1 that obscure the antibody epitope typically accessible in the light-adapted state.

To assess the visual consequences of the dark-induced changes to synaptic proteins, electroretinograms (ERGs) were recorded from mice that were dark adapted for increasingly long periods. Light adaptation at the photoreceptor synapse was measured by examining the amplitude ratio between the b-wave and a-wave, as adaptation in phototransduction would affect both the b- and a-waves, whereas adaptation at the photoreceptor synapse would affect only the b-wave. Evidence of light adaptation at the photoreceptor synapse was apparent by the reduced b/a-wave ratios in mice dark adapted for 72-hours compared to those dark adapted for the protocol standard of 16 hours (**Figure A2.1-1**). While this was true for all scotopic flash intensities, the effect was less pronounced for the brightest scotopic flash (2.41 cd•s/m^2). Dark adaptation for 48-hours produced a similar effect to that of 72-hours, although a less severe decrease in the b/a-wave ratio was observed. Although 72-hour dark adaptation reduced the b/a-wave ratio to 79-87% of standard (16-hour dark adaptation), ERGs from these mice were surprisingly robust considering the observed decrease in synaptic protein abundance and altered protein distribution. These findings demonstrate that light adaptation at the OPL is fast acting and is able to recover quickly despite dramatic changes to the biochemistry of the synapse

A2.1.2 Direct contribution

For this publication, I used the R programming language to perform ERG data processing, analysis, and visualization, which resulted in **Figure A2.1-1** (Figure 5 of the original article). The details of this analysis are documented in **Additional file 2**, which presents the raw code together with the code output and text narrative to yield a notebook-style exhibition of the analysis. In brief, variable parsing and data restructuring were performed to convert the data into a more tractable format from the original ERG Lab program output. Next, baseline offset was adjusted to 0 for all traces based on the average voltage during a pre-flash window (30-70 ms). Oscillating potentials were removed using a Butterworth Lowpass filter, then global minima and maxima for each trace were identified. For each trace, the b-wave was measured, then the b/a-wave ratio calculated. Averages were calculated and results were plotted in numerous styles before arriving upon the visualization that became Figure A2.1-1.

Figure[A2.1-1]

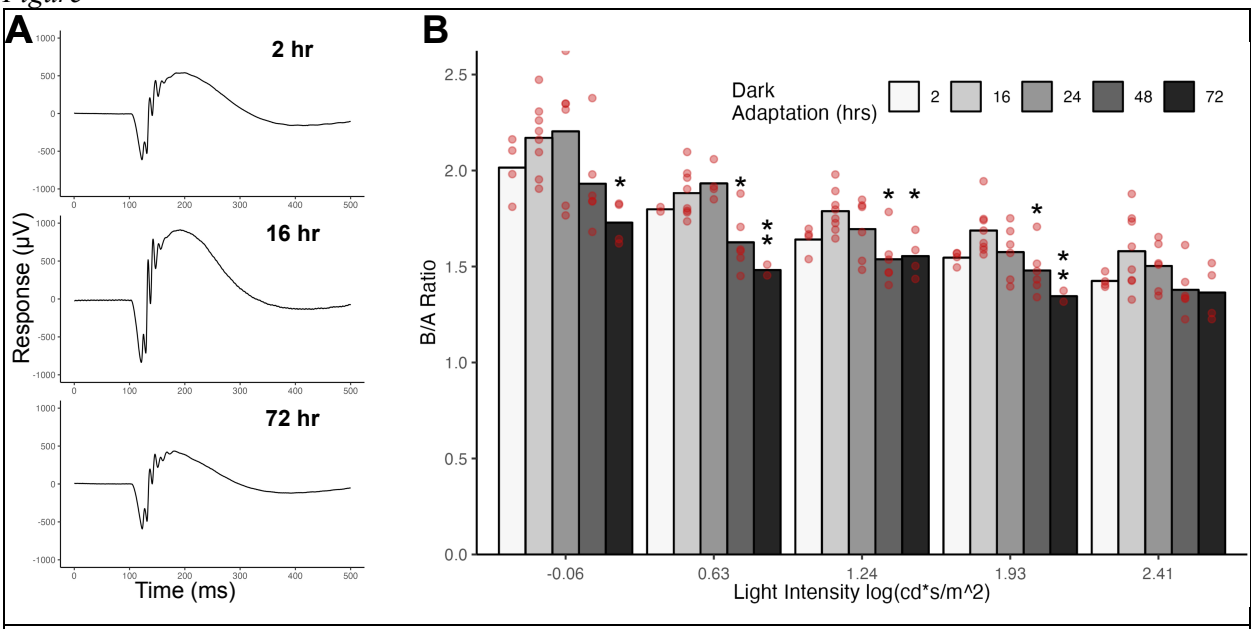

A2.1-1 Prolonged dark exposure decreases ERG amplitudes. ERGs from mice following different dark exposure times. (**A**) Representative ERG traces from mice that were dark exposed for 2, 16, or 72 hours. Flash strength = -0.06 log(cd*s/m2^). (**B**) Scotopic ERGs were recorded from mice that had been dark exposed for 2, 16, 24, 48, or 72 hours. The mean b-wave to a-wave ratios are plotted for light intensities that gave a measurable a-wave (-0.06 to 2.41 log(cd*s/m^2)). Values for individual eyes are indicated with red circles. Significant differences relative to the 16 hr dark-adapted state (our standard dark-adaptation time) are indicated with asterisks (*P ≤ 0.05, **P ≤ 0.01).

A2.2: Anti-TRPM1 Monoclonal Antibody Development

DOI: *unpublished work*

A2.2.1 Introduction

Transient receptor potential melastatin 1 (TRPM1) is a cation channel expressed by retinal ON-bipolar cells (ON-BCs) that enables ON-BCs to depolarize during the light response[5]. ON-BCs synapse directly with rod and cone photoreceptor and make several key processing contributions to image-forming vision[6]. If TRPM1 becomes dysfunctional, as can occur in disease, ON-BCs cannot depolarize, creating serious consequences for vision. Most notably, dysfunctional TRPM1 significantly compromises night vision due to the exclusive wiring of rod photoreceptors to ON-BCs[7]. Melanoma-associated retinopathy (MAR) is one such disease that involves the inhibition of TRPM1 by autoantibodies, causing night blindness, photopsia, contrast-sensitivity issues, and other visual deficits[8]. The trigger for autoantibody production against TRPM1 is unknown and remains an active area of research. Current hypotheses involve the formation of neoepitopes on TRPM1 due production of alternatively spliced mRNA isoforms within malignant cutaneous melanocytes (see **Appendix 1**). The detection and characterization of the mutant proteins encoded by these alternatively sliced transcripts will be an important step in understanding the cause for autoimmunity in MAR. Relatedly, the mechanism by which TRPM1 autoantibodies cross the ON-BC plasma membrane to reach intracellular target epitopes on the channel is another mystery under interrogation (see **Chapter 4**).

In the aforementioned areas of research, there is a pressing need for tools to study TRPM1 protein isoforms and the mechanism of TRPM1 autoantibody entry into ON-BCs. Specifically, antibodies targeting the TRPM1 N-terminus are required for detection of the truncated TRPM1 isoforms that arise from alternative splicing. Furthermore, antibodies that bind exclusively to TRPM1's intracellular cytoplasmic domains would be advantageous for exploring the mechanism of antibody uptake in ON-BCs. To address this deficiency, I generated four novel monoclonal antibodies against a region of the human TRPM1 N-terminus. As commercially available antibodies against TRPM1 are either specific to non-human sequences, or they target the protein's C-terminus, these antibodies fill a gap in the researcher's toolbox for the study of this essential ion channel.

A2.2.2 Antibody Characterization

From Chapter 4.3:

Two overlapping segments of the TRPM1 N-terminus (exons 2-7 and exons 6-10; NM_001252020.2; **Supplemental Table 4-S1**) were cloned from human M14 melanoma cells, then expressed in *E. coli (*Novagen (Sigma-Aldrich); Burlington, MA, USA; *pET-28a(+)*, Cat#: 69864) and the resulting his-tagged polypeptides were purified on a nickel column (Qiagen; Venlo, Netherlands; Ni-NTA Agarose; Cat#: 30210). Mice were immunized four times, three weeks apart, with the purified TRPM1 polypeptides in a Freund's adjuvant mixture. Serum from the immunized animals was used to confirm a positive immune response to TRPM1 by ELISA prior to splenic harvest and generation of hybridomas. Individual hybridoma clones were screened for reactivity with the purified TRPM1 proteins by ELISA. Supernatants from select clones were additionally screened for reactivity with TRPM1 in transfected HEK293T cells and mouse retina sections. Specificity for TRPM1 was confirmed with TRPM1 KO animals. Finally, monoclonal antibodies were isotyped (Thermo Fisher; Waltham, MA; Pro-Detect™ Rapid Antibody Isotyping Assay Kit, mouse; Cat#: A38550) and purified from the hybridoma supernatants with protein G sepharose columns (Cytiva; Marlborough, MA; Cat#: 17040401).

Figure[A2.2-1]

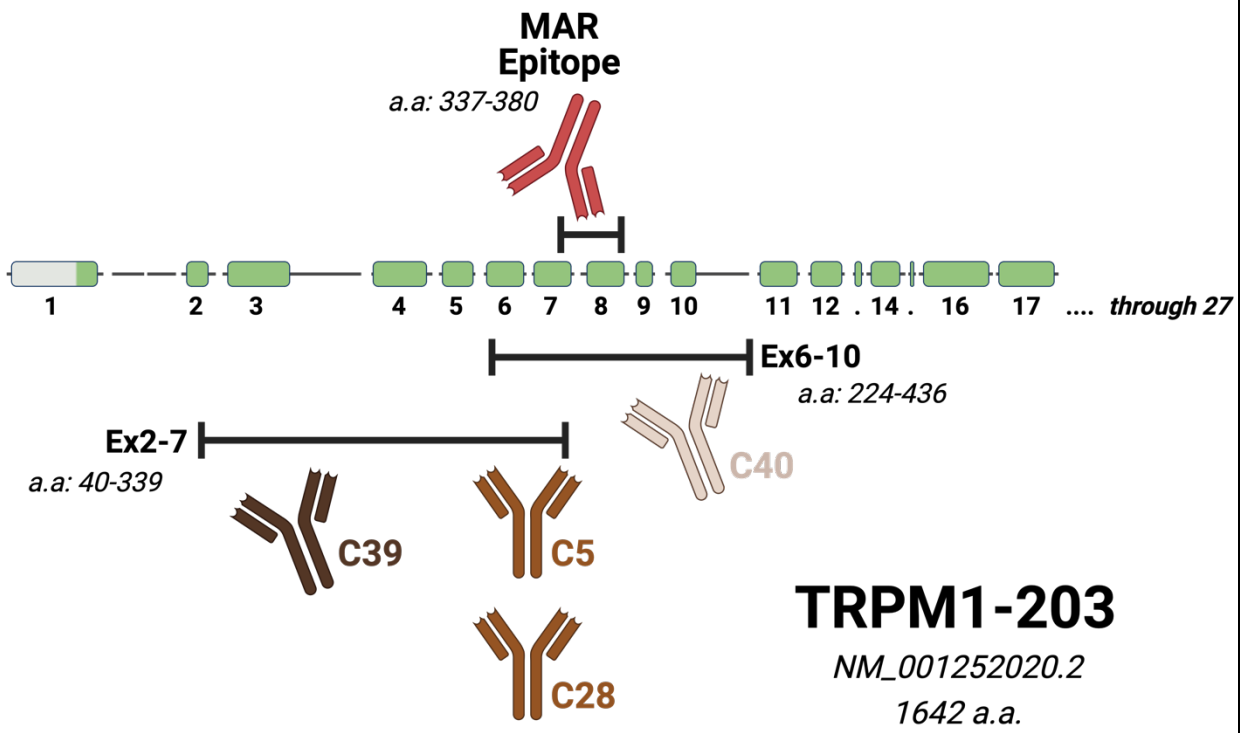

[A2.2-1] Epitopes of novel TRPM1 monoclonal antibodies. A gene schematic of a full-length TRPM1 isoform showing the approximate epitopes of the 4 novel TRPM1 monoclonal antibodies and the polypeptide immunogens they were raised against (black bars). Two of the four antibodies (C5, C28) bind the overlapping region between the two immunogens. Antibodies C39 and C40 bind exclusively to the ex2-7 and ex6-10 immunogens, respectively. The MAR epitope, as mapped in Duvoisin *et al.* –2017, is displayed for reference[9].

Figure[A2.2-2]

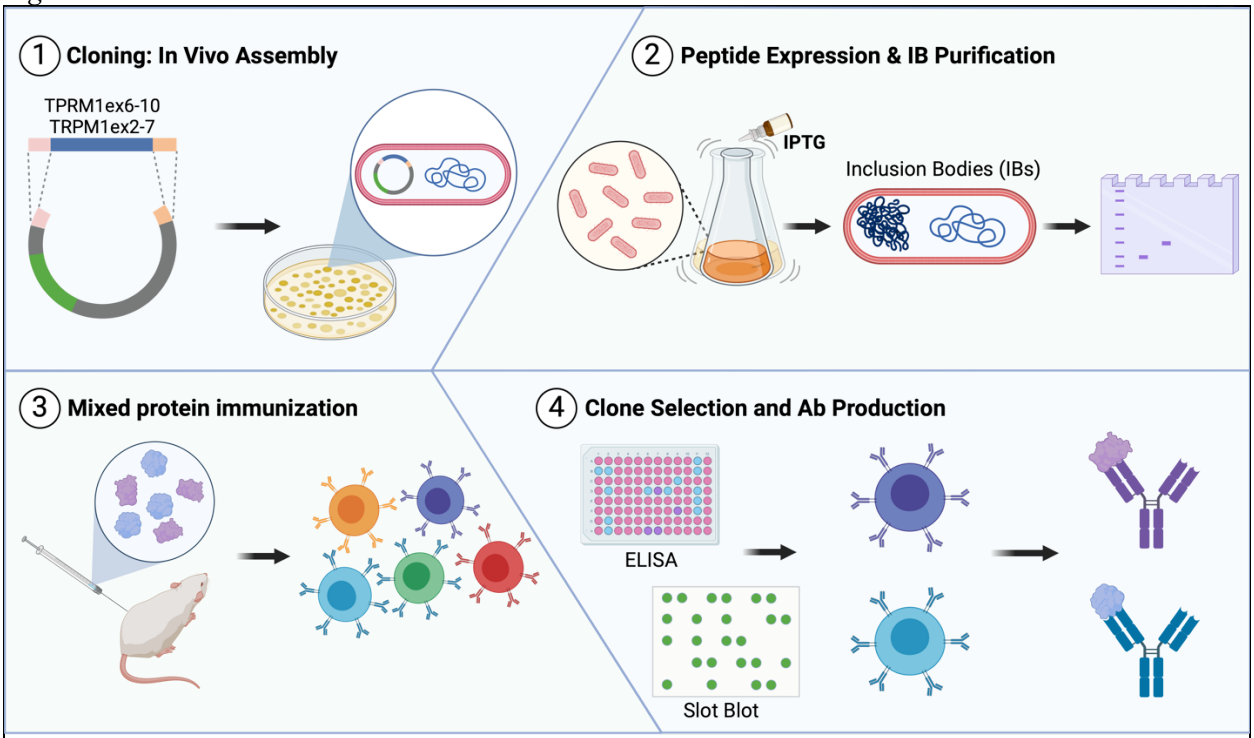

[A2.2-2] **Overview of TRPM1 monoclonal antibody production**. (**1**) TRPM1 sequences were amplified from M14 melanoma cells and subcloned into peET28a bacterial expression vectors. (**2**) BL21 *E.* coli were transformed with the TRPM1 vectors and expression was induced overnight (40μM IPTG, shaking at 225rpm at 30º O/N). Inclusion bodies containing the overexpressed proteins were purified from the bacteria, then solubilized in 8M urea and 1% SDS. Solubilized his-tagged proteins were then purified over Ni-NTA columns. (**3**) Both TRPM1 proteins were mixed in Freund's adjuvant and mice were immunized four times, three weeks apart. (**4**) After splenic harvest and hybridoma generation, single B cell clones were screened for TRPM1 reactivity by ELISA, western blotting, and immunohistochemistry.

Figure[A2.2-3]

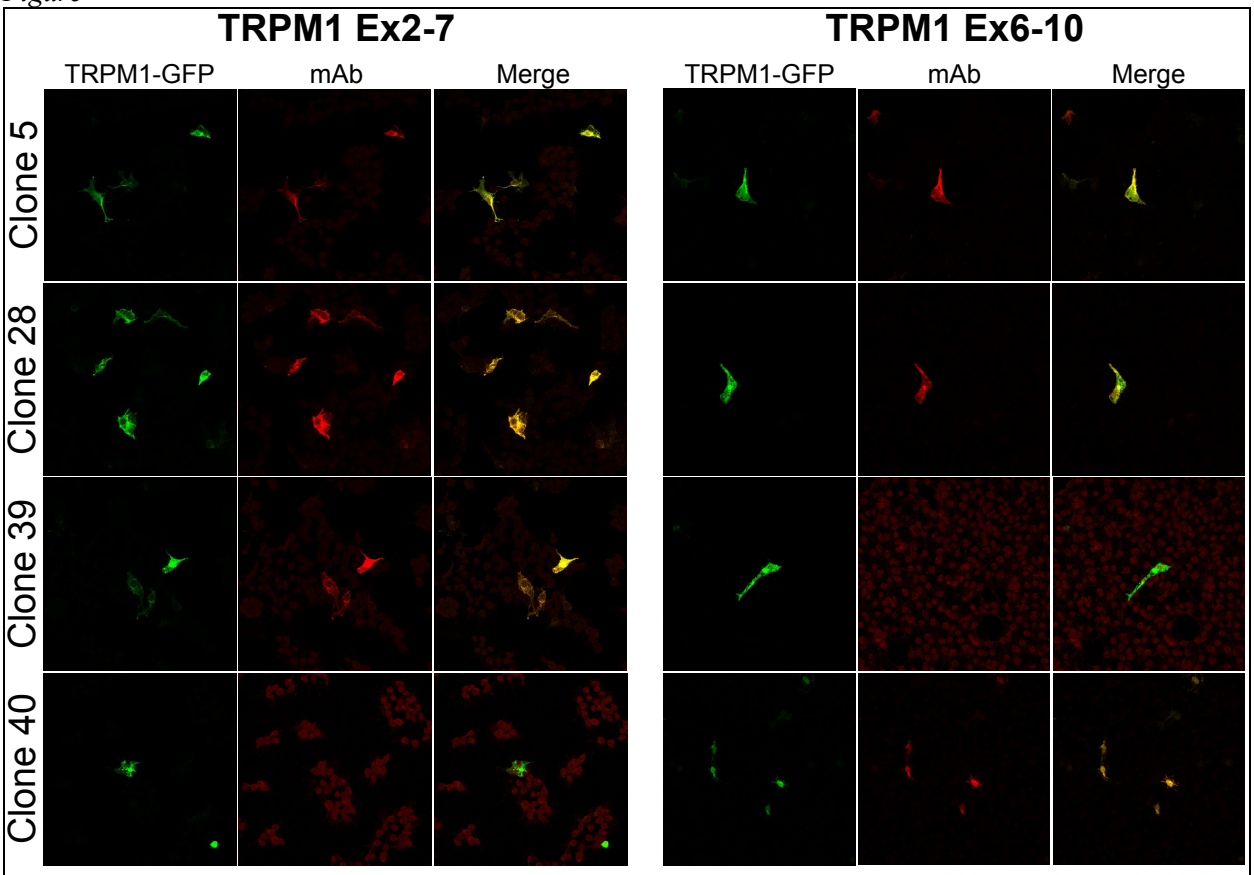

[A2.2-3] **Novel monoclonals react specifically with TRPM1**. HEK293T cells were transfected with plasmids encoding GFP-tagged versions of the two TRPM1 immunogens (TRPM1 Ex2-7 or TRPM1 Ex6-10). Following fixation and permeabilization, cells were incubated with supernatants from the hybridomas that produced the four TRPM1 monoclonal antibodies. Green and red colocalization indicates antibody reactivity with overexpressed TRPM1. Clones 5 and 28 react with both constructs, whereas clones 39 and 40 react only with TRPM1 Ex2-7 and TRPM1 Ex6-10, respectively.

Figure[A2.2-4]

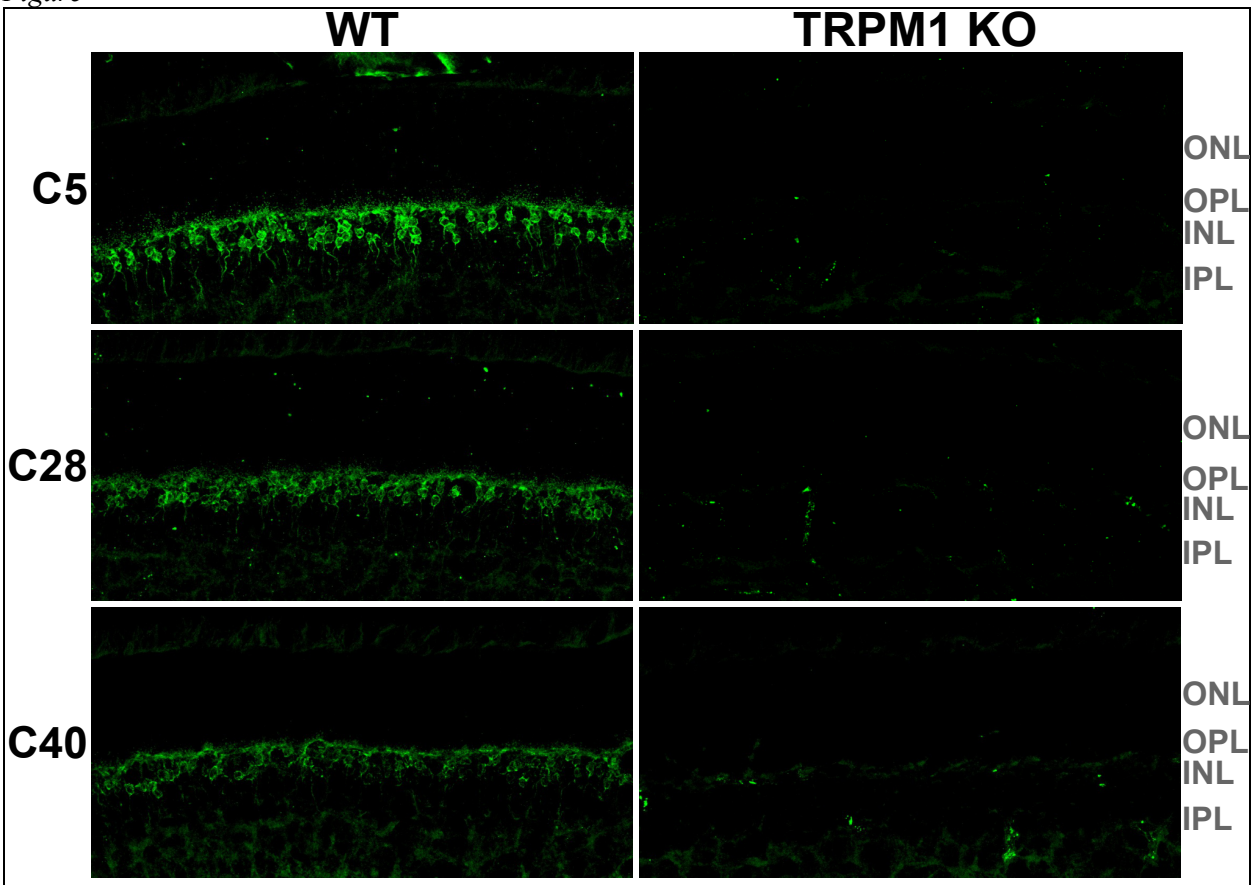

[A2.2-4] **TRPM1 monoclonals label bipolar cells in mouse retinal cryosections**. Prior to purification, dilutions of hybridoma supernatant (1:6 in Antibody Incubation Solution) were applied to retinal cryosections from wild-type and TRPM1 knockout mice for 1 hour at room temperature. Sections were washed 3 times in room temperature PBS, then incubated with an Alexa Fluor-488 conjugated anti-mouse secondary antibody to visualize the bound monoclonal antibodies from the supernatants. Clones C5, C28, and C40 labeled bipolar cells in WT, but not TRPM1 KO mice, demonstrating their specificity for TRPM1. Clone C39 (not shown) labels TRPM1 in transfected HEK cells (Figure A2.2-3) but not retinal cryosections, suggesting its binding epitope may exist in different conformational states in the two models. WT = wild type; ONL = outer nuclear layer; OPL = outer plexiform layer; INL = inner nuclear layer; IPL = inner plexiform layer.

Figure[A2.2-5]

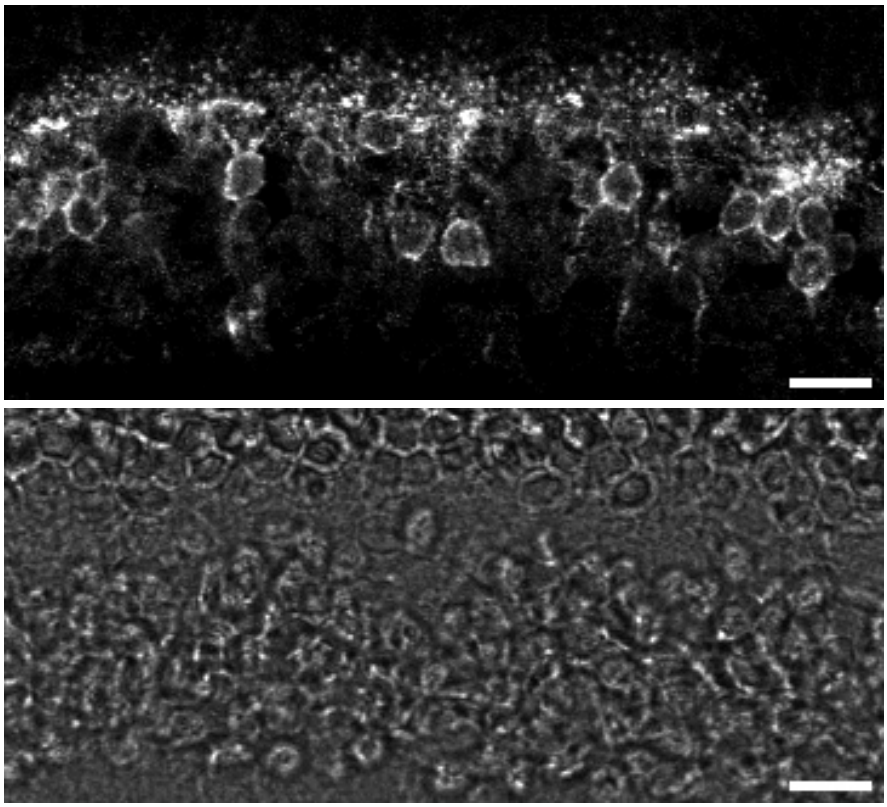

[A2.2-5] **TRPM1 C40 efficiently labels ON-BC cell bodies and dendrites at dilute concentrations**. For immunohistochemistry applications, the C40 clone produced the most efficient labeling of ON-BCs in mouse retinal cryosections. Puncta representing TRPM1 in the ON-BC dendritic tips are clearly visible above the cell bodies, and cell soma labeling remains strong even diluted 1:5K. For the other TRPM1 monoclonal antibodies (C5, C28, and C39), ON-BC labeling is no longer visible at 1:5K (data not shown). Scale bars = 10 μm.

Table [A2.2-1]

Summary of TRPM1 monoclonal antibodies. Amino acid epitope positions are based on the TRPM-203 transcript (NM_001252020.2). Listed concentrations do not account for 50% dilution in glycerol.

Clone	Plate Position	Isotype	Light Chain	Epitope (a.a.)	Retina IHC	Transfected HEK	Concentration (mg/mL)
5	1C5	IgG2b	kappa	224-339	+	+	18.983
28	3H11	IgG2b	kappa	224-339	+	+	30
39	5B2	IgG2a	kappa	40-223	-	+	83.6
40	5A3	IgG1	kappa	340-436	+	+	32.8

Appendix 2 Bibliography

1. Haley, T. L. *et al.* Light-dependent changes in the outer plexiform layer of the mouse retina. *Frontiers in Ophthalmology* **3**, (2023).

2. Lamb, T. D. Why rods and cones? *Eye* **30**, 179–185 (2016).

3. Joachimsthaler, A., Tsai, T. I. & Kremers, J. Electrophysiological Studies on The Dynamics of Luminance Adaptation in the Mouse Retina. *Vision* **1**, 23 (2017).

4. Li, D., Fang, Q. & Yu, H. The Shift of ERG B-Wave Induced by Hours' Dark Exposure in Rodents. *PLOS ONE* **11**, e0161010 (2016).

5. Morgans, C. W., Brown, R. L. & Duvoisin, R. M. TRPM1: The endpoint of the mGluR6 signal transduction cascade in retinal ON-bipolar cells. *Bioessays* **32**, 609–614 (2010).

6. Euler, T., Haverkamp, S., Schubert, T. & Baden, T. Retinal bipolar cells: elementary building blocks of vision. *Nat Rev Neurosci* **15**, 507–519 (2014).

7. Martemyanov, K. A. & Sampath, A. P. The Transduction Cascade in Retinal ON-Bipolar Cells: Signal Processing and Disease. *Annu. Rev. Vis. Sci.* **3**, 25–51 (2017).

8. Elsheikh, S., Gurney, S. P. & Burdon, M. A. Melanoma-associated retinopathy. *Clin Exp Dermatol* **45**, 147–152 (2020).

9. Duvoisin, R. M. *et al.* Autoantibodies in Melanoma-Associated Retinopathy Recognize an Epitope Conserved Between TRPM1 and TRPM3. *Invest. Ophthalmol. Vis. Sci.* **58**, 2732 (2017).